$D^0 - \bar{D}^0$ Mixing and Rare Charm Decays[*]

Gustavo Burdman

Theory Group, Lawrence Berkeley National Laboratory, Berkeley, California 94720
email: gaburdman@lbl.gov

Ian Shipsey

Department of Physics, Purdue University, West Lafayette, Indiana 47907
email: shipsey@physics.purdue.edu

KEYWORDS: flavor physics, flavor-changing neutral currents

ABSTRACT: We review the current status of flavor-changing neutral currents in the charm sector. We focus on the standard-model predictions and identify the main sources of theoretical uncertainties in both $D^0 - \bar{D}^0$ mixing and rare charm decays. The potential of these observables for constraining short-distance physics in the standard model and its extensions is compromised by the presence of large nonperturbative effects. We examine the possible discovery windows in which short-distance physics can be tested and study the effects of various extensions of the standard model. The current experimental situation and future prospects are reviewed.

CONTENTS

1 INTRODUCTION

The remarkable success of the standard model in describing all experimental information to date suggests that the quest for deviations from it should be directed either at higher energy scales or at small effects in low-energy observables. To the last group belong measurements (with precision surpassing 1%) of electroweak observables at CERN's Large Electron Positron

Collider (LEP) and the SLAC Linear Detector (SLD) as well as the Tevatron experiments (1). Tests of the standard model through quantum corrections are a powerful tool for probing the high energy scales possibly related to electroweak symmetry breaking and the flavor problem. The absence of flavor-changing neutral currents (FCNC) at tree level in the standard model implies that processes involving these currents are a primary test of the quantum structure of the theory. The study of FCNC has been focused on processes involving K and B mesons, such as K^0–$\bar{K}^0$ and B_d^0–$\bar{B}_d^0$ mixing, and on rare decays involving transitions such as $s \to d\ell^+\ell-$, $s \to d\nu\bar{\nu}$, $b \to s\gamma$, and $b \to s\ell^+\ell^-$.

The analogous FCNC processes in the charm sector have received considerably less scrutiny. This is perhaps because, on general grounds, the standard-model expectations are very small for both D^0–$\bar{D}^0$ mixing and FCNC decays. For instance, no large nondecoupling effects arise from a heavy fermion in the leading one-loop contributions. This is in sharp contrast with K and B FCNC processes, which are affected by the presence of the top quark in loops. In the standard model, D-meson FCNC transitions involve the rather light down-quark sector, which implies an efficient Glashow-Iliopoulos-Maiani (GIM) cancellation. In many cases, extensions of the standard model may upset this suppression and contributions may be orders of magnitude larger than the standard-model short-distance contributions.

As a first step, and in order to ponder the existence of a window for the observation of new physics in a given observable in charm processes, we must compute the standard-model contributions to such quantities. Attention to standard-model backgrounds is particularly important in this case owing to the presence of potentially large long-distance contributions that are nonperturbative in essence and therefore noncalculable by analytical methods. In general, the flavor structure of charm FCNC favors the propagation of light-quark intermediate states. Thus, if it turns out that the charm-quark mass is not heavy enough compared to a typical scale of hadronic effects, long-distance effects are likely to dominate. They will obscure the more interesting short-distance contributions that are the true test of the standard model. Large long-distance effects are expected in D^0–$\bar{D}^0$ mixing and FCNC charm decays. In the case of mixing, although the long-distance effects dominate over the standard-model short-distance contributions, there could still be a significant window between these and the current experimental limits. The predictions of numerous extensions of the standard model lie in this window. We examine this possibility in Section 2, where we also show that even the current experimental bounds on $D^0 - \bar{D}^0$ mixing constrain several new-physics scenarios.

Charm radiative decays are completely dominated by nonperturbative physics and do not constitute a suitable test of the short-distance structure of the standard model or its extensions. However, semileptonic modes such as $c \to u\ell^+\ell^-$ may be used to constrain various standard-model extensions, since their kinematics might allow measurements away from the resonance-dominated region, where the bulk of the long-distance contributions lie. We demonstrate this in detail in the case of supersymmetric (SUSY) theories with or without R-parity conservation. Purely leptonic flavor-violating modes such as $D^0 \to \mu^+e^-$ are free of standard-model backgrounds. We review the status and prospects of rare charm decays in Section 3.

2 D^0–$\bar{D}^0$ **MIXING**

The time evolution of the $D^0 - \bar{D}^0$ system is described by the Schrödinger equation as

$$i\frac{\partial}{\partial t}\left(\begin{array}{c} D^0(t) \\ \bar{D}^0(t) \end{array}\right) = \left(\mathbf{M} - \frac{i}{2}\mathbf{\Gamma}\right)\left(\begin{array}{c} D^0(t) \\ \bar{D}^0(t) \end{array}\right). \tag{1}$$

Here

$$\left(\mathbf{M} - \frac{i}{2}\mathbf{\Gamma}\right)_{ij} = \frac{\langle D_i|H_{\text{eff}}|D_j\rangle}{2m_D} = m_D^{(0)}\delta_{ij}$$

$$+ \frac{\langle D_i|H_w|D_j\rangle}{2m_D} + \frac{1}{2m_D}\sum_n \frac{\langle D_i|H_w|n\rangle\langle n|H_w|D_j\rangle}{m_D^{(0)} - E_n + i\epsilon}. \tag{2}$$

Noticing that

$$\frac{1}{m_D^{(0)} - E_n + i\epsilon} = P\left(\frac{1}{m_D^{(0)} - E_n}\right) + i\pi\delta(E_n - m_D^{(0)}), \tag{3}$$

where P denotes principal value, we see that the absorptive part, $\mathbf{\Gamma}$, comes from summing over real intermediate states

$$\Gamma_{ij} = \frac{1}{2m_D}\sum_n \langle D_i|H_w|n\rangle\langle n|H_w|D_j\rangle \, \delta(E_n - m_D). \tag{4}$$

On the other hand, the contributions to M_{ij} will include not only the second term in Equation 2 but also a dispersive piece from off-shell intermediate states. Because $\mathbf{M}$ and $\mathbf{\Gamma}$ are Hermitian matrices, $M_{12} = M_{21}^*$ and $\Gamma_{12} = \Gamma_{21}^*$. Invariance under CPT requires $M_{11} = M_{22}$ and $\Gamma_{11} = \Gamma_{22}$. The Hamiltonian eigenstates in terms of the weak eigenstates are

$$|D_{1,2}\rangle = p\,|D^0\rangle \pm q\,|\bar{D}^0\rangle. \tag{5}$$

Defining the "right-sign" amplitudes $A_{\bar{f}} \equiv A(D^0 \to \bar{f})$ and $\bar{A}_f \equiv A(\bar{D}^0 \to f)$, we can also define the "wrong-sign" amplitudes $\bar{A}_{\bar{f}} \equiv A(\bar{D}^0 \to \bar{f})$ and $A_f \equiv A(D^0 \to f)$, where f and $\bar{f}$ are CP-conjugate final states. Then the time evolution of states that start as weak eigenstates at $t = 0$ results in the time-dependent wrong-sign rate given by

$$r(t) = \frac{|\langle f|H|D^0\rangle|^2}{|\bar{A}_f|^2} = \left|\frac{q}{p}\right|^2 \left|g_+(t)\,\lambda_f^{-1} + g_-(t)\right|^2, \tag{6}$$

$$\bar{r}(t) = \frac{|\langle \bar{f}|H|\bar{D}^0\rangle|^2}{|A_{\bar{f}}|^2} = \left|\frac{p}{q}\right|^2 \left|g_+(t)\,\lambda_{\bar{f}} + g_-(t)\right|^2, \tag{7}$$

where we have normalized with the right-sign amplitudes and defined

$$g_\pm(t) \equiv \frac{1}{2}\left(e^{-i\gamma_1 t} \pm e^{-i\gamma_2 t}\right), \ \lambda_f \equiv \frac{q}{p}\frac{\bar{A}_f}{A_f}. \tag{8}$$

The eigenvalues of the Hamiltonian are $\gamma_{1,2} = (M_{11} - i\Gamma_{11}/2) \pm (q/p)(M_{12} - i\Gamma_{12}/2)$. We define

$$x \equiv \frac{m_1 - m2}{\Gamma} = \frac{\Delta m_D}{\Gamma}, y \equiv \frac{\Gamma_1 - \Gamma_2}{2\Gamma} = \frac{\Delta\Gamma_D}{2\Gamma}. \tag{9}$$

Section 2.4 discusses various ways of accessing the mixing parameters x and y.

2.1 Standard-Model Predictions for Mixing Parameter

In this section, we review our understanding of the standard-model predictions for $D^0 - \bar{D}^0$ mixing. As always in charm FCNC processes, the main issue is to estimate as accurately as possible the size of the long-distance contributions. Only then we can evaluate the potential of $D^0 - \bar{D}^0$ mixing to test the standard model and constrain its extensions.

2.1.1   SHORT-DISTANCE CONTRIBUTION TO Δm_D

In the standard model, the short-distance $\Delta C = 2$ transition occurs via box diagrams. The effective interactions at the m_c scale are described by the Hamiltonian (2):

$$\mathcal{H}_{\text{eff.}}^{\Delta C=2} = \frac{G_F^2}{4\pi^2}|V_{cs}^* V_{cd}|^2 \, \frac{(m_s^2 - m_d^2)^2}{m_c^2} \, (\mathcal{O} + 2\mathcal{O}') \,, \tag{10}$$

with $\mathcal{O} \equiv \bar{u}\gamma_\mu(1 - \gamma_5)c \, \bar{u}\gamma^\mu(1 - \gamma_5)c$ and $\mathcal{O}' \equiv \bar{u}(1 + \gamma_5)c \, \bar{u}(1 + \gamma_5)c$. The additional operator $\mathcal{O}'$ arises from the nonnegligible external momentum. The matrix elements of the operators can be parameterized by

$$\langle D^0|\mathcal{O}|\bar{D}^0\rangle = \frac{8}{3}m_D^2 f_D^2 B_D \quad ; \quad \langle D^0|\mathcal{O}'|\bar{D}^0\rangle = -\frac{5}{3}\left(\frac{m_D}{m_c}\right)^2 m_D^2 f_D^2 B_D'. \tag{11}$$

In the vacuum-insertion approximation, one has $B_D = B_D' = 1$ and the box diagrams' contribution to the mass difference is

$$\Delta m_D^{\text{box}} \simeq 1.4 \times 10^{-18} \text{ GeV} \left(\frac{m_s}{0.1\text{GeV}}\right)^4 \left(\frac{f_D}{0.2\text{GeV}}\right)^2. \tag{12}$$

The b-quark contribution is much smaller owing to additional Cabibbo-Kobayashi-Maskawa (CKM) suppression. Thus, for typical values of f_D and m_s, the box diagrams contribute with approximately $x_{\text{box}} \simeq (\text{few} \times 10^{-6}) - (10^{-5})$. In contrast to K and B mixing, the internal quarks in the box diagrams here are down-type quarks. The b-quark contribution, which would give in principle the largest GIM violation, is suppressed by small CKM mixing factors. The leading contribution, as shown in Equation 10, is given by the strange quark and therefore results in a very effective GIM suppression.

The box-diagram contributions to $\Delta\Gamma$ are further suppressed by m_s^2. This can be seen as the two powers of the helicity suppression factor from the matrix element of a 0^- meson to a pair of quarks.

2.1.2   LONG-DISTANCE CONTRIBUTIONS

The long-distance contributions to D^0–$\bar{D}^0$ mixing are inherently nonperturbative and cannot be calculated from first principles. It is however extremely important to estimate their size in order to understand the origin of a possible experimental observation.

A first step is to recall that $D^0 - \bar{D}^0$ mixing is an SU(3)-breaking effect (3, 7):

$$x, \ y \sim \sin\theta_c^2 \times [\text{SU(3) breaking}]. \tag{13}$$

Thus, the task is to estimate the amount of SU(3) breaking. An important observation (4, 11) is that the SU(3) breaking is a second-order effect in the quark masses. This circumstance would lead to the naive estimate

$$x, \ y \sim \sin\theta_c^2 \times \left(\frac{m_s}{\Lambda_{\text{hadr.}}}\right)^2 \lesssim O(10^{-3}), \tag{14}$$

with $\Lambda_{\text{hadr.}} \sim O(1)$ GeV a typical hadronic scale. There are two basic methods to estimate the contributions to mixing beyond box diagrams: the heavy-quark effective theory (HQET) approach pioneered by Georgi (4), which is essentially rooted in the operator product expansion (OPE); and an exclusive approach computing the contributions of hadrons in complete SU(3) multiplets to the dispersive and absorptive parts.

$D^0 - \bar{D}^0$ **Mixing in Heavy-Quark Effective Theory:** The applicability of the HQET ideas to $D^0 - \bar{D}^0$ mixing rests on the assumption that the charm-quark mass is much larger than the typical scale of the strong interactions. Georgi pointed out (4) that in this case there are no nonleptonic transitions to leading order in the effective theory, since they would require a large momentum transferred from the heavy quark to the light degrees of freedom. This means that, in the effective low-energy theory, mixing is a consequence of matching the full $\Delta C = 2$ theory at the scale m_c with the HQET and then running down to hadronic scales ($\ll m_c$). No new operators enter at low energy. The "long-distance" effects are provided by the tree-level matching of operators that are nonleading in the $1/m_c$ expansion but that are less GIM-suppressed than the box diagrams.

First let us consider the four-quark operators generated from the box diagrams by integrating out the Ws. The contribution of these operators to the mass difference behaves like (4)

$$\Delta m_D^{(4)} \simeq \frac{1}{16\pi^2} \frac{m_s^4}{m_c^2},\tag{15}$$

where the first factor comes from the loop and m_d is neglected. This presents the same amount of GIM suppression as the box diagrams and therefore causes no enhancement.

There will also be higher-dimension operators that, although suppressed by additional powers of $1/m_c$, can give important contributions. can give important contributions. For instance, six-quark operators arise by "cutting" one of the light-quark lines in the loop and then shrinking the connecting line leftover. As a consequence, two powers of m_s are lost and the contribution from six-quark operators goes like

$$\Delta m_D^{(6)} \simeq \frac{1}{m_c} \frac{m_s^2}{m_c^2} \left(m_s f^2 \right),\tag{16}$$

where the last factor comes from taking the hadronic matrix elements and f is the pseudo–Goldstone-boson decay constant. This constitutes an enhancement of $(4\pi f)^2/m_c\, m_s$ with respect to the four-quark operator contribution.

Finally, eight-quark operators are obtained by cutting the remaining light-quark line and bridging the two four-quark pieces with a gluon. The resulting contribution goes like

$$\Delta m_D^{(8)} \simeq \frac{\alpha_s}{4\pi} \frac{1}{m_c^2} \frac{\left(m_s f^2 \right)^2}{m_c^2}.\tag{17}$$

This is the least GIM-suppressed contribution, although it is suppressed by $1/m_c^2$ and, most important, by the factor $\alpha_s/4\pi$. Therefore, no enhancement is expected from these operators.

Ohl et al. performed a very detailed calculation in this approach, including QCD corrections to one loop (5). Their results can be summarized as

$$
\begin{aligned}
\Delta m_D^{(4)} &\simeq (0.8 - 1.5) \times 10^{-16} \text{ GeV} \left(\frac{m_s}{0.1 \text{ GeV}} \right)^4 \\
\Delta m_D^{(6)} &\simeq (0.6 - 1.6) \times 10^{-16} \text{ GeV} \left(\frac{m_s}{0.1 \text{GeV}} \right)^3 \\
\Delta m_D^{(8)} &\simeq (0.05 - 0.25) \times 10^{-16} \text{GeV} \left(\frac{m_s}{0.1 \text{GeV}} \right)^2.
\end{aligned}
\tag{18}
$$

The lower numbers correspond to adding the various coefficients in quadrature, since naive dimensional analysis does not predict the relative signs. The upper numbers come from adding all contributions coherently. This leads to

$$x \simeq (0.6 - 2) \times 10^{-4}\tag{19}$$

for $m_s = 0.1$ GeV. Thus, the "long-distance" enhancement observed in this approach is of about one order of magnitude.

More recently, Bigi & Uraltsev made similar arguments also in the context of the OPE (6). However, they found a larger eight-quark operator contribution than Equation 18 indicates. This results in $x \simeq 10^{-3}$. Bigi & Uraltsev also undertook (6) a study of $\Delta\Gamma$ in the OPE approach. They found that the most important contribution to y comes from the eight-quark operators, where the gluon connecting the two sets of four-quark operators is split to generate an imaginary part in the diagram. The "suppression" to be paid (relative to Δm_D) is given by $\beta\,\alpha_s/4\pi \simeq O(1)$, where $\beta = (11 - 2n_f/3)$ is the QCD beta function. This results in $y \simeq x \simeq 10^{-3}$.

Exclusive Approach: An estimate of the long-distance contributions can be obtained by assuming they come from the propagation of hadronic states to which both D^0 and $\bar{D}^0$ can decay. There will be one-, two-, three- ... particle intermediate states. Each of these groups can be further separated into sets whose contributions vanish separately in the SU(3) limit. For instance, one of these sets is formed by the two-charged-pseudoscalar intermediate states[1] $\pi^+\pi^-$, K^+K^-, $K^-\pi^+$, and $K^+\pi^-$. Thus, computing their contribution to the mass difference, as shown schematically in Figure 1, gives a concrete realization of the estimate in Equation 13 for an SU(3) set for which data are available. This was first done (7) in the massless limit. Although these "self-energy" diagrams will depend on the interaction chosen for the vertices, they have a universal imaginary part that typically comes from a logarithm.

The contribution of Figure 1 to the mass difference obeys a dispersion relation of the form (7)

$$\Sigma(p^2) = \frac{1}{\pi} \int_{s_0}^{\infty} \frac{Im[\Sigma(s)]\,ds}{(s - p^2 + i\epsilon)}, \tag{20}$$

where $s_0 \equiv (m_1 + m_2)^2$, and m_1 and m_2 are the masses in the loop. The mass difference is then given by $\Delta m_D = -Re[\Sigma(m_D^2)]/2m_D$. Taking into account a subtraction forcing the condition $\Sigma(0) = 0$, and keeping the masses, the implementation of a cutoff Λ in the dispersive integral (Equation 20) gives (8)

$$x \simeq \frac{m_D}{4\pi}\left\{\frac{B(\pi^+\pi^-)}{\mathbf{p}_{\pi\pi}}\,I(m_\pi, m_\pi, \Lambda) + \frac{B(K^+K^-)}{\mathbf{p}_{KK}}\,I(m_K, m_K, \Lambda)\right.$$
$$\left. -2\cos\delta\frac{\sqrt{B(K^-\pi^+)\,B(K^+\pi^-)}}{\mathbf{p}_{K\pi}}\,I(m_\pi, m_K, \Lambda)\right\}, \tag{21}$$

where $\mathbf{p}_{ij}$ is the magnitude of the three-momentum in the actual decay, δ is the strong phase between the Cabibbo-allowed and the doubly Cabibbo-suppressed decays, B is the branching fraction, and the integrals are

$$I(m_1, m_2, \Lambda) = -\int_{s_0}^{\Lambda^2} \frac{\sqrt{1 - \frac{s_0}{s}}\,ds}{s - m_D^2}. \tag{22}$$

By taking the massless limit in Equation 21, one recovers the result in Reference (7) with the identification $\mu^2 = 2\,m_D\,(\Lambda - m_D)$. Although the result depends strongly on the cutoff Λ, this can be interpreted as the value of s for which the internal momentum reaches its maximum. Not surprisingly, the value of Λ that gives an internal momentum of ~ 1 GeV also yields $\mu \sim 1$ GeV. This is $\Lambda \simeq (2\text{--}2.2)$ GeV, not far above m_D. Using this cutoff results in a

---

[1]Strictly speaking, this is a U-spin set.

contribution to the mass difference of

$$x \simeq 6.5 \times 10^{-4} \times [1 - \cos \delta \; b],\tag{23}$$

where we define b by

$$\frac{B(K^+\pi^-)}{B(K^-\pi^+)} = b^2 \left| \frac{V_{cd}^* V_{us}}{V_{cs}^* V_{ud}} \right|^2,\tag{24}$$

as a measure of the amount of SU(3) breaking in the absolute value of the amplitudes, in addition to the SU(3)-breaking relative phase δ. Measurements in doubly Cabibbo-suppressed (DCS) decays result in $b \sim 1.22$ (9).

It is clear that the cancellation in this SU(3) set is quite effective. Although the dependence on the cutoff Λ appears unsatisfactory, it has a clear physical interpretation. In order to derive Equation 21, we assumed that the couplings at the vertices in Figure 1 are pointlike and therefore constant in s. However, the hadrons participating in these interactions are composite, with the compositeness scale $\Lambda_{\text{hadr.}} \sim O(1)$ GeV, a typical hadronic scale. Thus, at or near $\Lambda_{\text{hadr.}}$, the couplings should develop a form-factor suppression determined by this energy scale that in turn would render the integrals in Equation 22 finite without ad hoc cutoff. Then we should replace $I(m_1, m_2, \Lambda)$ with

$$I(m_1, m_2) = -\int_{s_0}^{\infty} g^2(s) \frac{\sqrt{1 - \frac{s_0}{s}} \; ds}{s - m_D^2},\tag{25}$$

with the coupling of the interaction vertex normalized so that $g(s) \sim 1$ for $s < m_D^2$ and it falls off with $\Lambda_{\text{hadr.}}$ for $s \geq m_D^2$. Of course, the dependence on the cutoff is now hidden in $g(s)$, but its physical meaning is more transparent.

In principle, pseudoscalar-vector (PV), vector-vector (VV), and all other possible intermediate states can be treated similarly. However, in many cases, the data are incomplete. In some cases, phase space suppresses some of the modes, but unlike in $\Delta\Gamma$ (11) (see discussion below), there is no SU(3)-breaking effect induced by running out of phase space. Modes that are not accessible to the actual D decay (and thus to the absorptive part) still contribute to the dispersive part. We cannot express these in terms of branching ratios because the decays are not physical. But in principle the amplitudes for these "off-shell" contributions are well-defined. We then conclude that estimates provided by lighter, far-from-threshold sets, such as the one in Equation 21, are likely to be the most reliable ones in this approach. The underlying assumption is that the contributions of other sets, their signs being not fixed, should not conspire to add coherently and change significantly the order of magnitude of the effect. This reasoning results in

$$x \lesssim 10^{-3},\tag{26}$$

with large uncertainties. In sum, the exclusive approach seems to be consistent with our naive estimate of Equation 14. Additional sources of enhancement in $D^0 - \bar{D}^0$ mixing are discussed in Reference (10).

The exclusive approach can also be applied to $\Delta\Gamma_D$. For instance, for the PP (two pseudoscalars) set considered above, the contribution to y has an expression similar to Equation 21, so that the cancellation is still quite efficient (11). However, y receives contributions only from real intermediate states, so phase space could be a considerable source of SU(3) breaking, in a way that did not arise for the x case (11). In the most extreme cases, some states belonging to a given set would simply be absent because Ds are not allowed to decay into them. This could upset the SU(3) cancellations, perhaps to a large extent. This source of SU(3) violation is estimated by considering the effect of phase space in the contribution of a given intermediate

state F and within a given SU(3) representation R. Thus, one can write

$$y_{F,R} = \frac{\sum_n \langle \bar{D}^0 | H_w | n \rangle \rho_n \langle n | H_w | D^0 \rangle}{\sum_n \langle D^0 | H_w | n \rangle \rho_n \langle n | H_w | D^0 \rangle} = \frac{\sum_n \langle \bar{D}^0 | H_w | n \rangle \rho_n \langle n | H_w | D^0 \rangle}{\sum_n \Gamma(D^0 \to n)}, \tag{27}$$

where the sums are performed over intermediate states n belonging to the class F (PP, PV, etc.) and the representation R. Here, ρ_n is the phase space of state n and depends only on the masses of the particles in this intermediate state. The expression in Equation 27 would be y if the states n of (F, R) were the only states available for the D^0 to decay into. Then, in order to obtain the corresponding contribution to y, $y_{F,R}$ must be rescaled to the total branching ratio of the states in (F, R):

$$y = \frac{1}{\Gamma} \sum_{(F,R)} y_{F,R} \left[\sum_n \Gamma(D^0 \to n) \right]. \tag{28}$$

The scarcity of precise data makes it difficult to disentangle the various SU(3) contributions. A very rough estimate of the relevant branching ratios has been made (11) in order to estimate y in this approach. The states considered are PP, PV, VV, 3P (three pseudoscalars), and 4P. In most cases, the contributions to y are $O(10^{-3})$ at most. The only exception to this is the 4P intermediate states, where very large values of $y_{4P,R}$ are found. This dramatic effect comes mostly from the fact that some members of the SU(3) multiplets that should cancel have run out of phase space, since the average mass of the multiplet is not far from threshold to begin with. In this case, it is found that $y \simeq 10^{-2}$ can be obtained, although with large uncertainties.

In obtaining this estimate of the long-distance contributions to y, it was assumed that phase space is the only source of SU(3) breaking. This constitutes a good estimate if additional sources of breaking do not cancel the effect of phase space significantly. However, this cancellation would naturally occur if the charm quark is heavy enough so that quark-hadron duality, in the spirit of the OPE approach discussed above, is valid. Furthermore, in some cases SU(3) breaking occurs in the opposite direction to the one dictated by phase space: $B(D^0 \to K^+ K^-)/B(D^0 \to \pi^+ \pi^-) \simeq 2.9$. In any case, the effect found in Reference (11) is a reminder of the difficulty of estimating reliably the size of the standard-model effect.

In this examination of the long-distance contributions to mixing, we have seen that

$$x \lesssim 10^{-3}, \quad y \lesssim 10^{-2}. \tag{29}$$

The possibility of having y at the 1% level raises a serious question as to whether it will be possible to extract a smaller value of x from data with enough precision to constrain the short-distance physics contributions from the standard model and/or its extensions.

2.2   CP Violation

In the standard model, the D system is not as sensitive to CP violation as the K and B mesons are. Once again, the small effects predicted in the standard model could leave open a window to the observation of new-physics effects. Here—rather than going into specific calculations—we discuss some general features of CP violation in D mesons, both in the standard model and beyond.

2.2.1   DIRECT CP VIOLATION

Direct CP violation requires the presence of both weak and strong relative phases between two or more amplitudes contributing to a given final state. In the standard model, relative

weak phases can only be obtained in Cabibbo-suppressed decays, for instance, via the interference between spectator and penguin amplitudes. In order to estimate the size of the CP asymmetries this would generate, we write

$$
\begin{aligned}
A_{CP} &\simeq \frac{Im[V_{cd}\, V_{ud}^*\, V_{cs}\, V_{us}^*]}{\lambda^2} \;\; \sin\delta_{\rm st}\;\; \frac{P}{S} \\
&\simeq A^2\, \eta\, \lambda^4\; \sin\delta_{\rm st}\; \frac{P}{S} \qquad \lesssim 10^{-3},
\end{aligned}
\tag{30}
$$

where $\delta_{\rm st}$ is the strong relative phase between the penguin and the spectator amplitudes, P and S, and $A \sim 1$ and η are CKM parameters in the Wolfenstein parameterization. Specific model calculations (12) for $D \to KK, \pi\pi, K^*K$, three-body modes, etc. yield this order of magnitude for the effect. New physics could enter, for instance, through large phases in the penguin diagram. This could give asymmetries of the order of 1% or larger. On the other hand, Cabibbo-allowed decays do not have two amplitudes with different weak phases, and therefore the CP asymmetry is zero in the standard model. Some new-physics scenarios, e.g., some left-right–symmetric models, provide extra phases and could give asymmetries as large as 1%.

2.2.2 INDIRECT CP VIOLATION

When CP violation is negligible, the CP asymmetry is proportional to

$$
A_{CP} \sim -2\,(x\cos\delta + y\sin\delta)\,\sin\phi\,(\Gamma t).
\tag{31}
$$

In the standard model, $\phi \sim 2\,A^2\lambda^4\eta \lesssim 10^{-3}$. New physics in x could induce a large $\sin\phi$. Thus, even if $x \ll y$, provided there is a significant relative strong phase between the $K\pi$ final states, there could be sensitivity to CP-violating phases from new-physics contributions to x.

2.3 Constraints on Physics Beyond the Standard Model

Because the predictions for $D^0 - \bar{D}^0$ mixing in the standard model are quite uncertain, the existence of a discovery window between the current experimental limits and the standard-model prediction cannot be established accurately. On the other hand, several extensions of the standard model predict large enhancements in Δm_D. In many cases, even the current experimental limit is enough to severely constrain models. The situation is illustrated in Figure 2, where standard-model predictions for x and y are collected along with predictions from extensions of the standard model for x. Current experimental bounds already exclude or severely limit the parameter space of some standard-model extensions. In some of these models, theorists have been forced to choose either theoretical mechanisms or parameters that avoid FCNC signals in K and B physics. However, this often leads to large $D^0 - \bar{D}^0$ mixing effects. Thus, although a positive observation of $x \lesssim 10^{-2}$ may not be a clear indication of new physics, pushing the experimental bound as low as possible has a great impact on theoretical model building. We illustrate this point in two paradigmatic cases: weak-scale supersymmetry (SUSY) and strong dynamics at the TeV scale.

2.3.1 THE MINIMAL SUPERSYMMETRIC STANDARD MODEL and Δm_D

Weak-scale SUSY is a possible solution to the hierarchy problem. The minimal supersymmetric standard model (MSSM), the simplest SUSY extension of the standard model, involves a doubling of the particle spectrum by putting all standard-model fermions in chiral supermultiplets and placing the standard-model gauge bosons in vector supermultiplets. Many new

parameters are introduced. The soft SUSY-breaking sector generally includes three gaugino masses, as well as trilinear scalar interactions and Higgs and sfermion masses.

In general, sfermion masses are not related to fermion masses. In particular, if we choose to rotate the squark fields by the same matrices that diagonalize the quark mass matrices, squark mass matrices are not diagonal (14). In this "super-CKM" basis, squark propagators can be expanded so that nondiagonal mass terms result in mass insertions that change the squark flavor. These mass insertions can be parameterized in a model-independent fashion via

$$(\delta_{ij}^u)_{\lambda\lambda'} = \frac{(M_{ij}^u)^2_{\lambda\lambda'}}{M_{\tilde{q}}^2}, \tag{32}$$

where $i \neq j$ are generation indices, λ, λ' denote the chirality, $(M_{ij}^u)^2$ are the off-diagonal elements of the up-type squark mass matrix, and $M_{\tilde{q}}$ represents the average squark mass. This effect can be avoided in specific SUSY-breaking scenarios such as gauge mediation or anomaly mediation, but is present in most situations, e.g., if SUSY breaking is mediated by gravity. In most cases, the main contribution from these soft SUSY-breaking terms to FCNC transitions comes from the gluino-squark loops. Such contributions to rare K and B transitions have led to strong universality constraints on the charged $Q = -\frac{1}{3}$ squark sector (see, e.g., (15)). The most stringent bounds that apply to the nonuniversal soft breaking terms $(\delta_{12}^u)_{\lambda\lambda'}$ come from the experimental searches for D^0–$\bar{D}^0$ mixing.[2] For instance, the CLEO limit (16) implies (17)

$$\frac{1}{2}\left\{\left(\frac{\Delta m_D}{\Gamma_{D^0}}\right)\cos\delta + \left(\frac{\Delta\Gamma_D}{2\Gamma_{D^0}}\right)\sin\delta\right\}^2 < 4 \times 10^{-4}\%, \tag{33}$$

where δ is a strong relative phase between the Cabibbo-allowed and the DCS $D^0 \to K\pi$ decays. Neglecting this phase results in the constraints obtained in Reference (17), which we collect in Table 1. These bounds were obtained assuming that $(\delta_{12}^u)_{RR} = 0$ and $(\delta_{12}^u)_{LR} = (\delta_{12}^u)_{RL}$.

Similar bounds on $(\delta_{ij}^d)_{\lambda\lambda'}$ are obtained in K and B processes. In general, SUSY models naturally give $(\delta_{ij}^q)_{LL}$ and $(\delta_{ij}^q)_{LL}$ of order 1, whereas $(\delta_{ij}^q)_{LR} \simeq (m_Z/M_{\tilde{q}})$ is expected. This can be avoided if squark masses are assumed to be universal at some high energy scale. However, the renormalization group running will generate nondiagonal values of the (δ_{ij}^q)s in general. The mechanism of quark-squark alignment (19), in which squark mass matrices are diagonalized along with the quarks, are an alternative to squark degeneracy. This alignment occurs naturally in theories with an Abelian horizontal symmetry (20). In order to avoid K^0–$\bar{K}^0$ mixing bounds, the down-squark mass matrices are chosen to be diagonal. In order to obtain the correct Cabibbo angle, an off-diagonal term in the up-squark mass matrices must be allowed. This leads to the prediction of large $D^0 - \bar{D}^0$ mixing, saturating the experimental bound.

2.3.2   CONSTRAINTS ON STRONG DYNAMICS FROM $D^0 - \bar{D}^0$ MIXING

We briefly address the constraints arising from Δm_D on theories where the electroweak symmetry is broken by new strong interactions at the TeV scale (for a review, see (21)). These include technicolor (22) and extended technicolor (ETC) (23), top condensation models (24, 25), and composite Higgs models (26), among others. In fact, this may also cover the standard model if the Higgs is not light enough (27).

---

[2]Limits obtained from charge and color breaking and bounding the potential from below (18) apply to the trilinear terms but not to the squark mass terms. Thus, unless the squark mass matrices are kept diagonal, such arguments cannot be used to constrain the nonuniversal mass insertions.

If we consider the standard model as an effective theory, then its scalar sector depends on two quantities (28): Λ, the scale of the underlying physics (or scalar "compositeness" scale), and f, the amplitude for producing the scalars from the vacuum. The ratio of these two scales $\kappa = \Lambda/f$ is estimated to be $\kappa \simeq 4\pi$ in naive dimensional analysis (29). On the other hand, in order for fermions to acquire masses from their Yukawa couplings to the Higgs, they may interact with its constituents through additional interactions characterized by the mass scale M. Assuming that this flavor scale is associated with new gauge interactions, it is possible to make explicit the dependence of the Yukawa couplings on Λ and M (27):

$$-\frac{g^2}{M^2}\frac{\Lambda^2}{\kappa}\,\bar{f}_R\phi\psi_L \sim \sqrt{2}\,\frac{m_f}{v}\bar{f}_R\phi\psi_L, \tag{34}$$

where ψ_L is an SU(2)$_L$ doublet containing f_L and $v \simeq 246$ GeV is the vacuum expectation value of the Higgs field. Thus, in order to have the correct fermion mass, one has

$$\Lambda \gtrsim \frac{M}{g}\sqrt{\sqrt{2}\kappa\frac{m_f}{v}}. \tag{35}$$

The relation in Equation 35 between the Higgs compositeness scale and the scale of flavor physics will result in bounds on Λ. In particular, in addition to the interactions coupling the constituents of the Higgs to the standard-model fermions, there are diagonal interactions involving only the standard-model fermions leading to dimension-six operators of the form

$$\frac{g^2}{M^2}\,(\bar{f}_{L,R}\gamma_\mu f_{L,R})\,(\bar{f}_{L,R}\gamma_\mu f_{L,R}). \tag{36}$$

For instance, for quarks, the interactions in Equation 36 result in FCNC once the quark mass matrix is diagonalized. Thus, operators such as

$$\frac{g^2}{M^2}\,U_{L,R}^{cu*}\,U_{LR}^{cu*}\,(\bar{u}_{L,R}\gamma_\mu c_{L,R})\,(\bar{u}_{L,R}\gamma_\mu c_{L,R}), \tag{37}$$

where the matrices $U_{L,R}$ rotate the left-handed and right-handed up-quarks to their mass eigenbasis, will induce $D^0 - \bar{D}^0$ mixing. Similarly, there will be FCNC operators acting in the K and B sectors. Bounds on M/g then result in bounds on Λ. For instance, assuming $U_{L,R}^{cu} \simeq \sin\theta_C$, one obtains

$$\Lambda \gtrsim 22 \text{ TeV}\,\sqrt{\kappa\,\left(\frac{1.5 \text{ TeV}}{m_c}\right)} \tag{38}$$

from the LR product of color-octet currents. For the naive-dimensional-analysis value $\kappa \sim 4\pi$, we have $\Lambda \gtrsim 78$ TeV.

In principle, this bound could be weakened considerably by assuming $U_{L,R} \ll 1$. But to do so would invite bounds from the down-quark sector. For instance, if $D_L^{ds} \sim \sin\theta_C$, then $\Lambda \gtrsim 15$ TeV. This is a general result that applies not only to ETC theories but also to a host of other scenarios.

The constraints of FCNCs apply not only to the flavor-physics scale but also to the Higgs-compositeness scale. If we interpret the FCNC constraint as a bound on the cutoff scale, these theories are fine-tuned. Whatever the way out of the bounds, this analysis suggests that these scenarios tend to have plenty of flavor physics. Furthermore, we can interpret the cutoff scale Λ as an implied upper bound on the Higgs mass by making use of the triviality constraint (27):

$$m_H^2 \ln\left(\frac{\Lambda}{m_H}\right) \leq \frac{4\pi^2 v^2}{3}. \tag{39}$$

The typical flavor-physics bounds on $\Lambda \lesssim 80$ TeV yield $m_H \leq 400$ GeV. Then, if we consider the standard model as an effective theory valid up to a scale Λ, a light Higgs results in a more fine-tuned scenario, i.e., $m_H/\Lambda \ll 1$. In heavier-Higgs scenarios, the cutoff scale is lower and flavor physics is likely to saturate the experimental bounds on a variety of flavor-physics observables. This circumstance is typical in theories where the Higgs is a composite field and the standard-model fermions feel the interaction binding it. On the other hand, these bounds can be avoided in models with a GIM mechanism built in (30).

Topcolor: In top-condensation models (24), the constituents of the Higgs are the third-generation left-handed quarks as well as t_R. Hill (25) proposed that a new gauge interaction strongly coupled to the third-generation quarks is responsible for top condensation. The topcolor interactions break at the TeV scale as $\mathrm{SU}(3)_1 \times \mathrm{SU}(3)_2 \to \mathrm{SU}(3)_{\mathrm{color}}$, leaving, besides the massless gluons, a set of color-octet gauge bosons (the top-gluons) leading to the Nambu–Jona-Lasinio effective interactions that result in top condensation. This leads to electroweak symmetry breaking as well as to a large "constituent" top mass.

Tilting the vacuum in the top directions to avoid a large b-quark mass is typically accomplished through additional Abelian interactions that leave a Z' strongly coupled to third-generation fermions. In some models, the tilting is done by simply arranging that b_R not couple to the topcolor interactions. The top-gluon interactions (as well as the Z's if present) are nonuniversal, leading to FCNC at tree level. These arise after quarks are rotated to their mass eigenbasis by the rotations

$$U_{L,R}^i \to \mathcal{U}_{L,R}^{ij} U_{L,R}^j, \qquad D_{L,R}^i \to \mathcal{D}_{L,R}^{ij} D_{L,R}^j, \tag{40}$$

where the rotation matrices $\mathcal{U}_{L,R}$ and $\mathcal{D}_{L,R}$ are unitary. The CKM matrix is then $V_{\mathrm{CKM}} = \mathcal{U}_L^\dagger \mathcal{D}_L$.

Constraints on topcolor models are reviewed in Reference (31). The bounds from the down-quark sector impose severe constraints on the entries of $\mathcal{D}_{L,R}$ mainly coming from the exchange of bound states that couple strongly to the b quark. There are several contributions to Δm_D. First, if we consider theories where topcolor only partly breaks the electroweak symmetry, there will be a set of pseudo–Nambu-Goldstone bosons in the spectrum with masses of a few hundred GeV. They contribute (31)

$$\Delta m_D \simeq \frac{f_D^2 \, m_D^2}{2} \frac{m_t^2}{f_{\tilde\pi}^2 m_{\tilde\pi}^2} (\mathcal{U}_L^{tu*} \mathcal{U}_R^{tc})^2, \tag{41}$$

where $f_{\tilde\pi} \approx (50\text{–}70)$ GeV is the top-pion decay constant. If it is assumed that the entries of $\mathcal{U}_{L,R}$ are similar to those of V_{CKM}, we then obtain

$$\Delta m_D \simeq 2 \times 10^{-14} \left(\frac{200 \text{ GeV}}{m_{\tilde\pi}}\right)^2 \text{ GeV}, \tag{42}$$

which is just below the current experimental bound even if we consider $\delta = 0$.

However, the scalar sector of topcolor theories is somewhat model-dependent. For instance, in some scenarios there are no top-pions in the spectrum and topcolor interactions fully break the electroweak symmetry. The most model-independent aspect of topcolor theories is the top-gluon sector. The constraint that the third-generation coupling be supercritical leaves the top-gluon mass as the only free parameter, beyond the quark-rotation matrices. Top-gluon exchange also contributes to B^0–$\bar{B}^0$ (32) mixing, from which important bounds on topcolor models can be derived.

Here we examine the top-gluon contributions to $D^0 - \bar{D}^0$ mixing. In principle, many four-quark operators, upon quark rotation to the mass basis, contribute to Δm_D as a result of

top-gluon exchange. Before rotation, we have the product of third-generation currents, which is enhanced by a factor of (31) $\cot^2 \theta \simeq 22$; the product of one third-generation current and one light current, proportional to $\cot \theta \times \tan \theta = 1$; and the product of two light currents, which is suppressed by $\tan^2 \theta$. It appears at first that—although suppressed by $\tan^2 \theta$—the last group would result in the largest contribution, since the quark rotations in the first two generations are expected to be of the order of the Cabibbo angle. A typical contribution to Δm_D from the last group gives (99)

$$\Delta m_D \simeq 4\pi\alpha_s(M_G) \, \tan^2 \theta \frac{(\mathcal{U}_L^{cu})^2}{2M_G^2} \, (\bar{u}_L\gamma_\mu u_L)(\bar{u}_L\gamma^\mu u_L), \tag{43}$$

which by itself gives a very stringent constraint, $M_G/U_L^{cu} \geq 100$ TeV.

This inference is not necessarily correct. Not only are the matrices $\mathcal{U}_{L,R}$ unitary, but it is also very plausible that the 2×2 block of $\mathcal{U}_{L,R}$ rotating the first two generations is nearly unitary. This would be the most likely situation if both $\mathcal{U}_{L,R}$ have a form similar to V_{CKM}. If this is the case, then

$$\mathcal{U}_{L,R}^{uu*}\mathcal{U}_{L,R}^{uc} \simeq -\mathcal{U}_{L,R}^{cu*}\mathcal{U}_{L,R}^{cc}. \tag{44}$$

This implies that all contributions involving one or two light currents before rotation will almost cancel, thus leading to no real bound. We conclude that the only significant contributions to $D^0 - \bar{D}^0$ mixing come from

$$\Delta m_D \simeq 4\pi\alpha_s(M_G) \frac{\cot^2 \theta}{2M_G^2} \, (\mathcal{U}_{L,R}^{tu*}\mathcal{U}_{L,R}^{tc})^2 \, (\bar{u}_L\gamma_\mu u_L)(\bar{u}_L\gamma^\mu u_L). \tag{45}$$

Using $f_D = 0.2$ GeV, $\alpha_s(1 \text{ TeV}) = 0.09$, and $\cot^2 \theta = 22$, this leads to

$$\Delta m_D \simeq 1.8 \times 10^{-13} \left(\frac{\mathcal{U}_{L,R}^{tu*}\mathcal{U}_{L,R}^{tc}}{\sin^5 \theta_C} \right)^2 \left(\frac{1 \text{ TeV}}{M_G} \right)^2 \text{ GeV}, \tag{46}$$

where we assume that the elements of $\mathcal{U}_{L,R}$ scale with the Cabibbo angle $\theta_C \sim 0.22$ just as the elements of V_{CKM} do. This is compatible with the current experimental limit for Δm_D, e.g., for $M_G \geq 2$ TeV or with some of the elements of $\mathcal{U}_{L,R}$ being slightly smaller that the naive scaling. Thus we see that generically the contributions of top-gluons, although not in conflict with bounds from $D^0 - \bar{D}^0$ mixing, are not far from the current experimental sensitivity.

2.3.3 OTHER NEW-PHYSICS SCENARIOS

As is obvious from Figure 2, there is no shortage of theories beyond the standard model whose parameter space is either already constrained by the current experimental limit on $D^0 - \bar{D}^0$ mixing or sits just below it. Here we mention just a few more.

Extended Higgs sectors without natural flavor conservation: In these scenarios, scalars have tree-level FCNCs that may saturate the current limits on mixing just as in the case of topcolor scalars.

Fourth-generation down quarks: Whether a fourth-generation down quark is a member of a doublet or a singlet, its contributions to the box diagram dramatically break the GIM cancellation in Equation 10 if it has a large Yukawa coupling to the Higgs field. It could saturate the bound if its mixing with the standard-model quarks is judiciously chosen.

Extra dimensions: If gauge or matter fields propagate in compact extra dimensions, the low-energy effective theory below the compactification scale $1/R$ will contain the massless states, the zero-modes. Starting at the compactification scale there are massive Kaluza-Klein (KK) excitations of these fields. These towers may contribute to flavor observables and in particular to $D^0 - \bar{D}^0$ mixing through loops. In addition, if fermions propagating in the bulk have different bulk mass terms, their wave function in the extra dimensions will differ (see, e.g., (33)). This leads to nonuniversal couplings to the KK excitations of the gauge fields and therefore to tree-level FCNC interactions. For instance, the interactions with the first KK excitations of gluons may mimic those of top-gluons if the third-generation quarks are localized toward the TeV brane in a compact five-dimensional model with Randall-Sundrum metric. Of course, as discussed above, the observation of any nonvanishing value of x cannot be interpreted as evidence of new physics because of the proximity of the highest estimates from long-distance, hadronic physics. However, this observation may be complementary to any deviation from the standard model observed in other flavor-physics observables as well as at the energy frontier.

2.4   *Experimental Status and Prospects*

The charm quark was discovered in 1974 in e^+e^- annihilation at SPEAR at the Stanford Linear Accelerator Center and simultaneously in hadronic collisions at Brookhaven National Laboratory (34). Since then, charm hadrons have been produced by a wide range of experimental facilities. The principal production processes are $e^+e^- \rightarrow c\bar{c}$ at $\sqrt{s} = m[\Upsilon(4S)]$; $Z^0 \rightarrow c\bar{c}$; hadroproduction, both at fixed-target experiments and at the Fermilab Tevatron; photoproduction; and threshold production, $e^+e^- \rightarrow \psi(3770) \rightarrow D\bar{D}$. The cross sections vary from 1.3 nb in $e^+e^- \rightarrow c\bar{c}$ at $\sqrt{s} = m[\Upsilon(4S)]$ to microbarns for photoproduction, and to of order a millibarn at the Tevatron. However the ratio of signal cross section to background cross section varies from 1/2.5 in e^+e^- annihilation at the B factories to 1/100 at the Tevatron.

Trigger efficiencies vary by orders of magnitude between experiments, and detection efficiencies vary as well. In a typical (30 fb^{-1}) year at a B factory, 8×10^7 charm quarks are directly produced, with a similar number produced through the decay of B mesons. The trigger efficiency is close to unity, and the detection efficiency is of order $\sim 50\%$ for a two-body hadronic decay. Because of the high relative production rate of charm compared to background, excellent mass resolution, and excellent particle identification, there is no need to exploit the long lifetime of the charm hadrons to isolate a clean charm data sample. At the Z^0, the environment is similar but the charm hadrons have higher momenta, ~ 30 GeV/c compared to 3 GeV/c near B threshold (35). In contrast, fixed-target experiments measure the c-hadron decay time very precisely, which is crucial to isolate clean event samples from the large noncharm backgrounds. The early part of Run IIa at the Tevatron produced $\sim 3 \times 10^{11}$ charm quarks. Until recently, most of these particles would not have been observed. However, there was a tremendous breakthrough in 2002, when CDF (36) demonstrated the ability to trigger on the detached vertices produced by hadronic B- and D-meson decays (36). Some 450,000 $D^0 \rightarrow K^-\pi^+$ decays have now been reconstructed.

To give another idea of how significant an achievement this is, it is useful to define an effective reconstruction cross section for a given mode at a given experiment as the quantity which, when multiplied by the integrated luminosity, yields the number of reconstructed events in that mode for that experiment. For CDF the effective reconstruction cross section for $D^0 \rightarrow K^-\pi^+$ is about 7 nb. This should be compared to the effective reconstruction cross section of about 13 pb for $D^0 \rightarrow K^-\pi^+$ in $e^+e^- \rightarrow D^0 X$ at 10 GeV.

The Cabibbo-allowed two-body decay $D^0 \rightarrow K^-\pi^+$ is easy to reconstruct experimentally and has a large branching ratio, 3.85% (9). The number of reconstructed $D^0 \rightarrow K^-\pi^+$ decays

therefore serves as a benchmark to quantify the size of charm data samples and facilitates comparison between experiments. Using this benchmark, Table 2 compares experiments that have recently published results on charm mixing, rare decays, and searches for CP violation. Table 2 also lists the time resolution for these experiments, which is important in the measurement of lifetimes and mixing. Fixed-target experiments have excellent vertex and proper time resolution, five to eight times better than those of the e^+e^- experiments operating near B–$\bar{B}$ threshold (for a discussion of the measurement of proper time in heavy-flavor physics, see (43)). At the Tevatron, the proper time resolution is similar to that achieved in fixed target experiments.

These data samples have led to many beautiful measurements of the properties of charm hadrons (42). The lifetime of charm mesons is now known with exquisite precision; for example, the lifetime of the D^0 and D^+ are known to 3 and 6 per mille, respectively. However, the data samples collected so far have been too small to allow detection of charm mixing, CP violation, and (with one recent exception) rare decays. Although the fixed-target program at Fermilab is now complete, the outlook for much larger samples of charm hadrons in the near future is very promising. The experiments BaBar, Belle, and CDF expect to increase their data samples, compared to those used in current publications, by factors of 5, 10, and 30, respectively, over the next few years. Each of these experiments also has an upgrade path. There are plans to increase the luminosity of the KEK-B accelerator to $\sim 10^{35}$ cm^{-2}s^{-1} by about 2007, an order of magnitude greater than at present. The configuration is called Super-KEK-B. (The plans and current status of this project are described at http://www-kekb.kek.jp/SuperKEKB/Workshop.html.) This impressive luminosity corresponds to a production rate of 2×10^9 charm hadrons in a Snowmass year of 10^7 s. A five-year program is envisaged at KEK-B. The SLAC group is developing a proposal for a "super B factory" with a luminosity goal of $\sim 10^{36}$ cm^{-2}s^{-1}, corresponding to 2×10^{10} charm hadrons in 10^7 s. This requires a new machine and a very significant upgrade of the BaBar detector, known as SuperBaBar (see, e.g., (44)).

At CDF there is great potential, if charm stays within the trigger bandwidth, to reconstruct 30 million $D \to K^-\pi^+$ in the 4.4 fb^{-1} expected in Run II (our estimate is based on the first 65 pb$^-1$ of integrated luminosity), which would be the largest charm sample so far recorded. The sample could grow by another factor of five during Run IIb. The success of the CDF detached vertex trigger augurs well for future hadron collider experiments such as the proposed BTeV experiment (see, e.g., (45, 46)), which expects to collect $\sim 8 \times 10^8$ charm hadrons in 10^7 s. At the Large Hadron Collider (LHC), the charm cross section is twice as large as at the Tevatron, but most of the increase occurs at inaccessibly small angles to the beam direction. Detector background rates also increase. The design of the trigger for the dedicated B-physics experiment LHCb (see, e.g., (47)) is not expected to have significant acceptance for charm. At the LHC experiments, ATLAS and CMS, the emphasis is placed on triggers for high p_T physics. The experiments do not have detached vertex triggers, although they may be added as upgrades a few years after turn on. No projections for charm yields exist at this time (48).

The prospect of a multi-hundred-GeV e^+e^- linear collider has led to an investigation of the possibility of running at the Z pole, where the charm-quark cross section is ~ 6 nb. Although the linear collider would run well above the Z pole, a scheme exists to allow continuous Z running simultaneously, a so called Giga-Z machine (see, e.g., (49)). The production statistics of Giga-Z do not, in our view, make it competitive with other future facilities, so we do not discuss it here.

The reaction $\psi(3770) \to D\bar{D}$ occupies a special place in the charm experimentalist's and theorist's arsenal. It is the only charm production process in which the charm-quark/anticharm-quark pair produces two charm hadrons that are quantum-mechanically correlated. It is also the only experimental environment in which the probability to reconstruct two charm hadrons

in a single event is large. The $\psi(3770)$ therefore offers crucial experimental advantages for the determination of absolute charm branching ratios, charm-decay constants and charm semileptonic form factors, and the CKM matrix elements V_{cs} and V_{cd}. This suite of measurements is important to the international program in precision flavor physics (see, e.g., (49)) and is widely held to be the main motivation for a charm factory. Particularly pertinent to this review, the $\psi(3770)$ offers unique opportunities to search for charm mixing and CP violation by exploiting quantum coherence and to search for rare decays by exploiting a background-free environment.

Very limited data have been taken at the $\psi(3770)$ since 1984, when Mark III (50) ran there and accumulated 9.6 pb⁻1. More recently, the BESII experiment obtained 20 pb⁻1 at and nearby the resonance (51). At the $\psi(3770)$, CLEO-c (52) expects to accumulate a data sample 300 times larger than MARK III, whereas BES III[3] will have a sample 10 times larger than CLEO-c. To demonstrate the power of $\psi(3770)$ running, we also consider the reach of a purely hypothetical "Super Charm factory" with a luminosity 17 times larger than that of BEPC II, although it is considered unlikely that such a machine could be built. Table 3 summarizes the future charm data samples we use for projections in this review.

In the kaon and B_d^0 meson systems, the mixing rates are large, $(\Delta m/\Gamma) \simeq O(1)$. The mixing parameters can be measured directly from observation of flavor oscillations as a function of time. In the B_s^0 system, the mixing rate is expected to be so large in the standard model that excellent time resolution is required to detect the oscillations. The situation is different for D mesons, where the mixing rate is expected to be very small, precluding the direct observation of flavor oscillations. Alternative methods include the following:

1. Measurements of wrong-sign D^0 decays, using either semileptonic final states or hadronic final states.

2. Comparison of the lifetime of the D^0 measured in hadronic decays and to final states that are CP eigenstates.

3. Time-integrated measurements exploiting quantum coherence at the $\psi(3770)$.

We now consider each of these methods in turn. Only the first two have been attempted so far. A detailed discussion of recent results can be found elsewhere (53).

In order to detect mixing, which is a small effect, it is necessary to know the initial flavor of the D meson and the flavor at the time it decayed. In most measurements that have been performed so far, both at fixed-target and at e^+e^- facilities, the initial flavor of the D^0 is determined from the observation of the sign of the "slow pion" (also called the "soft pion") in the decays $D^{*+} \to D^0 \pi_s^+$ and $D^{*-} \to \bar{D}^0 \pi_s^-$, where s denotes soft. This strong decay is extremely useful in charm and beauty experiments because the branching ratio is large $D^{*+} \to D^0 \pi_s = 68.1\%$, and Q, the mass difference between the initial and final states, is small—$Q = m(D^{*+}) - [m(D^0) + m(\pi_s)] = 6$ MeV. Consequently, $D^{*+} \to D^0 \pi^+$ produces a narrow peak in the Q distribution. In addition, the background is extremely low, so the miss-tag rate is small, about one per thousand in current experiments.

2.4.1 SEMILEPTONIC FINAL STATES

In semileptonic decays, $A_f = \bar{A}_{\bar{f}} = 0$ and we can write (in the small mixing limit)

$$r(t) = \left|\frac{q}{p}\right|^2 |g_-(t)|^2 \simeq \frac{e^{-\Gamma t}}{4} \left|\frac{q}{p}\right|^2 (x^2 + y^2) (\Gamma t)^2. \tag{47}$$

[3]The plans and current status of this project are described at http://bes.ihep.ac.cn/besIII/index.html.

The value of $\bar{r}(t)$ is obtained by exchanging q and p in Equation 47. In the absence of CP violation, the integrated mixing rate is $R_M \simeq (x^2 + y^2)/2$. The charge of the soft pion tags the flavor of the initial state as a D^0 or $\bar{D}^0$. The Cabibbo-favored decay [with $B(D^0 \to K^- l^+ \nu) \simeq 7\%$] gives a $(pi_s^+ \ell^-)$ "right-sign" (RS) charge correlation. If the D^0 mixes, before it decays it is a source of "wrong-sign" (WS) decays: $D^0 \to \bar{D}^0 \to K^+ l^- \nu$. In the standard model, only one diagram exists for semileptonic decays and so there is no direct decay route for $D^0 \to K^+ l^- \nu$. Accordingly, we describe the measurement as theoretically clean: the WS pair $(\pi_s^+ \ell^-)$ is unambiguously a mixing signature. However, the time distribution of the mixing signal is quadratic in the mixing variables. Therefore, although the $(\Gamma t)^2 e^{-\Gamma t}$ term suits fixed-target experiments, the measurement is relatively insensitive to small values of x and y. Furthermore, x and y are not measured separately. Finally, the undetected neutrino complicates the measurement.

At fixed-target experiments, beginning with E791, the technique is to reconstruct the semileptonic decay using $m(\pi_s K^+ \ell^-) - m(K^+ \ell^-)$. The reconstructed peak has a large width due to the missing neutrino. However, the detached vertex leads to a very clean signal in both e and μ modes. The E791 result is (54) $R_M = \frac{1}{2}(x^2 + y^2) < 0.5\%$ at 90% CL. CLEO obtains $R_M < 0.87\%$ @ 90% CL) (55) measured in the channels $D^0 \to K^+ \mu^- \bar{\nu}_\mu$ and $D^0 \to K^{*+} e^- \bar{\nu}_e$, respectively. The most restrictive measurement of R_M comes from FOCUS (56) in the mode $D^0 \to K^+ \mu^- \bar{\nu}_\mu$.

$$R_M - \frac{1}{2}(x^2 + y^2) < 0.12\% \text{ at } 90\% \text{ CL} \tag{48}$$

The bound on R_M is a circle in the $x - y$ plane centered at the origin. In Figure 3 this bound is shown as a circle with horizontal shading.

The future outlook for searcher of charm mixing using semileptonic final states is as follows. B factory results are expected soon. The SuperBaBar working group estimates that, with a 10 ab^{-1} data sample, the sensitivity would be $R_M < 5 \times 10^{-4}$ (57). The technique can, in principle, also be employed by future experiments at hadron machines because the presence of the lepton in the final state helps triggering. However, the technique has the greatest sensitivity at $e^+ e^-$ machines operating at the $\psi(3770)$. In all cases, if mixing is detected in this channel and y turns out to be larger than or comparable to x, a separate measurement of y will be needed.

2.4.2 HADRONIC FINAL STATES

A D^0 can produce a WS hadronic final state either by undergoing a doubly Cabibbo-suppressed (DCS) decay or by first oscillating into a $\bar{D}^0$ that subsequently undergoes a Cabbibo-favored (CF) decay. The WS decay includes three components: one from the DCS decay, a second from mixing, and a third from the interference between the first two. Assuming CP conservation and expanding the decay rate up to $O(x^2)$ and $O(y^2)$ results in the following expression for the time evolution of the hadronic WS decay rate:

$$r(t) = e^{-\Gamma t} \left[R_D + \sqrt{R_D}\, y'\, (\Gamma t) + \tfrac{1}{2} \left(x'^2 + y'^2 \right) (\Gamma t)^2 \right], \tag{49}$$

whereas the RS decays have simple exponential time dependence $\propto \exp^{-\Gamma t}$. Here R_D is defined by

$$\frac{A_f}{\bar{A}_{\bar{f}}} \equiv -\sqrt{R_D}\, e^{-i\delta} \tag{50}$$

and gives the rate for the DCS component. The mixing contribution is quadratic, and hence very small, but the interference term is linear in y' and may result in a measurable deviation from a pure exponential decay.

The specific case $f = K^+\pi^-$ has been studied. The parameters x' and y' are related to the mixing parameters x and y by a rotation (58)

$$x' = x\cos\delta_{K\pi} + y\sin\delta_{K\pi}, \qquad y' = y\cos\delta_{K\pi} - x\sin\delta_{K\pi}. \qquad (51)$$

A strong-phase $\delta_{K\pi}$ exists between the DCS and CF decay amplitudes (59, 60). Although it vanishes in the SU(3) limit, this can be a badly broken symmetry. In a measurement based on the time evolution of the WS state, it is not possible to determine the phase. Since the expression is quadratic in x', its sign is also not determined. We discuss techniques to determine $\delta_{K\pi}$ in Section 2.4.5.

To search for CP violation in the time evolution of the WS hadronic state one applies Equation 49 to D^0 and $\bar{D}^0$ separately. One determines $\{R_{\mathrm{WS}}^+, x'^2_+, y'_+\}$ for D^0 candidates and $\{R_{\mathrm{WS}}^-, x'^2_-, y'_-\}$ for $\bar{D}^0$ candidates, where $R_{\mathrm{WS}}^\pm$ are the corresponding wrong-sign rates. The separate D^0 and $\bar{D}^0$ results can be combined to form the quantities

$$A_D = \frac{R_D^+ - R_D^-}{R_D^+ + R_D^-}; \qquad A_M = \frac{R_M^+ - R_M^-}{R_M^+ + R_M^-}, \qquad (52)$$

where $R_M^\pm \equiv (x'^2_\pm + y'^2_\pm)/2$. Here A_M parameterizes CP violation in the mixing amplitude and leads to

$$\frac{q}{p} = (1 + A_M)^{\frac{1}{2}} e^{i\phi}, \qquad (53)$$

where ϕ is responsible for CP violation in the interference between the DCS decay and mixing. Also, A_D is related to CP violation in the DCS decay amplitude and is defined by making the replacements $\sqrt{R_D} \to \sqrt{R_D}(1 + A_D)$ for the case of initial D^0 and $\sqrt{R_D} \to \sqrt{R_D}/(1 + A_D)$ for the $\bar{D}^0$. In this way, the measurement of the time dependence is sensitive to the combinations $y'\cos\phi \pm x'\sin\phi$ through

$$x'_\pm = \sqrt[4]{\frac{1 \pm A_M}{1 \mp A_M}}(x'\cos\phi \pm y'\sin\phi), \qquad (54)$$

$$y'_\pm = \sqrt[4]{\frac{1 \pm A_M}{1 \mp A_M}}(y'\cos\phi \pm x'\sin\phi). \qquad (55)$$

An offset in ϕ of $\pm\pi$ can be absorbed by a change in sign of both x' and y', effectively swapping the definition of the two physical D^0 states without any other observable consequence. In order to avoid this ambiguity, we use the convention that $|\phi| < \pi/2$. CLEO uses a different approximation (61) in its analysis, which is valid for $A_D, A_M \ll 1 : R_D^\pm = (1 \pm A_D)R_D, x'_\pm = \sqrt{1 \pm A_M}(x'\cos\phi \pm y'\sin\phi),\ y'_\pm = \sqrt{1 \pm A_M}(y\prime\cos\phi \mp x'\sin\phi)$.

The total time-integrated hadronic WS rate, assuming CP conservation and normalizing to the total RS rate, is

$$R_{\mathrm{WS}} = \frac{\int \Gamma_{\mathrm{WS}}(t)\,dt}{\int \Gamma_{\mathrm{RS}}(t)\,dt} = R_D + \sqrt{R_D}y' + 1/2(x'^2 + y'^2). \qquad (56)$$

In this approximation, the mixing rate is $R_M = 1/2(x'^2 + y'^2) = 1/2(x^2 + y^2)$. If there is no mixing in the D^0 system, Equation 56 reduces to $R_{\mathrm{WS}} = R_D$.

CLEO (61) and BaBar (62) have obtained results with 9.0 fb^{-1} and 57.1 fb^{-1} of data, respectively. A result from Belle should soon be available (63). All three experiments have results for the time-integrated WS decay rate R_{WS} (61, 62, 64).

WS candidate events of the types $D^0 \to K^+\pi^-$ and $\bar{D}^0 \to K^-\pi^+$ are selected by requiring the π_s from the D^* decay and the daughter K of the D^0 to have identical charge (WS tag). To

detect a deviation from an exponential time distribution in WS events, a likelihood fit to the distribution of the reconstructed proper decay time t is performed. The likelihood fit includes a signal and a background component and models each as the convolution of a decay-time distribution and a resolution function.

The WS sample is statistically limited, amounting to $\sim 1/300$ the size of the RS sample selected with the same criteria except for the WS tag. The RS sample is used to constrain aspects in the fit that are common to the two samples. CLEO and BaBar determine the resolution functions of WS and RS signals and of the common background types with the RS sample. In the WS sample, a significant additional complication arises from the much lower achievable purity, e.g., $\sim 50\%$ in the CLEO analysis.

CLEO and BaBar both fit using Equation 56 and consider the case with and without CP violation. The results of both experiments are consistent with the absence of mixing and CP violation. We first consider the case with CP conservation. CLEO finds one-dimensional limits of $(1/2)x'^2 < 0.038\%$ and $-5.2\% < y' < 0.2\%$ at the 95% CL. The systematic error is $\pm 0.2\%$ ($\pm 0.3\%$) for x' (y') dominated by knowledge of the background shapes and acceptances.

CLEO's two-dimensional result is a contour on the x'–y' plane that contains the true value of x' and y' with 95% confidence. The contour is constructed using a Bayesian approach. Systematic errors are small but are not included. The contour is shown as the cross hatched region in Figure 3, where the strong phase shift $\delta_{K\pi}$ between the Cabibbo-favored and DCS decays has been assumed to be zero so that the range in x' (y') corresponds to the range of the allowed region in x (y).

In their fit, the BaBar collaboration allows x'^2 to take nonphysical negative values and finds that the most likely fit point when CP is conserved has a negative value of x'^2. BaBar observe a correlation between x'^2 and y'. They present their results as a contour on the x'^2–y' plane (see (64)), where the contour has been constructed using a frequentist approach based on toy Monte Carlo and systematic errors have been included. BaBar made their contours available to the authors of this review and we have redrawn the x'^2–y contour on the x–y plane by converting x'^2 to $x\prime$ and assuming $\delta_{K\pi}$ to be zero. The BaBar redrawn contour is displayed in Figure 3. The numerical result is given in Table 4, where the BaBar limits on x'^2 and y' are obtained by projecting their contour onto the corresponding axis. Also shown in Figure 3, and numerically in Table 4, is a preliminary contour from FOCUS (65) derived from WS $D^0 \to K^+\pi^-$.

The BaBar upper limit for x'^2 is almost three times larger than CLEO's but is based on a data sample six times larger. However, CLEO and BaBar have used different techniques to obtain the 95% CL limits, and the treatment of the fit output parameter x' differs as well, as can be seen in Figure 3. The region allowed by the BaBar result is about a factor of two more restrictive than that from CLEO. This is to be expected, since the measurement of x (y) using this technique scales as $1/L^{1/4}$. For a discussion with an alternative point of view see Reference (53). The sensitivity of this technique to x and y will improve by a factor of two for each B factory with 500 fb^{-1}.

A direct comparison of the CLEO and BaBar results is not possible when CP violation is allowed in the fit, because CLEO uses as fit output parameters x', y', R_D and A_D, A_M, and $\sin\phi$, whereas BaBar uses $A_D, x'^2_+, y'_+, R_D^+, R_M^+$ (x'^2_-, and y'_-, R_D^-, R_M^-) for the D^0 ($\overline{D^0}$) case. Fits that allow for CP violation lead to slightly less restrictive limits on x' and y' (se Table 4). In no case is evidence for CP violation found, i.e. BaBar finds A_D and R_M consistent with zero, and CLEO finds A_M, A_D and $\sin\phi$ consistent with zero.

Extraction of the time-integrated WS decay rate R_{WS}: CLEO and BaBar measure R_{WS} by repeating the fits described in the previous section with the assumption of no mixing in

the D^0 system, i.e., $x = y = 0$ (61, 62). CP violation is allowed, so the fit returns $R_{WS} = R_D$ and A_D. Belle uses a fit in the $M_D - \delta m$ plane to determine the time-integrated number of signal events in the candidate samples (64). The ratio of the number of signal events in the WS and RS candidate samples yields R_{WS}, where the systematic error is dominated by the uncertainty on the background shapes used in the fit. Table 5 compares results from CLEO, BaBar, and Belle to earlier measurements of WS decays by E791 (66), ALEPH (67), and FOCUS (68).

The results are in reasonable agreement. We compute the world average to be

$$\langle R_{\text{WS}} \rangle = (0.368 \pm 0.021)\%. \tag{57}$$

The WS rate is at roughly the level expected in the standard model (see Equation 24). If mixing were present, the WS integrated rate would differ from the standard-model expectation.

D^0 **Decays to Multibody Final States:**   CLEO has also measured R_{WS} in the multibody channels $D^0 \rightarrow K^+\pi^-\pi^0$ and $D^0 \rightarrow K^+\pi^-\pi^+\pi^-$ with the results $R_{\text{WS}} = (0.43^{+0.11}_{-0.10} \pm 0.07)\%$ and $R_{\text{WS}} = (0.41^{+0.12}_{-0.11} \pm 0.04)\%$, respectively (69, 70). R_{WS} need not be the same for different decay modes, but within the errors, R_{WS} is the same for all decay modes measured so far. With the large data samples from the B factories, it may be possible to set D^0–$\bar{D}^0$ mixing limits using combined Dalitz plot and proper time fits in multibody modes. These modes may prove useful in searching for CP violation and understanding strong-phase shifts (71).

The decay $D^0 \rightarrow K^0_S\pi^+\pi^-$ may be used to measure x and y directly, since the strong-phase difference may be extracted simultaneously in a time-dependent fit to the Dalitz plot. This is possible because both the RS and WS decays in the submode $D^0 \rightarrow K^{*\pm}\pi^\mp$ have the same final state. Thus, one can fit for the phase difference directly. The sign of x can also be extracted from such a fit. CLEO presented evidence for a WS amplitude and measured the branching fraction relative to the RS mode to be

$$\frac{B(D^0 \rightarrow K^{*+}\pi^-)}{B(D^0 \rightarrow K^{*-}\pi^+)} = (0.5 \pm 0.2^{+0.5}_{-0.1} \pm^{+0.4}_{-0.1})\% \tag{58}$$

and the strong-phase difference between the RS and WS to be $(189° \pm 10 \pm 3^{+15}_{-5})°$ using a time-independent Dalitz plot fit (72). The last uncertainty is due to the choice of resonances and model. No CP-violating effects were observed when the sample was separated into D^0 and $\bar{D}^0$ subsamples. Results of a time-dependent fit with limits on x, y, and CP violation are expected soon from CLEO, BaBar, and Belle. This channel may offer the greatest sensitivity to x at the large integrated luminosities already collected by Belle and BaBar.

2.4.3   THE MEASUREMENT OF y

The mixing parameter y can be determined by measuring the lifetime difference between D^0 decays to CP-even and CP-odd final states.

$$y_{CP} = \frac{\Gamma(CP \text{ even}) - \Gamma(CP \text{ odd})}{\Gamma(CP \text{ even}) + \Gamma(CP \text{ odd})} \simeq \frac{\Gamma(D^0 \rightarrow K^+K^-)}{\Gamma(D^0 \rightarrow K^-\pi^+)} - 1, \tag{59}$$

which then results in

$$y_{CP} = y \cos\phi - x \sin\phi \, (A_M + A_{\text{prod}}), \tag{60}$$

where the production asymmetry is defined as

$$A_{\text{prod}} \equiv \frac{N(D^0) - N(\bar{D}^0)}{N(D^0) + N(\bar{D}^0)}. \tag{61}$$

It is assumed that $(A_M, A_{\mathrm{prod}}) \ll 1$, where A_M and ϕ are defined as in the previous section.

Then y_{CP} is determined from the slope of the decay-time distributions in samples of $D^0 \rightarrow K^-\pi^+$, which is an equal mixture of CP-even and CP-odd final states, and $D^0 \rightarrow K^-K^+$ or $\pi^-\pi^+$, which are even final states. An unbinned maximum likelihood fit to the distribution of the reconstructed proper decay time t of the D^0 candidates at e^+e^- machines, and the reduced proper time at fixed-target experiments, is performed. Because y_{CP} is measured from the ratio of lifetimes, many systematic effects cancel.

A fixed-target experiment, FOCUS, was the first to make this measurement and found a value of y_{CP} of about 3% that was several standard deviations from zero (68). The e^+e^- experiments BaBar, Belle, and CLEO have now all made this measurement with greater precision than FOCUS.

The three experiments determine y from unbinned maximum-likelihood fits to the distribution of the reconstructed proper decay time, t, of the D^0 candidates. Small biases may occur in the measured lifetimes; these are at the 1% level or below. The precision with which they are known is limited by the statistics of the simulation and is the dominant source of systematic uncertainty for BaBar, whereas for Belle and CLEO knowledge of the background contributions to the signal is the largest source of systematic uncertainty.

The technique, resolution, and systematic errors at $\sqrt{s} = 10$ GeV are quite different from those in fixed-target experiments. D^0 candidates are selected by searching for pairs of tracks with opposite charge and combined invariant mass near the expected D^0 mass. The interception point of the D^0 momentum vector with the envelope of the interaction point (IP) provides the production vertex of the D^0 candidate. The proper decay time of a D^0 candidate is derived from its mass and flight length.

BaBar and CLEO employ a D^* tag. They refit each π_s candidate track with the constraint that it coincide with the D^0 candidate production vertex. This reduces substantially the mismeasurement of the π_s, momentum caused by multiple scattering. Then $\delta m = m(D^{*+}) - m(D^0)$ is required to be consistent with the known value. Belle does not use a D^* tag but requires that the D^0 candidate flight path be consistent with originating at the IP. All three experiments reject events with secondary charm production from B-meson decays with a momentum cut. The analyses by BaBar and Belle are for a subsample of the full data sets. Table 6 lists the subsample sizes and the number of events.

Recently BaBar reported an improved analysis that allows for CP violation. If CP violation occurs, the $D^0(\tau^+)$ and the $\bar{D}^0(\tau^-)$ will have different lifetimes to decay to CP-even states. The effective lifetimes can be combined to form

$$Y = \frac{\tau^0}{\langle\tau\rangle} - 1, \quad \langle\tau\rangle = (\tau^+ + \tau^-)/2 \tag{62}$$

$$\Delta Y = \frac{A_\tau \tau^0}{\langle\tau\rangle} \quad A_\tau = \frac{(\tau^+ - \tau^-)}{(\tau^+ + \tau^-)}. \tag{63}$$

Both Y and ΔY are zero if mixing is absent. Otherwise, in the limit of CP conservation in the mixing amplitude (and little production asymmetry), $Y = y\cos\phi$ and $\Delta Y = x\sin\phi$. All BaBar data (91 fb^{-1}) have been used. Four independent samples were isolated, three tagged with a D^*: $K^-\pi^+$ measures τ^0; K^-K^+ measures $\langle\tau\rangle$, and A_τ; $\pi^+\pi^-$ measures $\langle\tau\rangle$, and A_τ; and an untagged sample of $\approx 146,000$ K^-K^+ measures $\langle\tau\rangle$. An unbinned likelihood fit to m_{D^0}, t, σ_t yields $\langle\tau\rangle, \tau_0$, and A_τ. The statistical uncertainty is small; for example, for $K^-\pi^+$, it is ≈ 0.9 fs, corresponding to 0.5% in y. Assuming the same value of ϕ, the modes K^+K^- and $\pi^+\pi^-$ can be averaged. BaBar combines the modes to find

$$Y = (0.8 \pm 0.4^{+0.5}_{-0.4})\% \tag{64}$$

$$\Delta Y = (-0.8 \pm 0.6 \pm 0.2). \tag{65}$$

This is the single most precise value of Y and the first measurement of ΔY. [4] Because Y and ΔY are consistent with zero, there is no evidence for mixing or CP violation.

In the limit of CP conservation $Y = y$. We average Y with previous measurements of y_{CP}. Figure 4 summarizes the experimental situation: the FOCUS measurement is high, whereas the recent BaBar and Belle results move the world average closer to zero. The new measurement of Y continues this trend. Within the errors, the measured values are consistent. To compute the world average, we exclude the first BaBar measurement because the new measurement of Y supersedes it. We find

$$\langle y_{CP} \rangle = (0.8 \pm 0.5)\%. \tag{66}$$

The average is consistent with the standard-model expectation of a value of $|y|$ close to zero. Figure 3 shows the world-average value of y_{CP} on the x–y plane.

We note that ΔY is not systematically limited and so the precision with which it is determined can be expected to improve by a factor of $\sqrt{5}$ with a 500-fb^{-1} data sample at BaBar or Belle. With the 10 ab^{-1} sample expected at SuperBaBar, the collaboration estimates the following reach: $|Y| < 0.1\%$ and $|\Delta Y| < 0.06\%$ (57).

Figure 3 combines the constraints on the x–y plane for all measurements of mixing from hadronic and semileptonic decays discussed so far. The strong-phase difference is assumed to be zero for this comparison. It is seen that the BaBar measurement of $x'^2 - y'$ is in reasonable agreement with the horizontal band corresponding to the world average of y. If $\delta = 40°$ (the estimated maximum in Reference (73)), the elliptical constraints on x and y from $D^0 \to K^- \pi^+$ would be rotated by δ in a counterclockwise direction, resulting in greater overlap of the CLEO and FOCUS measurements with the world average value of y. These results would be even more consistent if $\delta > 90°$ (58). The overlap of the BaBar measurement with the y band is not significantly improved by rotation. The errors are too large to permit any strong conclusion at this time. However, it is clearly very important to obtain a measurement of the strong phase.

2.4.4   MIXING VIA QUANTUM COHERENCE AT THRESHOLD

At the $\psi(3770)$ and at the $\psi(4140)$, reactions $\psi(3770) \to D^0$–$\bar{D}^0$ and $\psi(4140) \to \gamma D^0 \bar{D}^0$ produce a $D^0 \bar{D}^0$ pair in a state that is quantum-mechanically coherent. This enables simple new methods to measure the $D^0 - \bar{D}^0$ mixing parameters (74) in a way similar to that proposed in Reference (75). Consider, for instance, $D^0 \bar{D}^0 \to (K^- \pi^+)(K^- \pi^+)$. The initial $D^0 \bar{D}^0$ state is

$$|i> = \frac{1}{\sqrt{2}}\{|D^0(k_1, t_1)\bar{D}^0(k_2, t_2)\} + \eta_C |D^0(k_2, t_2)\bar{D}^0(k_1, t_1)\}\}, \tag{67}$$

where $\eta_C = \pm$ is the charge-conjugation eigenvalue of the $D^0 \bar{D}^0$ pair. At the $\psi(3770)$, $\eta_C = -1$, so the system is in the antisymmetric initial state. The case where the D^0 decay is Cabibbo-favored (CF) and the $\bar{D}^0$ decay is DCS (e.g. $D^0 \to K^- \pi^+$ $\bar{D}^0 \to K^- \pi^+$) is indistinguishable from the the case where the $\bar{D}^0$ decay is CF and the D^0 decay is DCS. Upon adding the amplitudes, the DCS contribution cancels. Therefore, for $D^0 \bar{D}^0$ pairs produced from the decay of the $\psi(3770)$, the time-dependent rate is

$$\Gamma(t) \propto \frac{\Gamma^2}{8} e^{-\Gamma(t_1 + t_2)} |\frac{p^2}{q}|B(k_1)|^2 |B(k_2)|^2 (x+y)^2 (t_1 - t_2)^2, \tag{68}$$

---

[4] As this review was going to press, the Belle collaboration announced the preliminary result of a new analysis allowing for CP violation in mixing and interference. Using 91 fb^{-1} of data (82). They find $y_{CP} = (1.15 \pm 0.69)\%$. They also measure $A_\Gamma = (-0.2 \pm 0.6 \pm 0.3)\%$, where A_Γ differs from ΔY by a factor $(1 + y_{CP})$.

where $B \equiv B_{K^-\pi^+} = A(D^0 \to K^-\pi^+)$, i.e., the decay amplitude. Normalizing to $\Gamma[D^0\bar{D}^0 \to (K^-\pi^+)(K^+\pi^-)]$, which is given by

$$\Gamma(t) \propto \tfrac{1}{2}e^{-\Gamma(t_1+t_2)}|B_{K^-\pi^+}(k_1)|^2|B_{K^+\pi^-}(k_2)|^2, \tag{69}$$

implies for the time-integrated ratio

$$R\left(\frac{(K^-\pi^+)(K^-\pi^+)}{(K^-\pi^+)(K^+\pi^-)}\right) = \frac{x^2+y^2}{2}\left|\frac{p}{q}\right|^2\frac{|B_{K^-\pi^+}|^2}{|B_{K^+\pi^-}|^2}. \tag{70}$$

This is similar to the case of semileptonic final states,

$$R\left(\frac{l^\pm l^\pm}{l^\pm l^\mp}\right) = \frac{x^2+y^2}{2}. \tag{71}$$

We note that the DCS amplitude does not cancel for all decay modes (75). For the case where one final state is hadronic and the other semileptonic, we have

$$R\left(\frac{l^+(K^-\pi^+)}{l^+(K^+\pi^-)}\right) = R_D + \frac{x^2+y^2}{2}. \tag{72}$$

These unambiguous signatures for D^0–$\bar{D}^0$ mixing arise because of the quantum coherence of the initial state and are analogous to the situation for B^0–$\bar{B}^0$ pairs at the $\Upsilon(4S)$.

The measurement of R_M can be performed unambiguously with the decays $\psi'' \to K^-\pi^+K^-\pi^+$ and $\psi'' \to \ell^\pm(KX)^\mp\nu\ell^\mp(KX)^\mp\nu$. The hadronic final state cannot be produced from DCS decays. This final state is also very appealing experimentally, because it involves a two-body decay of both charm mesons, with energetic charged particles in the final state that form an overconstrained system. Particle identification is crucial in this measurement because if both the kaon and pion are misidentified in one of the two D-meson decays in the event, it becomes impossible to discern whether mixing has occurred.

The number of RS events in the all-hadronic and hadronic-semileptonic channels combined produced in 3 fb^{-1} is expected to be about 50,000, corresponding to $\sqrt{R_M} \leq 1\%$ at 95% CL. At threshold, the sensitivity scales as $x \propto L^{-1/2}$, whereas at a B factory, for the measurement of mixing through the time evolution of $D^0 \to K^+\pi^-$, the scaling goes like $x \propto L^{-1/4}$. This implies that a 3-fb^{-1} data sample at charm threshold has similar reach to a B-factory data sample of 500 fb^{-1}. Because the charm-threshold measurement is background-free, it is statistically limited rather than systematically limited. At BES III, where the data sample is expected to be 10 times greater, the limit will improve to $\sqrt{R_M} \leq 0.3\%$, but only if the particle identification capabilities are adequate. If it were possible to obtain 500 fb^{-1} at the $\psi(3770)$, the limit would be $\sqrt{R_M} \leq 0.08\%$.

The investigation of mixing parameters at the $\psi(4140)$ provides valuable complementary constraints and a useful consistency check. Note that the final-state $(K^-\pi^+)$ $(K^-\pi^+)$ and $(K^-\pi^+)$ (ℓ^+) from the $\eta_C = +1$ initial state have a decay width proportional to y'. Because R_M is bigger than x or y, the determination of y' from $\eta_C = +1$ initial states is comparable in sensitivity to measurements from the higher-statistics $\eta_C = -1$ initial state.

2.4.5   STRONG PHASES AT CHARM THRESHOLD

We can also take advantage of the coherence of the D mesons produced at the ψ'' to extract the strong-phase difference δ between the direct and DCS amplitudes that appears in the time-dependent mixing measurements. Because the CP properties of the final states produced in the decay of the $\psi(3770)$ are anticorrelated, one D state decaying into a final state with

definite CP properties immediately identifies or tags the CP properties of the state "on the other side." If one state decays into, for example, $\pi^0 K_S$ with $CP = -1$, the other state is "CP-tagged" as being in the $CP = +1$ state. This allows measurement of the branching ratio $B(D_{CP} \to K^-\pi^+)$ and $\cos\delta$. A triangle relation follows from the definition of D_{CP}:

$$\sqrt{2}A(D_{CP} \to K^-\pi^+) = A(D^0 \to K^-\pi^+) \pm A(\bar{D}^0 \to K^-\pi^+). \tag{73}$$

This implies

$$1 \pm 2\cos\delta\sqrt{R_D} = 2\frac{B(D_\pm \to K^-\pi^+)}{B(D^0 \to K^-\pi^+)}, \tag{74}$$

where R_D is the ratio of the DCS decay to the CF mode. We have used the fact that $R_D \ll \sqrt{R_D}$ and neglected CP violation in mixing, which could undermine the CP-tagging procedure by splitting the CP-tagged state on one side into a linear combination of CP-even and CP-odd states, thus requiring time-dependent studies. Both effects, however, are negligible. Now, if decays of both D_+ and D_- are measured, $\cos\delta$ can be obtained from the asymmetry,

$$A = \frac{B(D_+ \to K^-\pi^+) - B(D^- \to K^-\pi^+)}{B(D^+ \to K^-\pi^+) + B(D^- \to K^-\pi^+)} = 2\sqrt{R_D}\cos\delta. \tag{75}$$

The asymmetry A is expected to be small. Thus we have

$$\Delta(\cos\delta) \approx \frac{1}{2\sqrt{R_D}\sqrt{N}}, \tag{76}$$

where N is the total number of CP-tagged $K^-\pi^+$ from the $C = -1$ initial state. At CLEO-c, the total number N is expected to be about 32,000 in one year run of CLEO-c, leading to an expected accuracy of about ± 0.05 in $\cos\delta$.

Reference (83) outlines an alternative method to extract $\delta_{K\pi}$ from a measurement of the rates of the DCS and CF decays of the type $D \to K\pi$. This method requires the determination of rate asymmetries in D meson decays to $K_L\pi$ and $K_S\pi$, and makes the assumption that the two $\Delta I = 1/2$ DCS amplitudes have equal phase. Belle (84) finds that the relevant measurements of K_L and K_S mesons are possible with a statistical precision sufficient to constrain $\delta_{K\pi}$, but their preliminary measurement is not yet sensitive enough to do so:

$$A = \frac{\Gamma(D^0 \to K_S^0\pi^0) - \Gamma(D^0 \to K_L^0\pi^0)}{\Gamma(D^0 \to K_S^0\pi^0) + \Gamma(D^0 \to K_L^0\pi^0)} = 0.06 \pm 0.05 \pm 0.05. \tag{77}$$

As the data sample grows, this measurement will become interesting, but it will not be as precise as the determination of $\delta_{K\pi}$ at threshold. Because the two measurements have entirely different systematic errors, the B-factory measurement will serve as a useful cross check.

2.4.6   SEARCHES FOR CP VIOLATION IN THE D-MESON SYSTEM

Searches for CP violation in charm decays have reached accuracies of several percent (85, 86). In order to measure an asymmetry, one must know the flavor of the decaying meson. Charged D mesons are self-tagging; the neutral D meson requires the above-mentioned D^* tag to determine whether the decaying particle was a D^0 or $\bar{D}^0$.

The fixed target experiments E791 and FOCUS have made some of the most sensitive searches for direct CP violation in the charm system. A subtlety in the measurement is that there is a production asymmetry between D^+ and D^- and between D^0 and $\bar{D}^0$, and so these experiments normalize all asymmetries to some known CF mode where there can be no CP violation—for example,

$$A_{CP}(KK\pi) = \frac{\eta(D^+) - \eta(D^-)}{\eta(D^+) + \eta(D^-)}, \tag{78}$$

where

$$\eta(D^\pm) = \frac{N(D^\pm \to K^\mp K^\pm \pi^\pm)}{N(D^\pm \to K^\mp \pi^\pm \pi^\pm)}. \tag{79}$$

Signals are isolated according to (a) the significance of the longitudinal separation between the decay (secondary) vertex and production (primary) vertex (L/σ), where L is the longitudinal separation and σ is the calculated resolution in L; (b) the confidence level of the decay vertex fit; (c) the vector sum of the momenta from decay vertex tracks, which is required to point to the production vertex in the plane perpendicular to the beam; and (d) particle identification and momentum cuts that are specific to a given final state.

CDF recently presented their first search for CP violation in the charm system using the two-track hadronic trigger (88). Using 65 pb^{-1} of data collected during 2002, about 100,000 $D^0 \to K^-\pi^+$, $8,000$ $D^0 \to K^-K^+$ and $4,000$ $D^0 \to \pi^+\pi^-$ candidates pass selection cuts including $\delta m(D^*)$, the impact parameter of the D^0, and the projected decay length of the D^0. The already impressive statistics yield the most sensitive searches for asymmetries in the following modes:

$$A_{CP}(D^0 \to K^+K^-) = (2.0 \pm 1.7 \pm 0.6)\%, \tag{80}$$

$$A_{CP}(D^0 \to \pi^+\pi^-) = (3.0 \pm 1.9 \pm 0.6)\%. \tag{81}$$

The dominant systematic error comes from the correction for the charge asymmetry for low-momentum tracks in the CDF tracking system.

CLEO has made numerous searches for CP violation in the charm sector. There is no production asymmetry or appreciable detection asymmetry in the $\Upsilon(4S)$ energy region, but statistics are limited. Selected recent asymmetry measurements from all of these experiments are tabulated in Tables 7 and 8 and in Figures 5 and 6. We compute the following averages:

$$\langle A_{CP}(D^0 \to K^+K^-) \rangle = (0.8 \pm 1.2)\%, \tag{82}$$

$$\langle A_{CP}(D^0 \to \pi^+\pi^-) \rangle = (2.7 \pm 1.6)\%. \tag{83}$$

There is no evidence for CP violation at the current level of sensitivity.

An entirely different way to search for CP violation is to exploit quantum coherence at the ψ''. The production process

$$e^+e^+ \to \psi'' \to D^0\bar{D}^0 \tag{84}$$

produces an eigenstate of $CP+$, in the first step, since the ψ'' has J^{PC} equal to 1^{--}. Consider the case where both the D^0 and the $\bar{D}^0$ decay into CP eigenstates. Then the decays

$$\psi'' \to f^i_+ f^i_+ \text{ or } f^i_- f^i_- \tag{85}$$

are forbidden, where f_+ denotes a $CP+$ eigenstate and f_- denotes a $CP-$ eigenstate. This is because

$$CP(f^i_\pm f^i_\pm) = (-1)^\ell = -1 \tag{86}$$

for the $\ell = 1$ ψ''. Thus, observation of a final state such as $(K^+K^)(\pi^+\pi^-)$ constitutes evidence of CP violation. Moreover, all pairs of CP eigenstates, where both eigenstates are even or both are odd, can be summed over for this measurement. This provides a sensitive way to detect CP violation in charm decays and could become sensitive enough to see standard-model mechanisms.

Table 9 estimates the total number of events that would be observed for maximal CP violation in a one-year run at CLEO-c. The event samples are not large, but the measurement is essentially background free. Moreover, this method is important because it has unique sensitivity to the quantum-mechanical phase in the amplitude. This measurement can also

be performed at higher energies, where the final state $D^{*0}\bar{D}^{*0}$ is produced. When either D^* decays into a π^0 and a D^0, the situation is the same as above. When the decay is $D^{*0} \to \gamma D^0$, the CP parity is changed by a multiplicative factor of 1, and all decays $f^i_+ f^i_-$ violate CP (92).

The coherent nature of the wave function prevents measurements of time-integrated mixing-induced CP asymmetries from CP-odd $D^0\bar{D}^0$ pairs produced at the $\psi(3770)$. Thus, at this energy, nonzero time-integrated asymmetries would be a manifestation of direct CP violation. The measurement of direct CP violation in D^0 decays at the $\psi(3770)$ uses a different tagging technique from that at higher energies because the decay $D^{*+} \to D^0\pi^+$ is kinematically forbidden. One D^0 meson in the event, the tag, is partially or fully reconstructed. One example of partial reconstruction is lepton flavor tagging, in which the lepton in the decay $D^0 \to \ell^+ X$ is detected and the charge of the lepton determined. With the flavor of the tag established, the flavor of the other D^0 meson in the event is fixed. Table 10 summarizes the expected sensitivity for direct CP violation in a one-year run at the $\psi(3770)$ at CLEO-c.

CP-even initial states, such as those produced at the $\psi(4140) \to \gamma D^0\bar{D}^0$, are amenable to time-integrated CP asymmetries that are nonvanishing and depend only linearly on the mixing parameter x. In this case, there is a smaller statistical accuracy,due to the smaller cross section, and the overall CLEO-c sensitivity is of the order of 3% using lepton flavor tags only. Backgrounds are expected to be modest and to have a negligible effect on the measured asymmetries, in agreement with previous studies (93, 94).

The studies described here are only some examples of the many possible search strategies (92). Dalitz plot analyses uncover interference effects that are sensitive probes of CP-violating phases. Although some of these measurements can be performed with comparable accuracy at the B factories, the number of studies that can be performed at threshold is very broad and includes some unique measurements exploiting the quantum coherence of the initial state.

Current measurements of CP violation in D^0 decay are at the several-percent sensitivity level. The limits are considerably worse in D^+ and D_S decay. There are significant opportunities to search for the effects of new physics via the mechanism of CP violation both at charm threshold and at the B factories and CDF.

The most reliable way to compare the reach of future experiments for A_{CP} would be to compile a list of sensitivities estimated by each experiment based on detailed simulations. In almost all cases the simulations, or other detailed estimates, do not exist. Instead we will use the simplistic benchmark of the number of reconstructed $D^0 \to K^-\pi^+$ to estimate sensitivities. The CP asymmetry scales like $1/\sqrt{N(D^0 \to K^-\pi^+)}$. To test this method, we note that the experiments E687, E791, and CLEO II, which each reconstructed a few $\times 10^4$ of these decays, had a similar CP reach of $\delta A_{CP} \sim 5\%$. Using this result as a normalization, one expects $\delta A_{CP} \sim 3\%$ for FOCUS and $\delta A_{CP} \sim 2\%$ for CDF. Both are in agreement with the precision reported by the experiments. We compute the sensitivities for future experiments in Table 11. Experiments can be expected to probe CP asymmetries at the 10^{-3} level during this decade. In the early part of the next decade, we can hope to see CP asymmetries probed at the 10^{-4} level.

3   RARE CHARM DECAYS

We have seen that charm processes tend to be affected by large nonperturbative effects. However, for some modes, a window exists in which theoretical predictions are sufficiently under control to allow tests of the short-distance structure of the FCNC transition. This is, to some extent, the case in $c \to u\ell^+\ell^-$ modes, and therefore we concentrate on their potential. On the other hand, radiative charm decays, such as those mediated by $c \to u\gamma$, are largely dominated by long-distance physics. Their experimental accessibility presents an

opportunity to study purely nonperturbative effects in radiative weak decays. We first review the standard-model predictions for the leptonic, semileptonic, and radiative decays. Then we study the potential for new-physics signals in $c \to u\ell^+\ell^-$. Finally, we survey present experimental knowledge and future prospects in rare charm decays.

3.1 The Standard-Model Predictions

The short-distance contributions to the $c \to u$ transitions are induced at one loop in the standard model. It is convenient to use an effective description with the W boson and the b quark being integrated out as their respective thresholds are reached in the renormalization group evolution (96). The effective Hamiltonian is given by (97–99)

$$
\begin{aligned}
\mathcal{H}_{\text{eff}} &= -\frac{4G_F}{\sqrt{2}} \left[\sum_{q=d,s,b} C_1^{(q)}(\mu)O_1^{(q)}(\mu) + C_2^{(q)}(\mu)O_2^{(q)}(\mu) \right. \\
&\quad \left. + \sum_{i=3}^{8} C_i(\mu)O_i(\mu) \right], \quad m_b < \mu < M_W \\
\mathcal{H}_{\text{eff}} &= -\frac{4G_F}{\sqrt{2}} \left[\sum_{q=d,s} C_1^{(q)}(\mu)O_1^{(q)}(\mu) + C_2^{(q)}(\mu)O_2^{(q)}(\mu) \right. \\
&\quad \left. + \sum_{i=3}^{8} C_i'(\mu)O_i'(\mu) \right], \quad \mu < m_b,
\end{aligned}
\tag{87}
$$

with $\{O_i\}$ being the complete operator basis, $\{C_i\}$ the corresponding Wilson coefficients, and μ the renormalization scale; the primed quantities are those for which the b quark has been eliminated. In Equation 87, the Wilson coefficients contain the dependence on the CKM matrix elements $V_{qq'}$. The CKM structure of these transitions differs drastically from that of the analogous B-meson processes. The operators O_1 and O_2 are explicitly split into their CKM components,

$$
O_1^{(q)} = (\bar{u}_L^\alpha \gamma_\mu q_L^\beta)(\bar{q}_L^\beta \gamma^\mu c_L^\alpha), \qquad O_2^{(q)} = (\bar{u}_L^\alpha \gamma_\mu q_L^\alpha)(\bar{q}_L^\beta \gamma^\mu c_L^\beta),
\tag{88}
$$

where $q = d, s, b$, and α, β are contracted color indices. The rest of the operator basis is defined in the standard way. The QCD penguin operators are given by

$$
\begin{aligned}
O_3 &= (\bar{u}_L^\alpha \gamma_\mu c_L^\alpha) \sum_q (\bar{q}_L^\beta \gamma^\mu q_L^\beta), & O_4 &= (\bar{u}_L^\alpha \gamma_\mu c_L^\beta) \sum_q (\bar{q}_L^\beta \gamma^\mu q_L^\alpha), \\
O_5 &= (\bar{u}_L^\alpha \gamma_\mu c_L^\alpha) \sum_q (\bar{q}_R^\beta \gamma^\mu q_R^\beta), & O_6 &= (\bar{u}_L^\alpha \gamma_\mu c_L^\beta) \sum_q (\bar{q}_R^\beta \gamma^\mu q_R^\alpha).
\end{aligned}
\tag{89}
$$

The electromagnetic and chromomagnetic dipole operators are

$$
O_7 = \frac{e}{16\pi^2} m_c(\bar{u}_L \sigma_{\mu\nu} c_R)F^{\mu\nu}, \qquad O_8 = \frac{g_s}{16\pi^2} m_c(\bar{u}_L \sigma_{\mu\nu} T^a c_R)G_a^{\mu\nu};
\tag{90}
$$

and finally the four-fermion operators coupling directly to the charged leptons are

$$
O_9 = \frac{e^2}{16\pi^2}(\bar{u}_L \gamma_\mu c_L)(\bar{\ell}\gamma^\mu \ell), \qquad O_{10} = \frac{e^2}{16\pi^2}(\bar{u}_L \gamma_\mu c_L)(\bar{\ell}\gamma^\mu \gamma_5 \ell).
\tag{91}
$$

The matching conditions at $\mu = M_W$ for the Wilson coefficients of the operators O_{1-6} are

$$
C_1^q(M_W) = 0, \qquad C_{3-6}(M_W) = 0, \qquad C_2^q(M_W) = -\lambda_q,
\tag{92}
$$

with $\lambda_q = V_{cq}^* V_{uq}$. The corresponding conditions for the coefficients of the operators O_{7-10} are

$$
\begin{aligned}
C_7(M_W) &= -\frac{1}{2}\left\{\lambda_s F_2(x_s) + \lambda_b F_2(x_b)\right\}, \\
C_8(M_W) &= -\frac{1}{2}\left\{\lambda_s D(x_s) + \lambda_b D(x_b)\right\}, \\
C_9^{(')}(M_W) &= \sum_{i=s,(b)} \lambda_i \left[-\left(F_1(x_i) + 2\bar{C}(x_i)\right) + \frac{\bar{C}(x_i)}{2s_w^2}\right], \\
C_{10}^{(')}(M_W) &= -\sum_{i=s,(b)} \lambda_i \frac{\bar{C}(x_i)}{2s_w^2}.
\end{aligned}
\tag{93}
$$

In Equation 93, we define $x_i = m_i^2/M_W^2$; the functions $F_1(x)$, $F_2(x)$, and $\bar{C}(x)$ are those derived in Reference (100), and the function $D(x)$ was defined in Reference (97). To compute the $c \to u\ell^+\ell^-$ rate at leading order, operators in addition to O_7, O_9, and O_{10} must contribute. Even in the absence of the strong interactions, the insertion of the operators $O_2^{(q)}$ in a loop would give a contribution sometimes referred to as leading-order mixing of C_2 with C_9. When the strong interactions are included, further mixing of the four-quark operators with O_{7-10} occurs. The effect of these QCD corrections in the renormalization group running from M_W down to $\mu = m_c$ is particularly important in $C_7^{\text{eff}}(m_c)$, the coefficient determining the $c \to u\gamma$ amplitude. As was shown in Reference (97), the QCD-induced mixing with $O_2^{(q)}$ dominates $C_7^{\text{eff}}(m_c)$. The fact that the main contribution to the $c \to u\gamma$ amplitude comes from the insertion of four-quark operators inducing light-quark loops signals the presence of large long-distance effects. This was confirmed (97, 98) when these nonperturbative contributions were estimated and found to dominate the rate. Therefore, we must take into account effects of the strong interactions in $C_7^{\text{eff}}(m_c)$. On the other hand, the operator O_9 mixes with four-quark operators even in the absence of QCD corrections (101). Finally, the renormalization-group running does not affect O_{10}, i.e., $C_{10}(m_c) = C_{10}(M_W)$. Thus, in order to estimate the $c \to u\ell^+\ell^-$ amplitude, it is a good approximation to consider the QCD effects only where they are dominant, namely in $C_7^{\text{eff}}(m_c)$, whereas we expect these to be less dramatic in $C_9^{\text{eff}}(m_c)$.

The leading-order mixing of $O_2^{(q)}$ with O_9 results in

$$
C_9^{(') \text{ eff}} = C_9(M_W) + \sum_{i=d,s,(b)} \lambda_i \left[-\frac{2}{9}\ln\frac{m_i^2}{M_W^2} + \frac{8}{9}\frac{z_i^2}{\hat{s}} - \frac{1}{9}\left(2 + \frac{4z_i^2}{\hat{s}}\right)\sqrt{\left|1 - \frac{4z_i^2}{\hat{s}}\right|}\,\mathcal{T}(z_i)\right], \tag{94}
$$

where we have defined

$$
\mathcal{T}(z) = \begin{cases}
2\arctan\left[\dfrac{1}{\sqrt{\frac{4z^2}{\hat{s}}-1}}\right] & \text{(for } \hat{s} < 4z^2) \\[3ex]
\ln\left|\dfrac{1+\sqrt{1-\frac{4z^2}{\hat{s}}}}{1-\sqrt{1-\frac{4z^2}{\hat{s}}}}\right| - i\pi & \text{(for } \hat{s} > 4z^2),
\end{cases}
\tag{95}
$$

and $\hat{s} \equiv s/m_c^2$, $z_i \equiv m_i/m_c$. The logarithmic dependence on the internal quark mass m_i in the second term of Equation 94 cancels against a similar term in the Inami-Lim function $F_1(x_i)$ entering in $C_9(M_W)$, leaving no spurious divergences in the $m_i \to 0$ limit.[5]

---

[5]Fajfer et al. (107) do not take the mixing of O_9 with O_2 into account. This results in a prediction for the short-distance components that is mainly given by these logarithms.

3.1.1 THE $c \to u\ell^+\ell^-$ DECAY RATES

To compute the differential decay rate in terms of the Wilson coefficients, we use the two-loop QCD corrected value of $C_7^{\text{eff}}(m_c)$ as obtained in Reference (98); we compute $C_9^{\text{eff}}(m_c)$ from Equation 94 and $C_{10}(m_c) = C_{10}(M_W)$ from Equation 93. The differential decay rate in the approximation of massless leptons is given by

$$
\begin{aligned}
\frac{d\Gamma_{c \to u\ell^+\ell^-}}{d\hat{s}} \;=\; & \tau_D \, \frac{G_F^2 \alpha^2 m_c^6}{768\pi^5} \, (1 - \hat{s})^2 \left[\left(\left| C_9^{(')\ \text{eff}}(m_c) \right|^2 + |C_{10}|^2 \right) (1 + 2\hat{s}) \right. \\
& \left. + 12 \, C_7^{\text{eff}}(m_c) \, \text{Re}\left[C_9^{(')\ \text{eff}}(m_c) \right] + 4 \left(1 + \frac{2}{\hat{s}} \right) \left| C_7^{\text{eff}}(m_c) \right|^2 \right],
\end{aligned}
\tag{96}
$$

where τ_D refers to the lifetime of either $D^\pm$ or D^0. We estimate the inclusive branching ratios for $m_c = 1.5$ GeV, $m_s = 0.15$ GeV, $m_b = 4.8$ GeV and $m_d = 0$,

$$
\mathcal{B}r^{(\text{sd})}_{D^+ \to X_u^+ e^+ e^-} \simeq 2 \times 10^{-8}\,, \qquad \mathcal{B}r^{(\text{sd})}_{D^0 \to X_u^0 e^+ e^-} \simeq 8 \times 10^{-9}\,.
\tag{97}
$$

The dominant contributions to the rates in Equation 97 come from the leading-order mixing of O_9 with the four-quark operators $O_2^{(q)}$, the second term in Equation 94. When considering the contributions of various new-physics scenarios, one should remember that their magnitudes must be compared to the mixing of these operators. Shifts in the matching conditions for the Wilson coefficients C_7, C_9, and C_{10}, even when large, may not be enough to give an observable deviation.

3.1.2 THE $c \to u\gamma$ RATE

The short-distance $c \to u\gamma$ contribution to radiative charm decays was first studied in detail by Burdman et al. (97), who found that the effects of the leading logarithms on $C_7(mc)^{\text{eff.}}$ enhanced the branching ratio by several orders of magnitude. Even with such enhancement, the rates were too small. However, Greub et al. noted (98) that the leading logarithmic approximation was still affected by a fair amount of GIM suppression because the quark mass dependence on the resummed expressions was still mild. Going to two loops in the matrix elements of the operators in Equation 87, specifically in $O_2^{(q)}$, leads to a more substantial mass dependence that in turn breaks GIM more efficiently. These two-loop contributions dominate the short-distance radiative amplitude, giving, for instance (98),

$$
B^{(\text{sd})}(D^0 \to X\gamma) \simeq 2.5 \times 10^{-8}.
\tag{98}
$$

Although this represents a very large enhancement even with respect to the leading logarithmic approximation (about five orders of magnitude!), it is still small, especially when compared with the estimated size of long-distance contributions (see below).

3.1.3 EXCLUSIVE SEMILEPTONIC DECAY MODES

The exclusive modes corresponding to $c \to u$ transitions are known to be dominated by long-distance dynamics. This is true for both the radiative and the semileptonic decays. For the $D \to X\gamma$ exclusive modes, long-distance physics dominates all observables. However, in $D \to X\ell^+\ell^-$, it is in principle possible to escape the largest long-distance contributions by looking at regions of phase space away from resonances. We now discuss in some detail the computation of $D \to \pi\ell^+\ell^-$ and $D \to \rho\ell^+\ell^-$ as presented in Reference (99). For completeness, the expectations in the exclusive radiative and neutrino modes are surveyed at the end of this section.

As a crude first estimate of the contributions of long-distance physics, we can consider the resonance process $D \to XV \to X\ell^+\ell^-$, where $V = \phi, \rho, \omega$. We isolate contributions from this particular mechanism by integrating $d\Gamma/dq^2$ over each resonance peak associated with an exchanged vector or pseudoscalar meson. The branching ratios thus obtained are in the $\mathcal{O}(10^{-6})$ range (102).

This result suggests that the long-distance contributions overwhelm the short-distance physics and any new physics that might be present. However, this is not always the case. A more thorough treatment requires looking at all the kinematically available regions in $D \to X_u\ell^+\ell^-$, not just the resonance region. The effect of these states can be thought of as a shift in the short-distance coefficient C_9^{eff} in Equation 94, since $V \to \ell^+\ell^-$ selects a vector coupling to the leptons. This follows from Reference (103), which incorporates in a similar manner the resonant contributions to $b \to q\ell^+\ell^-$ decays via a dispersion relation for $\ell^+\ell^- \to$ hadrons. This procedure is manifestly gauge-invariant. The new contribution can be written via the replacement (103)

$$C_9^{\text{eff}} \to C_9^{\text{eff}} + \frac{3\pi}{\alpha^2} \sum_i \kappa_i \frac{m_{V_i}\Gamma_{V_i \to \ell^+\ell^-}}{m_{V_i}^2 - s - im_{V_i}\Gamma_{V_i}}, \tag{99}$$

where the sum is over the various relevant resonances, m_{V_i} and Γ_{V_i} are the resonance mass and width, and the factor $\kappa_i \sim \mathcal{O}(1)$ is a free parameter adjusted to fit the nonleptonic decays $D \to XV_i$ when the V_i are on shell. We obtain $\kappa_\phi \simeq 3.6$, $\kappa_\rho \simeq 0.7$, and $\kappa_\omega \simeq 3.1$. The latter result comes from assuming $B(D^+ \to \pi^+\omega) = 10^{-3}$, since a direct measurement is not available yet.

$D^+ \to \pi^+ e^+ e^-$: The main long-distance contributions come from the ϕ, ρ, and ω resonances. The η and η' effects are negligible. The dilepton mass distribution for this decay takes the form (99)

$$\frac{d\Gamma}{ds} = \frac{G_F^2\alpha^2}{192\pi^5}|\vec{p}_\pi|^3 |f_+(s)|^2 \left(\left|\frac{2m_c}{m_D}C_7^{\text{eff}} + C_9^{\text{eff}}\right|^2 + |C_{10}|^2\right), \tag{100}$$

where $s = m_{ee}^2$ is the square of the dilepton mass. Here we have used the heavy-quark spin-symmetry relations that relate the matrix elements of O_7 to the "semileptonic" matrix elements of O_9 and O_{10} (104). An additional form factor is formally still present, but its contribution to the decay rate is suppressed by $(m_\ell/m_D)^2$ and is neglected here. Precise measurements of $D \to \pi\ell\nu$ will give us $f_+(q^2)$. In the meantime, we make use of the prediction of chiral perturbation theory for heavy hadrons (ChPTHH) (105), which at low recoil gives

$$f_+(s) = \frac{f_D}{f_\pi} \frac{g_{D^*D\pi}}{(1 - s/M_{D^*}^2)}. \tag{101}$$

Here we use the recent CLEO measurement (106) $g_{D^*D\pi} = 0.59 \pm 0.1 \pm 0.07$, and we take $f_D = 200$ MeV. In Figure 7, we present this distribution as a function of the dilepton mass. The two narrow peaks are the ϕ and the ω, which sits on top of the broader ρ. The total rate results in $B(D^+ \to \pi^+e^+e^-) \simeq 2 \times 10^{-6}$. Although most of this branching ratio arises from the intermediate $\pi^+\phi$ state, we can see from Figure 7 that new-physics effects as low as 10^{-7} can be observed as long as such sensitivity is achieved in the regions away from the ω and ϕ resonances, both at low and high dilepton mass squared.

Fajfer et al. use a different approach to compute the long-distance effects in $D \to \pi\ell^+\ell^-$ (107). They estimate individual contributions to the amplitude by using a combination of vector meson dominance (VMD), factorization, ChPTHH, and hidden local symmetry. In

addition to the large inherent uncertainties associated with each of these methods, there is no clear prescription of how to fix the relative signs of the various contributions, nor—in contrast to the previous approach—the sign relative to the short-distance contribution. Within these large uncertainties, the results of Reference (107) and Reference (99) do not differ by much.

$D^+ \to \rho^+ e^+ e^-$: Once again, we follow closely the calculation of Burdman et al. (99). Because fewer data are currently available on the $D \to VV'$ modes, we take the values of the κ_i in Equation 99 from the fits to the $D^+ \to \pi^+ V$ case studied above. Again, once precise measurements of the $D \to \rho\ell\nu$ form factors are available, heavy quark spin symmetry relations can be used to turn these into $D \to \rho\ell^+\ell^-$ form factors. Lacking these at the moment, we use the extracted values from the $D \to K^*\ell\nu$ data (108) and assume SU(3) symmetry (113). The total integrated branching ratio is $B(D^0 \to \rho^0 e^+ e^-) = 1.8 \times 10^{-6}$ (i.e., $B(D^+ \to \rho^+ e^+ e^-) = 4.5 \times 10^{-6}$). As Figure 8 shows, once again most of this rate comes from the resonance contributions. However, there is also a region—in this case confined to low values of m_{ee} owing to the kinematics—where sensitive measurements could test the standard-model short-distance structure of these transitions.

Fajfer et al. (109) studied these modes, following the approach of Reference (107). Their results (109) show a large enhancement at low m_{ee} when compared with Figure 8. If this long-distance enhancement is present, it could dominate the low m_{ee} region, rendering the $D \to V\ell^+\ell^-$ modes useless to test short-distance physics at any level. Therefore, we examine this discrepancy carefully. A $1/m_{ee}^2$ enhancement can only appear as a result of nonfactorizable contributions. This is clear from References (110) and (111): the factorization amplitude for $D \to \rho V$, when combined with a gauge-invariant $(\gamma - V)$ mixing, leads to a null contribution to $D \to V\ell^+\ell^-$. This is reflected also in the fact that the mixing of the operator O_2 with O_7 is nonfactorizable (111). A resonant contribution to O_7, leading to a $1/q^2$ behavior, is then proportional to C_7^{eff}, which is mostly given by the O_2 mixing. In addition, when compared with the usual short-distance matrix element of O_7, this resonant contribution will be further suppressed by the factor $g_V(q^2)A^{\text{nf}}(q^2)$, where $g_V(q^2)$ is the $(\gamma - V)$ mixing form factor, and $A^{\text{nf}}(q^2)$ parameterizes the nonfactorizable amplitude $\langle \rho V|O_7|D\rangle$, which is of $\mathcal{O}(\Lambda_{\text{QCD}}/m_c)$ (112). Thus, even if we take the on-shell values for these quantities, the resonant contribution to O_7 is likely to be below 10% of the standard-model short-distance contribution. The actual off-shell values at low q^2 far from the resonances are likely to be even smaller. We then conclude that the $1/q^2$ enhancement is mostly given by the short-distance contribution. This is only noticeable at extremely small values of the dilepton mass, so that it is likely to be beyond the experimental sensitivity in the electron modes (due to Dalitz conversion), whereas in the muon modes it lies beyond the physical region. On the other hand, the factorizable pieces contribute to the matrix elements of O_9, just as in Equation 99, and give no enhancement at low values of q^2. We then conclude that there should be no very large long-distance contributions at low m_{ee}.

The ρ modes also contain angular information in the form of a forward-backward asymmetry for the lepton pair. Because this asymmetry results from the interference between the vector and the axial-vector couplings of the leptons, it is negligible in the standard model, since vector couplings due to vector mesons overwhelm axial-vector couplings. This is true even away from the resonance region, since the coefficients $C_9^{(\prime)\text{eff}}$ and C_7^{eff} get large enhancements due to mixing with O_2 and QCD corrections, whereas C_{10}—the axial-vector coupling—is not affected by any of these, which results in a very small interference.

For both the π and ρ modes, the sensitivity to new-physics effects is reserved for large $\mathcal{O}(1)$ enhancements because the long-distance contributions are still important even away from the resonances. Table 14 summarizes theoretical predictions from Reference (99). In addition,

some modes are almost exclusively long-distance physics. Examples are $D^0 \to \bar{K}^{0(*)}\ell^+\ell^-$ and the radiative $D^0 \to \bar{K}^{0(*)}\gamma$, dominated by W exchange diagrams, as well as $D^\pm \to \bar{K}^{\pm(*)}\ell^+\ell^-$ and the radiative $D^\pm \to \bar{K}^{\pm(*)}\gamma$, which contain both W annihilation and exchange. The measurements of these modes, although not directly constraining new physics, will help us understand long-distance physics. This may prove crucial to test the short-distance physics in the π and ρ modes.

Exclusive Radiative Decays: Exclusive decays mediated by the $c \to u\gamma$ transition are expected to be plagued by large hadronic uncertainties. As mentioned, the large mixing of the O_7 operator with the four-quark operators, especially O_2, and the propagation of light quarks in the loops indicate the presence of potentially large nonperturbative effects. These are not calculable from first principles nor in a controlled approximation (other than lattice gauge theory). Moreover, even if lattice computations of these effects become available, they typically overwhelm the standard-model short-distance contributions. Thus, modes such as $D \to \rho\gamma$ are not expected to be a probe of the short-distance structure of the standard model to the extent $B \to K^*\gamma$ can be if the transition form factor is known precisely.

On the other hand, one can try to estimate the size of the long-distance contributions and therefore the branching fractions of these modes. This is interesting in its own right; experimental observation of these modes will give us guidance in our otherwise limited understanding of these nonperturbative effects.

Several attempts at estimating the long-distance contributions have been made (97, 115–118). An example is the decay $D^0 \to \rho^0\gamma$. We can identify two types of long-distance contributions: pole-mediated and vector-meson dominance (VMD) transitions. Pole contributions can be thought of as driven by "annihilation" diagrams. The effective weak Hamiltonian underlying these transitions is

$$H_w = -\frac{4G_F}{\sqrt{2}} \left[a_1(\bar{u}_L\gamma_\mu d'_L)(\bar{s}'_L\gamma^\mu c_L) + a_2\,(\bar{s}'_L\gamma_\mu d'_L)(\bar{u}_L\gamma^\mu c_L) \right], \tag{102}$$

with $d' \equiv V_{ud}d + V_{us}s$ and $s' \equiv V_{cs}s + V_{cd}d$. There are two pole diagrams giving (97)

$$\begin{aligned} A(D^0 \to \rho^0)_{\text{pole}} &= \frac{g_{\rho\pi\gamma}}{m_D^2 - m_\pi^2}\langle\pi^0|H_w|D^0\rangle \\ &+ \frac{g_{D^{*0}D^0\gamma}}{m_D^2 - m_{D^*}^2}\langle\rho^0|H_w|D^{*0}\rangle. \end{aligned} \tag{103}$$

Here, H_w refers to the four-fermion weak Hamiltonian governing nonleptonic weak decays. For instance,

$$\langle\pi^0|H_w|D^0\rangle = -\frac{G_F}{\sqrt{2}}a_2(m_c)V_{ud}^*V_{cd}\frac{f_\pi}{\sqrt{2}}f_D m_D^2, \tag{104}$$

where $a2(m_c)$ is determined in D nonleptonic decays. These two pole diagrams may cancel rather efficiently. Since the details are extremely model-dependent, we could ask what branching ratio would be implied by one of them alone. This typically leads to (97) $B(D^0 \to \rho^0\gamma)_{\text{pole}} \leq$ few $\times 10^{-7}$. However, QCD sum rules may be used (115) to compute the annihilation contributions, and these are found to give $B(D^0 \to \rho^0\gamma) \simeq$ few $\times 10^{-6}$.

On the other hand, VMD contributions come from considering the nonleptonic intermediate states. In this case, this corresponds to $D^0 \to \rho^0 V \to \rho^0\gamma$, where the neutral vector boson V turns into an on-shell photon. Various methods have been used to compute the nonleptonic and $V \to \rho$ amplitudes (97, 116, 117). A common assumption to estimate the VMD amplitude has been that of factorization (119). However, the contribution of the factorized nonleptonic amplitude vanishes when the photon is on-shell (110, 111). This is a consequence

of gauge invariance and is related to the fact that the mixing of four-quark operators with the photon penguin operator O_7 vanishes unless nonfactorizable gluons are exchanged. Thus, nonfactorizable contributions to the nonleptonic amplitude constitute the leading effect in the VMD amplitude. It is therefore possible that the VMD contributions to weak radiative decays of charm mesons are overestimated. At the same time, it is possible that the charm quark is not heavy enough for the nonfactorizable effects to be suppressed. The suppression is formally $O(\Lambda/m_c)$, with Λ a typical scale of strong interactions. We conclude that uncertainties in these modes are still very large. Table 12 summarizes predictions for these decays in different model computations. The Belle collaboration recently announced a measurement of $D^0 \to \phi\gamma$, with a branching ratio of (138) $B(D^0 \to \phi\gamma) = (2.60^{+0.70+0.15}_{-0.61-0.17}) \times 10^{-5}$. As one can see from Table 11, this is consistent with the upper end of the predictions in Reference (97), which were obtained by making use of VMD plus the data on the relevant nonleptonic decay in addition to the pole contributions. If this trend is confirmed in this as well as other modes, this might point in the direction of large nonfactorizable contributions. Experimental bounds are closing in on some of these predictions and will undoubtedly shed light on the size of these long-distance effects.

3.1.4 OTHER DECAY MODES

Our discussion has neglected many decay modes to focus on those that can potentially test the short-distance structure of the standard model and are reachable in present or planned experiments. Here is a sample of other modes studied in the literature.

$D^0 \to \gamma\gamma$: The standard-model short-distance contributions can be obtained from the two-loop $c \to u\gamma$ amplitude. This results in (99) $B^{\mathrm{SD}}(D^0 \to \gamma\gamma) \simeq 3 \times 10^{-11}$. There are several types of long-range effects. Fajfer et al. (120) estimate these effects using ChPTHH to one loop. This gives $B^{\mathrm{LD}}(D^0 \to \gamma\gamma) \simeq (1 \pm 0.5) \times 10^{-8}$. Burdman et al. (99) consider various long-distance effects and obtain similar results. In this case, the main contributions are found to come from VMD and the K^+K^- unitarity contribution.

$D^0 \to \ell^+\ell^-$: The short-distance contributions to this mode are also extremely suppressed, not only by helicity but also by the quark masses in the loop. Unlike in $c \to u\gamma$, the mixing with O_2 does not help. In Reference (99), the short distance is estimated at $B^{\mathrm{SD}}(D^0\ell^+\ell^-) \lesssim 10^{-18}$. The most important source of long-distance effects is the two-photon unitary contribution, which gives

$$B^{\mathrm{LD}}(D^0 \to \ell^+\ell^-) \simeq 3 \times 10^{-5} \; B(D^0 \to \gamma\gamma). \tag{105}$$

$D \to X\nu\bar{\nu}$: Short- and long-distance contributions to $c \to u\nu\bar{\nu}$ processes in the standard model are extremely small, typically resulting in (99) $B(c \to u\nu\bar{\nu}) \lesssim 10^{-15}$.

3.2 Rare Charm Decays and New Physics

As mentioned, charm-changing neutral-current processes such as D^0–$\bar{D}^0$ mixing and rare charm decays complement the constraints on extensions of the standard model obtained from processes initiated by down quarks, such as kaon and B-meson transitions. Although we have seen that bounds on Δm_D are quite constraining in a variety of models, new physics may still show itself in rare charm decays. We mainly review the potential for signals from supersymmetric theories (with and without R-parity conservation) and from new strong dynamics at the TeV scale. We briefly comment on the sensitivity to other new physics, such as theories with extra dimensions and extended gauge and matter sectors.

3.2.1   THE MINIMAL SUPERSYMMETRIC STANDARD MODEL

The MSSM adds to the standard-model description of loop-mediated processes contributions due to gluino-squark exchange, chargino/neutralino-squark exchange, and charged Higgs-quark exchange. This last contribution carries the same CKM structure as in the standard-model loop diagram and is proportional to the internal and external quark masses; thus, its effects in rare charm transitions are small and we neglect it here. The gluino-squark contribution proceeds via flavor-diagonal vertices proportional to the strong coupling constant and in principle dominates the CKM-suppressed, weak-scale strength chargino/neutralino-squark contributions. We therefore consider only the case of gluino-squark exchange here as an estimate of the potential size of SUSY effects in rare charm decays.

A typical squark-gluino contribution is depicted in Figure 9. The corresponding effects in the $c \to u$ transitions were studied for $D \to X_u\gamma$ (17) and for $D \to X_u\ell^+\ell^-$ (99). Within the context of the mass insertion approximation (14), the effects are included in the Wilson coefficients corresponding to the decay $D \to X\ell^+\ell^-$ via

$$C_i = C_i^{\mathrm{SM}} + C_i^{\tilde{g}}, \tag{106}$$

for $i = 7, 9, 10$. Allowing for only one insertion, the explicit contributions from the gluino-squark diagrams are (17, 99, 121)

$$C_7^{\tilde{g}} = -\frac{8}{9} \frac{\sqrt{2}}{G_F M_{\tilde{q}}^2} \pi\alpha_s \left\{ (\delta_{12}^u)_{LL} \frac{P_{132}(u)}{4} + (\delta_{12}^u)_{LR} P_{122}(u) \frac{M_{\tilde{g}}}{m_c} \right\}, \tag{107}$$

and

$$C_9^{\tilde{g}} = -\frac{8}{27} \frac{\sqrt{2}}{G_F M_{\tilde{q}}^2} \pi\alpha_s (\delta_{12}^u)_{LL} P_{042}(u), \tag{108}$$

with the contribution to C_{10} vanishing at this order because of the helicity structure.

If we allow for two mass insertions, there is a contribution to $C_{9,10}$ given by

$$C_{10}^{\tilde{g}} = -\frac{1}{9} \frac{\alpha_s}{\alpha} (\delta_{22}^u)_{LR}(\delta_{12}^u)_{LR} P_{032}(u) = -\frac{C_9}{1 - 4\sin^2\theta_W}. \tag{109}$$

Here, $u = M_{\tilde{g}}^2/M_{\tilde{q}}^2$ and the functions $P_{ijk}(u)$ are defined as

$$P_{ijk}(u) \equiv \int_0^1 dx \, \frac{x^i(1-x)^j}{(1-x+ux)^k}. \tag{110}$$

In addition, the operator basis can be extended by the "wrong chirality" operators $\hat{O}_7$, $\hat{O}_9$, and $\hat{O}_{10}$, obtained by switching the quark chiralities in Equations 90 and 91. The gluino-squark contributions to the corresponding Wilson coefficients are

$$\hat{C}_7^{\tilde{g}} = -\frac{8}{9} \frac{\sqrt{2}}{G_F M_{\tilde{q}}^2} \pi\alpha_s \left\{ (\delta_{12}^u)_{RR} \frac{P_{132}(u)}{4} + (\delta_{12}^u)_{LR} P_{122}(u) \frac{M_{\tilde{g}}}{m_c} \right\}, \tag{111}$$

$$\hat{C}_9^{\tilde{g}} = -\frac{8}{27} \frac{\sqrt{2}}{G_F M_{\tilde{q}}^2} \pi\alpha_s (\delta_{12}^u)_{RR} P_{042}(u) - (1 - 4\sin^2\theta_W)\hat{C}_{10}^{\tilde{g}},$$

$$\hat{C}_{10}^{\tilde{g}} = -\frac{1}{9} \frac{\alpha_s}{\alpha} (\delta_{22}^u)_{LR}(\delta_{12}^u)_{LR} P_{032}(u),$$

where the expression for $\hat{C}_{10}^{\tilde{g}}$ is again obtained with a double insertion.

As noted in References (121) and (17), in both $C_7^{\tilde{g}}$ and $\hat{C}_7^{\tilde{g}}$ the term in which the squark chirality labels are mixed introduces the enhancement factor $M_{\tilde{g}}/m_c$. In the standard model,

the chirality flip that appears in O_7 occurs by a flip of one external quark line, resulting in a factor of m_c included in the operator's definition.[6] However, in the gluino-squark diagram, the insertion of $(\delta^u_{12})_{RL}$ forces the chirality flip to take place in the gluino line, thus introducing a $M_{\tilde{g}}$ factor instead of m_c. This yields a significant enhancement in the short-distance contributions to the process $D \to X_u \gamma$ (17), which is unfortunately obscured by the large long-range effects. This is not the case in $c \to u\ell^+\ell^-$ processes.

In order to estimate the effects in $c \to u\ell^+\ell^-$ transitions from the gluino contributions, we make use of the bounds of Table 1. Figures 10 and 11 show the dilepton mass distribution as a function of the dilepton mass for $D^+ \to \pi^+ e^+ e^-$ and $D^0 \to \rho^0 e^+ e^-$, respectively (from Reference (99)). Four sample cases are considered there (99): (I) $M_{\tilde{g}} = M_{\tilde{q}} = 250$ GeV, (II) $M_{\tilde{g}} = 2\,M_{\tilde{q}} = 500$ GeV, (III) $M_{\tilde{g}} = M_{\tilde{q}} = 1000$ GeV, and (IV) $M_{\tilde{g}} = (1/2)\,M_{\tilde{q}} = 250$ GeV.

We first examine the $D^+ \to \pi^+ e^+ e^-$ case. Although the net effect is relatively small in the integrated rate (an increase $\simeq 20\%$ or smaller), the enhancement due to the SUSY contributions is most conspicuous away from the vector resonances, particularly for low dilepton masses. Experiments sensitive to the dilepton mass distribution at the branching fraction of $10^{-7} - 10^{-8}$ can detect these SUSY contributions. However, the decays to a vector meson, such as $D \to \rho e^+ e^-$, are more sensitive to the gluino exchange, as Figure 11 shows.

The effect is quite pronounced and lies almost entirely in the low m_{ee} region. This is mostly due to the contributions of $(\delta^u_{12})_{RL}$ to C_7 and C_7', which contain the $M_{\tilde{g}}/m_c$ enhancement as advertised above. This effect is intensified at low $q^2 = m^2_{ee}$ owing to the photon propagator (see, e.g., Equation 96 for the inclusive decays). This low-q^2 enhancement of the O_7 contribution is present in exclusive modes with vector mesons, such as $D \to \rho\ell^+\ell^-$, but not in modes with pseudoscalars, such as $D \to \pi\ell^+\ell^-$, since gauge invariance forces a cancellation of the $1/q^2$ factor in the latter case (see, e.g., Equation 100). This is apparent from a comparison of the low dilepton mass regions in Figures 10 and 11. Thus we see that rare charm decays are indeed sensitive to a generic extension of the standard model such as the MSSM. This is particularly true of the $D \to \rho\ell^+\ell^-$ modes.

3.2.2 SUPERSYMMETRY WITH R-PARITY VIOLATION

Imposing R-parity conservation in the MSSM prohibits baryon- and lepton-number–violating terms in the superpotential. However, other symmetries can be invoked to prohibit rapid proton decay, such as baryon parity or lepton parity (see, e.g., (122)), and hence allow for R-parity violation. The R-parity–violating superpotential can be written as[7]

$$\mathcal{W}_{R_p} = \epsilon_{ab} \left\{ \tfrac{1}{2}\lambda_{ijk} L_i^a L_j^b \bar{E}_k + \lambda'_{ijk} L_i^a Q_j^b \bar{D}_k + \tfrac{1}{2}\epsilon_{\alpha\beta\gamma}\lambda''_{ijk} \bar{U}_i^\alpha \bar{D}_j^\beta \bar{D}_k^\gamma \right\}, \qquad (112)$$

where L, Q, $\bar{E}$, $\bar{U}$, and $\bar{D}$ are the chiral superfields in the MSSM. The SU(3) color indices are denoted by $\alpha, \beta, \gamma = 1, 2, 3$, the SU(2)$_L$ indices by $a, b = 1, 2$, and the generation indices by $i, j, k = 1, 2, 3$. The fields in Equation 112 are in the weak basis.

The λ'_{ijk} term is the relevant one for the rare charm decays we consider here because it can give rise to tree-level squark-exchange contributions to decay channels such as $D \to X\ell^+\ell^-$, $D \to \ell^+\ell^-$, as well as the lepton-flavor–violating $D \to X\mu^+ e^-$ and $D \to \mu^+ e^-$ modes. Before considering the FCNC effects in D decays, we need to rotate the fields to the mass basis. This leads to

$$\mathcal{W}_{R_p} = \tilde{\lambda}'_{ijk} \left[N_i V_{jl} D_l - E_i U_j \right] \bar{D}_k + \cdots, \qquad (113)$$

where V is the CKM matrix and we define

$$\tilde{\lambda}'_{ijk} \equiv \lambda'_{irs} \mathcal{U}^L_{rj} \mathcal{D}^{*R}_{sk}. \qquad (114)$$

---

[6]The m_u term, proportional to the $(1 - \gamma_5)$ in the operator, is neglected.

[7]We ignore bilinear terms that are not relevant to our discussion of FCNC effects.

Here, $\mathcal{U}^L$ and $\mathcal{D}^R$ are the matrices used to rotate the left-handed up- and right-handed down-quark fields to the mass basis. Written in terms of component fields, this interaction now reads

$$\mathcal{W}_{\lambda'} = \tilde{\lambda}'_{ijk} \left\{ V_{jl}[\tilde{\nu}^i_L \bar{d}^k_R d^l_L + \tilde{d}^l_L \bar{d}^k_R \nu^i_L + (\tilde{d}^k_R)^* (\nu^i_L)^c d^l_L] \right.$$
$$\left. - \tilde{e}^i_L \bar{d}^k_R u^j_L - \tilde{u}^j_L \bar{d}^k_R e^i_L - (\tilde{d}^k_R)^* (e^i_L)^c u^j_L \right\}. \tag{115}$$

The last term in Equation 115 can give rise to the processes $c \to u\ell\ell^{(')}$ at tree level via the exchange of a down squark. This leads to effects that are proportional to $\tilde{\lambda}'_{i2k}\tilde{\lambda}'_{i1k}$ with $i = 1, 2$ (owing to kinematical restrictions).

Constraints on these coefficients have been derived (for a recent review, see (123)). For instance, Agashe & Graesser (124) obtain tight bounds from $K^+ \to \pi^+ \nu\bar{\nu}$ by assuming that only one R-parity–violating coupling satisfies $\tilde{\lambda}'_{ijk} \neq 0$. We update this bound by using the latest experimental result (125) $B(K^+ \to \pi^+ \nu\bar{\nu}) = (1.57^{+1.75}_{-0.82}) \times 10^{-10}$, which yields $\tilde{\lambda}'_{ijk} < 0.005$. However, this bound can be avoided in the single-coupling scheme (124), where only one R-parity–violating coupling is taken to be nonzero in the weak basis. In this case, it is possible that flavor rotations may restrict the R-parity-breaking–induced flavor violation to be present in either the charge $-\frac{1}{3}$ or $+\frac{2}{3}$ quark sectors, but not both. Then large effects are possible in the up sector for observables such as D^0–$\bar{D}^0$ mixing and rare decays without affecting the down-quark sector.

Agashe & Graesser (124) obtain a rather loose constraint on the R-parity–breaking couplings from D^0 mixing, which could result in large effects in $c \to u\ell\ell^{(')}$ decays. Here, we take a conservative approach and use more model-independent bounds. The constraints on the R-parity–breaking couplings for the processes of interest here are collected in Table 13 from Reference (123). The charged-current universality bounds assume three generations. The π-decay constraint is given by the quantity $R_\pi = \Gamma(\pi \to e\nu)/\Gamma(\pi \to \mu\nu)$. The limits obtained from $D \to K\ell\nu$ were first obtained in Reference (126).

We first consider the contributions to $c \to u\ell^+\ell^-$. The tree-level exchange of down squarks results in the effective interaction (99)

$$\delta\mathcal{H}_{\text{eff}} = -\frac{\tilde{\lambda}'_{i2k}\tilde{\lambda}'_{i1k}}{m^2_{\tilde{d}^k_R}} (\bar{\ell}_L)^c c_L \ \bar{u}_L(\ell_L)^c, \tag{116}$$

which, after Fierz rearrangement, gives

$$\delta\mathcal{H}_{\text{eff}} = -\frac{\tilde{\lambda}'_{i2k}\tilde{\lambda}'_{i1k}}{2m^2_{\tilde{d}^k_R}} (\bar{u}_L\gamma_\mu c_L)(\bar{\ell}_L\gamma^\mu \ell_L). \tag{117}$$

This corresponds to contributions at the high-energy scale to the Wilson coefficients C_9 and C_{10} given by

$$\delta C_9 = -\delta C_{10} = \frac{\sin^2\theta_W}{2\alpha^2} \left(\frac{M_W}{m_{\tilde{d}^k_R}}\right)^2 \tilde{\lambda}'_{i2k}\tilde{\lambda}'_{i1k}. \tag{118}$$

If we now specify $\ell = e$ and use the bounds from Table 13, we arrive at the constraint

$$\delta C_9^e = -\delta C_{10}^e \leq 1.10 \left(\frac{\tilde{\lambda}'_{12k}}{0.04}\right) \left(\frac{\tilde{\lambda}'_{11k}}{0.02}\right). \tag{119}$$

Notice that these are independent of the squark mass, which cancels. Taking this upper limit on the Wilson coefficients results in the dotted-dashed lines of Figures 7 and 8 corresponding

to $D^+ \to \pi^+ e^+ e^-$ and $D^0 \to \rho^0 e^+ e^-$, respectively. The effect in these rates is small, of order 10% at most, whereas the experimental bounds are a factor of 20 above this level in the most restrictive case (given by the pion mode). On the other hand, for $\ell = \mu$, we obtain

$$\delta C_9^\mu = -\delta C_{10}^\mu \leq 17.4 \left(\frac{\tilde{\lambda}'_{22k}}{0.21} \right) \left(\frac{\tilde{\lambda}'_{21k}}{0.06} \right). \tag{120}$$

When the existing constraints on $\tilde{\lambda}'_{1jk}$ are taken into account, R-parity violation results in small deviations in $D \to (\pi, \rho)e^+ e^-$. However, the bounds on $\tilde{\lambda}'_{2jk}$ are loose and lead to very large effects in the $\ell = \mu$ modes. In fact, the allowed values from other observables saturate the current experimental limits for $D \to \pi \mu^+ \mu^-$ and $D \to \rho \mu^+ \mu^-$, resulting in the bound (99)

$$\tilde{\lambda}'_{22k} \tilde{\lambda}'_{21k} < 0.004. \tag{121}$$

These large effects would be clearly observable away from the resonances.

In addition, the angular information in $D \to \rho \mu^+ \mu^-$ can be used to confirm the new-physics origin of the large deviations. If we define the forward-backward asymmetry for leptons as

$$A_{FB}(q^2) = \frac{\int_0^1 \frac{d^2\Gamma}{dx dq^2} dx - \int_{-1}^0 \frac{d^2\Gamma}{dx dq^2} dx}{\frac{d\Gamma}{dq^2}} \quad , \tag{122}$$

where $x \equiv \cos\theta$, with θ being the angle between the ℓ^+ and the decaying D meson in the $\ell^+ \ell^-$ rest frame (as mentioned in Section 3.1.3), the standard-model prediction for this quantity is nearly zero. This is because the rate comes almost entirely from the long-distance contributions to the lepton vector coupling (e.g., O_9), making the interference with the axial-vector couplings negligible. This can be seen by inspecting the numerator of the asymmetry (113, 127)

$$A_{FB}(q^2) \sim 4 \, m_D \, k \, C_{10} \left\{ C_9^{\text{eff}} \, g \, f + \frac{m_c}{q^2} C_7^{\text{eff}} \, (f \, G - g \, F) \right\}, \tag{123}$$

where k is the vector meson three-momentum in the D rest frame, and f, g, F, and G are form factors. Because the standard-model amplitude is dominated by the long-distance vector intermediate states, we have $C_9^{\text{eff}} \gg C_{10}$. New-physics contributions that make $C_{10} \simeq C_9^{\text{eff}}$ will hence generate a sizeable asymmetry. This is actually the case in R-parity-violating SUSY. Burdman et al. (99) show that the asymmetry in $D \to \rho \mu^+ \mu^-$ is predicted to be quite large for the allowed values of the R-parity–violating parameters.

The effective Wilson coefficients of Equation 118 also lead to a contribution to the two-body decay $D^0 \to \mu^+ \mu^-$. The R-parity–violating contribution to the branching ratio then reads

$$B^{\mathcal{R}_p}(D^0 \to \mu^+ \mu^-) = \tau_{D^0} \, f_D^2 \, m_\mu^2 \, m_D \sqrt{1 - \frac{4m_\mu^2}{m_D^2}} \, \frac{\left(\tilde{\lambda}'_{22k} \tilde{\lambda}'_{21k} \right)^2}{64\pi \, m_{\tilde{d}_k}^4}. \tag{124}$$

Applying the bound in Equation 121 gives the constraint[8]

$$B^{\mathcal{R}_p}(D^0 \to \mu^+ \mu^-) < 3.5 \times 10^{-7} \left(\frac{\tilde{\lambda}'_{22k} \tilde{\lambda}'_2 1k}{0.004} \right)^2. \tag{125}$$

Thus, R-parity violation could give an effect that could soon be probed in these modes.

[8]In Reference (99), this expression (Equation 86) was incorrectly given. Also, the branching ratio stated there did not reflect the bound from Equation 122, but the less restrictive bounds to the individual couplings.

Next, we consider the products of R-parity–violating couplings that lead to lepton flavor violation. For instance, the products $\tilde{\lambda}'_{11k}\tilde{\lambda}'_{22k}$ and $\tilde{\lambda}'_{21k}\tilde{\lambda}'_{12k}$ will give rise to $D^+ \to \pi^+\mu^+e^-$. This leads to

$$\delta C_9^{\mu e} = -\delta C_{10}^{\mu e} = 4.6 \times \left\{ \left(\frac{\tilde{\lambda}'_{11k}}{0.02}\right)\left(\frac{\tilde{\lambda}'_{22k}}{0.21}\right) + \left(\frac{\tilde{\lambda}'_{21k}}{0.06}\right)\left(\frac{\tilde{\lambda}'_{12k}}{0.04}\right) \right\}, \tag{126}$$

which results in $B^{R_p}(D^+ \to \pi^+\mu^+e^-) < 3 \times 10^{-5}$. Here again, experiment is on the verge of being sensitive to R-parity–violating effects. Similarly, for the corresponding two-body decay we have

$$B^{R_p}(D^0 \to \mu^+e^-) < 0.5 \times 10^{-6} \times \left\{ \left(\frac{\tilde{\lambda}'_{11k}}{0.02}\right)\left(\frac{\tilde{\lambda}'_{22k}}{0.21}\right) + \left(\frac{\tilde{\lambda}'_{21k}}{0.06}\right)\left(\frac{\tilde{\lambda}'_{12k}}{0.04}\right) \right\}. \tag{127}$$

Last, we consider the R-parity–violation contributions to $D^\pm \to e^\pm\nu$ and $D_s^\pm \to e^\pm\nu$. These decay modes receive large enhancements mostly from the s-channel exchange of sleptons (128). Unlike the t-channel squark exchange discussed above, this results in amplitudes that are unsuppressed by helicity. The largest lepton-number violation occurs in $D^\pm \to e^\pm\nu_\tau$ through the product $|\lambda^*_{231}\tilde{\lambda}'_{221}|$, and in $D_s^\pm \to e^\pm\nu_\tau$ through $|\lambda^*_{231}\tilde{\lambda}'_{222}|$. Here λ_{ijk} is the strength of the cubic lepton superfield interactions in the R-parity–violating superpotential term $\epsilon_{ab}L_i^a L_j^b \bar{E}_k$. When current bounds are taken into account, it is found that R-parity violation could result in (128) $B^{R_p}(D^\pm \to e^\pm\nu) \simeq 10^{-4}$, several orders of magnitude above the standard-model prediction. Even more dramatically, we could have $B^{R_p}(D_s^\pm \to e^\pm\nu) \simeq 5 \times 10^{-3}$. Table 14 summarizes the predictions from Reference (99) in both the standard model and R-parity–violating SUSY.

3.2.3   STRONG DYNAMICS

Technicolor Models: In standard technicolor theories, both fermions and technifermions transform under the new gauge interaction of extended technicolor (ETC). As we saw in Section 2.3.2, this leads to the presence of four-quark operators coming from the diagonal ETC generators and characterized by a mass-scale M bounded by $D^0 - \bar{D}^0$ mixing to be greater than 100 TeV or so. However, additional operators are generated at low energies that are not suppressed by M. The condensation of technifermions leading to electroweak symmetry breaking leads to fermion mass terms of the form

$$m_q \simeq \frac{g_{\text{ETC}}^2}{M_{\text{ETC}}^2}\langle \bar{T}T\rangle_{\text{TC}}. \tag{128}$$

Operators arising from the technifermion interactions have been shown (129) to give rise to FCNC involving the Z boson,

$$\xi^2 \frac{m_c}{8\pi v}\frac{e}{\sin 2\theta_W}\mathcal{U}_L^{cu}Z^\mu\,(\bar{u}_L\gamma_\mu c_L) \quad \text{and} \quad \xi^2 \frac{m_t}{8\pi v}\frac{e}{\sin 2\theta_W}\mathcal{U}_L^{tu}\mathcal{U}_L^{tc*}Z^\mu\,(\bar{u}_L\gamma_\mu c_L), \tag{129}$$

where $\mathcal{U}_L$ is the unitary matrix rotating left-handed up-type quark fields into their mass basis and ξ is a model-dependent quantity of $\mathcal{O}(1)$. The induced flavor-conserving Z coupling was first studied in Reference (129), and flavor-changing effects in B decays have been examined in References (130) and (131).

The flavor-changing vertices in Equation 129 induce contributions to $c \to u\ell^+\ell^-$. These appear mostly as a shift in the Wilson coefficient $C_{10}(M_W)$,

$$\delta C_{10} \simeq \mathcal{U}_{cu}^L\frac{m_c}{2v}\frac{\sin^2\theta_W}{\alpha} \simeq 0.02, \tag{130}$$

where we assume $\mathcal{U}_L^{cu} \simeq \lambda \simeq 0.22$ (i.e., one power of the Cabibbo angle) and we take $m_c = 1.4$ GeV. Although this represents a very large enhancement with respect to the standard-model value of $C_{10}(M_W)$, it does not translate into a large deviation in the branching ratio. As we have seen, these are dominated by the mixing of the operator O_2 with O_9, leading to a very large value of C_9^{eff}. The contribution in Equation 130 represents only a few-percent effect in the branching ratio with respect to the standard model. However, the effect is quite large in the region of low dilepton mass.

Furthermore, the interaction in Equation 129 can also mediate $D^0 \to \mu^+ \mu^-$. The corresponding amplitude is

$$\mathcal{A}_{D^0 \mu^+ \mu^-} \simeq \mathcal{U}_{cu}^L \, \frac{m_c}{2\pi v} \, \frac{G_F}{\sqrt{2}} \, \sin^2 \theta_W f_D \, m_\mu \, . \tag{131}$$

This results in the branching ratio $B^{\text{ETC}}(D^0 \to \mu^+ \mu^-) \simeq 0.6 \times 10^{-10}$, which, although still small, is not only several orders of magnitude larger than the standard-model short-distance contribution but also more than two orders of magnitude larger than the long-distance estimates.

Finally, the FCNC vertices of the Z boson in Equation 129 also give large contributions to $c \to u \nu \bar{\nu}$. The enhancement is considerable and results in the branching ratio

$$B^{\text{ETC}}_{D^+ \to X_u \nu \bar{\nu}} \simeq \xi^4 \left(\frac{\mathcal{U}_L^{cu}}{0.2} \right)^2 2 \times 10^{-9}. \tag{132}$$

Topcolor: As discussed in Section 2.3.2, the topcolor interactions must be nonuniversal, and so they mediate FCNCs at tree level. After the rotations of quark fields defined in Equation 40, the exchange of top-gluons generates four-fermion couplings of the form

$$\frac{4\pi \alpha_s \cot \theta^2}{M_G^2} \mathcal{U}^{tc*} \mathcal{U}^{tu} \left(\bar{u} \gamma_\mu T^a t \right) \left(\bar{t} \gamma^\mu T^a c \right) \tag{133}$$

where $\mathcal{U}^{ij} = \mathcal{U}_L^{ij} + \mathcal{U}_R^{ij}$ and M is the mass of the exchanged color-octet gauge boson. The one-loop insertion of this operator results in contributions to the operators $\mathcal{O}_9$ and $\mathcal{O}_{10}$ in $c \to u \ell^+ \ell^-$ as well as in the purely leptonic decays. These could lead to large effects when compared to the standard model

$$\delta C_{10} \simeq 2 \, \delta C_9 \simeq 0.01 \times \left(\frac{\mathcal{U}^{tc*} \mathcal{U}^{tu}}{\sin^5 \theta_c} \right) \left(\frac{1 \text{ TeV}}{M_G} \right)^2 , \tag{134}$$

where the effects are rather modest unless the quark rotation matrices are larger than expected. This would not be unnatural, for instance, for $\mathcal{U}_R$, since the rotations of right-handed quarks are not related to any known observable in the standard model.

3.2.4 OTHER NEW-PHYSICS SCENARIOS

Extensions of the standard model leading to effects in rare charm decays also tend to result in large contributions to $D^0 - \bar{D}^0$ mixing. Burdman et al. have evaluated a long list of these scenarios in detail (99). Generically, the effects are either negligible or amount to $O(1)$ enhancement over the standard-model short-distance contributions.

As mentioned in Section 2.3.3, compact extra dimensions may lead not only to massive scalar and fermionic states but also to nonuniversal couplings of the standard-model fermions to Kaluza-Klein excitations of gauge bosons that may induce flavor-violating loop effects. In general, the largest effects in rare charm decays are associated with massive neutral gauge

bosons (e.g., KK excitation of a Z'), which generate a FCNC current in the up-quark sector and then decay into either charged leptons or neutrinos. With masses starting around the TeV scale, these states could lead to $O(1)$ enhancements in $c \to u\ell^+\ell^-$ modes, when compared to the standard-model short-distance predictions. Thus, in the charged-lepton modes this can translate into observable effects in the low $m_{\ell\ell}$ window. The enhancement in the $c \to u\nu\bar{\nu}$ modes could be several orders of magnitude above the standard-model predictions, although they may be very difficult to observe.

Many other new-physics scenarios involving additional matter and/or gauge fields would lead to contributions to flavor physics and in particular to rare charm decays. Most contributions that are potentially large tend to be constrained by $D^0 - \bar{D}^0$ mixing. Such is the case, for instance, with extra down-type quarks and extra gauge bosons.

3.3   Experimental Bounds and Prospects

Experiments that can measure rare D decay branching ratios at the level of a part per million will start to confront models of new physics in an interesting way. Although current experimental limits are, in most cases, well above this level of sensitivity, the arsenal of experiments opening up from CDF to the B factories and charm factory may allow observation of rare decays within the decade.

We first review the present experimental status of charm rare decays. We then provide estimates of the reach of the currently running experiments CLEO-c and BaBar/Belle made by the CLEO-c collaboration, estimate the rare-decay reach of future facilities, and finally briefly consider the experimental dilepton mass resolution in decays of the type $D \to \pi e^+ e^-$.

Fixed-target experiments have traditionally had the best rare-decay limits for low-multiplicity final states involving charged particles. In fixed-target experiments, rare decays are isolated using the same procedure used to isolate nonrare charm decays. The procedure is described in Section 2.4.6 of this review.

Table 15 and Figure 12 show some of the best recent results and compare them to theory. At CDF, the search strategy for rare charm decays is still being refined but it will be similar to that developed for rare B decays such as $B^+ \to K^+\mu^+\mu^-$ (87). Recently CDF has produced the best upper limit for $D^0 \to \mu^+\mu^-$ (88).

At e^+e^- B factories operating at the $\Upsilon(4S)$, the background to rare charm decays is very large, and so far searches have been performed only for D^0 modes where the D^* tag can be used to remove the significant combinatoric background. Using this technique, the first observation of a FCNC mode in the charm system has recently been made by BELLE (138), as shown in Figure 13. The measured branching ratio is $B(D^0 \to \phi\gamma) = (2.60^{+0.70+0.15}_{-0.61-0.17}) \times 10^{-5}$.

Tables 16 and 17 list a collection of rare D^0 nodes. The second column is the best limit currently available from an e^+e^- experiment running at or near the $\Upsilon(4S)$ resonance. The third column shows cases where the best limit was not obtained on the $\Upsilon(4S)$. The next-to-last column estimates the sensitivity of an e^+e^- experiment with 400 fb^{-1} of integrated luminosity at or near the $\Upsilon(4S)$, based on the efficiencies and background levels found by CLEO, and the final column shows the projected CLEO-c limits based on Monte Carlo estimates of efficiency and tagging rates, and assuming an integrated luminosity of 3 fb^{-1} on the $\psi(3770)$ with a 10% tagging probability. This amount of data could be accumulated in one year. At the $\psi(3770)$ the assumption is made for all modes that the signal is background-free.

Tables 18 and 19 show the current experimental status as well as projected sensitivities for a collection of rare D^+ decays. In these cases, there are no recent limits available from e^+e^- experiments, so only the current world best measurement and the projected CLEO-c sensitivity [again based on 3 fb^{-1} of integrated luminosity on the $\psi(3770)$] are shown.

If tagging is not needed, the limits at CLEO-c will improve by a factor of ten. Although

these estimated limits are quite rough, we can draw some general conclusions from them. In general, CLEO-c and the B-factory experiments have complementary strengths. For some final states, CDF will have the greatest sensitivity.[9]

The most reliable way to compare the reach of future experiments for rare decays would be to compile a list of sensitivities estimated by each experiment based on detailed simulations. However, as with δA_{CP}, in almost all cases the simulations or other detailed estimates are nonexistent. Instead, to compare the reach of future experiments for rare decays we again use the number of $D^0 \to K^-\pi^+$ reconstructed by each experiment. The mode we choose for the extrapolation for hadron experiments is $D^+ \to \pi^+\mu^+\mu^-$. The normalization is provided by the E791 search for that mode, which found $B(D^+ \to \pi^+\mu^+\mu^-) < 5.2 \times 10^{-5}$ at 90% CL. Because background is present, we scale this result by $1/\sqrt{N(D^0 \to K^-\pi^+)}$. For the e^+e^- experiments, the mode we choose for the extrapolation is $D^0 \to \pi^0 e^+e^-$. The normalization for machines operating in the B-meson threshold region is the result of the CLEO II search, which found $B(D^0 \to \pi^0 e^+e^-) < 4.5 \times 10^{-5}$ at 90% CL. We scale this by $1/\sqrt{N(D^0 \to K^-\pi^+)}$ in order to obtain upper limits for the B-factory and super-B-factory experiments. For the charm factories, reconstructing the second charm meson in the event ensures a background-free situation and the scaling is $1/L$ using the CLEO-c estimated sensitivity as the normalization. The results of this exercise are in Table 11.

To estimate the number of events each experiment will observe, we use $B(D^+ \to \pi^+\mu^+\mu^-) \sim 6.2 \times 10^{-6}$ and $B(D^0 \to \pi^0 e^+e^-) \sim 8 \times 10^{-7}$. As can be seen from the results in Table 11, sensitivity to interesting physics in these modes can be achieved by BES III, BTeV, or the "super" machines.

For the case of the dilepton modes $D \to \pi\ell^+\ell^-$ and $D \to \rho\ell^+\ell^-$, as emphasized in Section 3.1.3, the sensitivity to short-distance physics, whether it is that of the standard model or one of its extensions, is in the region of low dilepton mass away from the resonances. Figure 14 shows our Monte Carlo simulation of the experimental dilepton mass resolution in the decay $D^+ \to \pi^+ e^+e^-$ for D mesons produced at the $\Upsilon(4S)$ and for D mesons produced at threshold. The dilepton mass resolution is excellent in both cases. The dilepton mass resolution will also be very good at hadron facilities. In all cases, the dilepton resolution is expected to be adequate to sort between the standard-model and new-physics predictions for this class of decays.

4   SUMMARY

D^0–$\bar{D}^0$ mixing and rare charm decays will be further probed by experiment in the coming years. We have examined the potential of these measurements to test the standard model and its extensions. In the case of D^0–$\bar{D}^0$ mixing, the irreducible background from long-distance physics makes it difficult for a future positive observation to be attributed to short-distance physics. However, tight limits on Δm_D result in very important complementary constraints on physics beyond the standard model. On the other hand, although they are also generally affected by large theoretical uncertainties, we have seen that some rare charm decay modes can be used to probe short-distance physics. Such is the case with $c \to u\ell^+\ell^-$ decay modes. Sensitivity to the nonresonant regions in these modes could be achieved by experiments in the near future. In sum, these charm physics observables, when considered together with the results from the various B and kaon physics experiments, constitute a necessary low-energy

---

[9]We note that there is no commonly agreed prescription for calculating expected experimental upper limits. For an alternative, and more optimistic, estimate of the sensitivity to rare charm decays at a B factory, see Reference (57).

complement to direct searches for new physics at high energies.

References

1. Alcaraz J, et al. (combined LEP and SLD Electroweak Working Groups). LEPEWWG/96-02, SLD Physics Note 52

2. Datta A, Kumbhakar D. *Z. Phys. C* 27:515 (1985)

3. Wolfenstein L. *Phys. Lett.* B164:170 (1985)

4. Georgi H. *Phys. Lett.* B297:353 (1992)

5. Ohl T, Ricciardi G, Simmons EH. *Nucl. Phys. B* 403:605 (1993)

6. Bigi II, Uraltsev NG. *Nucl. Phys. B* 592:92 (2001)

7. Donoghue JF, Golowich E, Holstein BR, Trampetic J. *Phys. Rev. D* 33:179 (1986)

8. Burdman G. *Potential for discoveries in charm meson physics.* Presented at Workshop on Tau Charm Factory, Argonne, IL, Jun. 21–23 (1995), hep-ph/9508349

9. Hagiwara K, et al. (Particle Data Group Collab.) *Phys. Rev. D* 66:010001 (2002)

10. Petrov AA. *Phys. Rev. D* 56:1685 (1997); Golowich E, Petrov AA. *Phys. Lett.* B427:172 (1998)

11. Falk AF, Grossman Y, Ligeti Z, Petrov AA. *Phys. Rev. D* 65:054034 (2002)

12. Bucella F, et al. *Phys. Lett.* B302:319 (1993)

13. Nelson HN. In *Proc. 19th Int. Symp. Photon and Lepton Interactions at High Energy LP99,* ed. JA Jaros, ME Peskin, hep-ex/9908021

14. Misiak M, Pokorski S, Rosiek J. In *Heavy Flavors II,* ed. AJ Buras, M Lindner, *Adv. Ser. Direct. High Energy Phys.* 15:795 (1998)

15. Ellis J, Nanopoulos DV. *Phys. Lett.* 110B:44 (1982)

16. Brandenburg G, et al. (CLEO Collab.) *Phys. Rev. Lett.* 87:071802 (2001)

17. Prelovsek S, Wyler D. *Phys. Lett.* B500:304 (2001)

18. Casas JA, Dimopoulos S. *Phys. Lett.* B387:107 (1996)

19. Nir Y, Seiberg N. *Phys. Lett.* B309:337 (1993)

20. Leurer M, Nir Y, Seiberg N. *Nucl. Phys. B* 398:319 (1993); *Nucl. Phys. B* 420:468 (1994)

21. Hill CT, Simmons EH. *Phys. Rep.* 381:235 (2003)

22. Weinberg S. *Phys. Rev. D* 19:1277 (1979); Susskind L. *Phys. Rev. D* 20:2619 (1979)

23. Eichten E, Lane K. *Phys. Lett.* B90:125 (1980); Dimopoulos S, Susskind L. *Nucl. Phys. B* 155:237 (1979)

24. Hill CT. *Phys. Lett.* B266:419 (1991); Martin SP. *Phys. Rev. D* 45:4283 (1992); Martin SP. *Phys. Rev. D* 46:2197 (1992); Martin SP. *Nucl. Phys. B* 398:359 (1993); Lindner M, Ross D. *Nucl. Phys. B* 370:30 (1992); Bönisch R. *Phys. Lett.* B268:394 (1991); Hill CT, Kennedy D, Onogi T, Yu HL. *Phys. Rev. D* 47:2940 (1993)

25. Hill CT. *Phys. Lett.* B345:483 (1995); Lane K, Eichten E. *Phys. Lett.* B352:382 (1995); Lane K. *Phys. Rev. D* 54:2204 (1996); Lane K. In *Proc. 1996 Workshop on Strongly Coupled Gauge Theories, Nagoya, Jpn., Nov. 1996,* p. 72, ed. J Nishimura, K Yamawaki. Singapore: World Sci (1997); Lane K. *Phys. Lett.* B433:96 (1998)

26. Kaplan DB, Georgi H, Dimopoulos S. *Phys. Lett.* B136:187 (1984); Georgi H, Kaplan DB. *Phys. Lett.* B145:216 (1984); Dugan MJ, Georgi H, Kaplan DB. *Nucl. Phys. B* 254:299 (1985)

27. Chivukula RS, Dobrescu BA, Simmons EH. *Phys. Lett.* B401:74 (1997)

28. Georgi H. *Phys. Lett.* B298:187 (1993)

29. Manohar A, Georgi H. *Nucl. Phys. B* 234:189 (1984)

30. Randall L. *Nucl. Phys. B* 403:122 (1993); Burdman G, Evans N. *Phys. Rev. D* 59:115005 (1999)

31. Buchalla G, Burdman G, Hill CT, Kominis D. *Phys. Rev. D* 53:5185 (1996)

32. Burdman G, Lane KD, Rador T. *Phys. Lett.* B514:41 (2001)

33. Chang S, et al. *Phys. Rev. D* 62:084025 (2000); Hewett JL, Petriello FJ, Rizzo TG. *JHEP* 0209:030 (2002); Burdman G. *Phys. Rev. D* 66:076003 (2002); Huber SJ. hep-ph/0303183

34. Aubert JJ, et al. *Phys. Lett.* 33:1404 (1974); Augustin JE, et al. *Phys. Rev. Lett.* 33:1406 (1974)

35. Barate M, et al. (ALEPH Collab.) *Eur. Phys. J. C* 16:597 (2000)

36. Donati S. *First Run II results from CDF.* Presented at XXXVIth Rencontres de Moriond, Les Arcs, France, March 2002

37. Appel JA. *Annu./ Rev./ Nucl./ Part./ Sci.* 42:367 (1992); Summers DJ, et al. hep-ex/0009015; Amato S, et al. *Nucl. Instrum. Methods A* 324:535 (1993); Bracker S, et al. *IEEE Trans. Nucl. Sci.* 43:2457 (1996); Aitala EM, et al. *Eur. Phys. J. C* 4:1 (1999)

38. Fabretti PL, et al. *Nucl. Instrum. Methods A* 329:62 (1993); Fabretti PL, et al. *Nucl. Instrum. Methods A* 320:519 (1992); Link JM, et al. *Nucl. Instrum. Methods A* 484:270 (2002)

39. Kubota Y, et al. (CLEO Collab.) *Nucl. Instrum. Methods A* 320:66 (1992); Hill TS. *Nucl. Instrum Methods A* 428:32 (1998)

40. Aubert, et al. (BaBar Collab.) *Nucl. Instrum. Methods A* 479:1 (2002)

41. Abashian A, et al. (Belle Collab.) *Nucl. Instrum. Methods A* 479:117 (2002)

42. Hagiwara K (Particle Data Group). *Phys. Rev. D* 66:010001 (2002)

43. Bellini G, Bigi II, Dornan PJ. *Phys. Rep.* 289:1 (1997); Cheung H. In *Proc. 9th Int. Symp. Heavy Flavor Physics,* ed. A Ryd, F Porter, 618:321–28, AIP Conf. Proc. (2002)

44. Hitlin D. In *Proc. 9th Int. Symp. Heavy Flavor Physics,* ed. A Ryd, F Porter, 618:422–26, AIP Conf. Proc. (2002)

45. Kaplan D. *Hadron collider charm physics reach.* Presented at Meet. Div. Particles and Fields, Williamsburg, VA, May 2002

46. Stone S. In *Proc. 9th Int. Symp. Heavy Flavor Physics,* ed. A Ryd, F Porter, 618:415–21, AIP Conf. Proc. (2002)

47. Straumann UD. In *Proc. 9th Int. Symp. Heavy Flavor Physics,* ed. A Ryd, F Porter, 618:422–26, AIP Conf. Proc. (2002)

48. Hinchliffe I (ATLAS Collab.), and Sphicas P (CMS Collab.), private communications.

49. Zhao Z, et al. *Report of Snowmass 2001 Working Group E2: Electron-positron colliders from the ϕ to the Z,* hep-ex/0201047 (2002)

50. Coffman D, et al. (Mark III Collab.) *Phys. Lett.* B263:135 (1991)

51. J. Z. Bai (for the BESII collaboration), hep-ex/0307028; and L. Weiguo, private communication.

52. Briere RA, et al.

53. Grothe M. *Mod. Phys. Lett.* A18:1 (2003); Petnor A. *CP violation in charmed mesons.* Invited talk at Continuous Advances in QCD, Minneapolis, MN, May 2002, hep-ph/0209049

54. Aitala EM, et al. *Phys. Rev. Lett.* 88:32 (1999)

55. Smith A. *Recent charm results from CLEO.* Presented at XXXVIIth Rencontres de Moriond QCD, Les Arcs, France, March 2002

56. Malvezzi S (FOCUS Collab.) In *Proc. Int. Conf. High Energy Physics (ICHEP02) Amsterdam 2002,* pp. 636–40; Hosack M. *A search for D^0–$\bar{D}^0$ mixing in semileptonic decays from Focus.* PhD thesis. Vanderbilt Univ. 2003 (unpublished)

57. Williams D. *Charm/tau physics.* Presented at Worskhop on the Discovery Potential of an Asymmetric B Factory at 10^{36} Luminosity, SLAC, Stanford, CA, May 8–10, 2002

58. Bergmann S, et al. *Phys. Lett.* B486:418 (2000)

59. Blaylock G, Seiden A, Nir Y. *Phys. Lett.* B355:555 (1995)

60. Browder TE, Pakvasa S. *Phys. Lett.* B:383:475 (1996)

61. Godang R, et al. (CLEO Collab.) *Phys. Rev. Lett.* 84:5038 (2000)

62. Aubert B, et al. (BaBar Collab.) hep-ex/0304007

63. Ban Y (Belle Collab.) *Preliminary D^0 anti-D^0 mixing search at Belle.* Presented at Int. Conf. Flavor Physics (ICFP 2001), Zhang-Jia-Jie City, Hunan, China, May 31–Jun 6, 2001

64. Abe K, et al. (Belle Collab.) BELLE-CONF-0254, hep-ex/0208051

65. Link JM. In *Proc. 36th Rencontres de Moriond, Les Arcs, France, March 2001,* hep-ex/0106093

66. Aitala EM, et al. (E791 Collab.) *Phys. Rev. D* 57:13 (1998)

67. Barate R, et al. (ALEPH Collab.) *Phys. Lett.* B436:211 (1998)

68. Link JM, et al. (FOCUS Collab.) *Phys. Rev. Lett.* 86:2955 (2001)

69. Brandenburg G, et al. *Phys. Rev. Lett.* 87:071802 (2001)

70. Dytman SA, et al. *Phys. Rev. D* 64:111101 (2001)

71. Chiang C, Rosner JL. *Phys. Rev. D* 65:054007 (2002)

72. Muramatsu H, et al. (CLEO Collab.) *Phys. Rev. Lett.* 89:251802 (2002); erratum, *Phys. Rev. Lett.* 90:059901 (2003)

73. Falk AF, Nir Y, Petrov AA. *JHEP* 9912:019 (1999)

74. Gronau M, Grossman Y, Rosner JL. *Phys. Lett.* B508:37 (2001); Silva J, Soffer A. *Phys. Rev. D* 61:112001 (2000)

75. Bigi II, Sanda AI. *Phys. Lett.* B171:320 (1986);

76. Aitala EM, et al. *Phys. Rev. Lett.* 83:32 (1999)

77. Link JM, et al.

78. Csorna SE, et al. (CLEO Collab.) *Phys. Rev. D* 65:092001 (2002)

79. Abe K, et al. (Belle Collab.) *Phys. Rev. Lett.* 88:162001 (2002)

80. Grothe M. hep-ex/0112002

81. Meadows B. *Charm physics in BaBar.* Presented at Moriond QCD Les Arcs, France, March 22–29, 2003

82. Yabsley B. *Experimental limits on new physics from charm decay.* Presented at Lepton Photon 2003, XXI Int. Symp. Lepton Photon Interactions, Aug. 11–16, FNAL, Batavia, IL, and BELLE CONF-0347

83. Golowich E, Pakvasa S. *Phys. Lett.* B505:94 (2001)

84. Abe K, et al. (Belle Collab.) BELLE-CONF-0129, hep-ex/0107078

85. Smith AB (CLEO Collab.) In *Proc. 4th Int. Conf. B Physics & CP Violation,* hep-ex/0104008

86. Link JM, et al. (FOCUS Collab.) *Phys. Lett.* B491:232 (2000); erratum, *Phys. Lett.* B465:232 (2001); Bonvicini G, et al. *Phys. Rev. D* 63:071101 (2001)

87. Abe F et al. (CDF Collab.) , *Phys. Rev. Lett.* 76:4675 (1996).

88. Korn A (DØ Collab.) hep-ex/0305054

89. Aitala EM, et al. *Phys. Lett.* B421:405 (1998)

90. Link JM, et al. *Phys. Lett.* B491:232 (2000)

91. Aitala EM, et al. *Phys. Lett.* B403:377 (1997)

92. Bigi II, Sanda AI. *CP Violation,* p. 180. Cambridge, UK: Cambridge Univ. Press (2000)

93. Gladding G. In *Proc. Tau-Charm Factory Workshop,* Stanford, CA, May 23–27, p. 152. SLAC-Report-343 (1989)

94. Fry JR, Ruf T. CERN-PPE/94-20 (1994)

95. Aitala EM, et al. *Phys. Rev. D* 57:13 (1998)

96. Gilman FJ, Wise MB. *Phys. Rev. D* 20:2392 (1979)

97. Burdman G, Golowich E, Hewett J, Pakvasa S. *Phys. Rev. D* 52:6383 (1995)

98. Greub C, et al. *Phys. Lett.* B382:415 (1996)

99. Burdman G, Golowich E, Hewett J, Pakvasa S., *Phys. Rev. D* 66:014009 (2002)

100. Inami T, Lim CS. *Prog. Theor. Phys.* 65:1772 (1981)

101. Buchalla G, Buras AJ, Lautenbacher ME. *Rev. Mod. Phys.* 68:1125 (1996)

102. Singer P, Zhang DX. *Phys. Rev. D* 55:1127 (1997)

103. Lim CS, Morozumi T, Sanda AI. *Phys. Lett.* B218:343 (1989)

104. Isgur N, Wise MB. *Phys. Rev. D* 42:2388 (1990); Burdman G, Donoghue JF. *Phys. Lett.* B270:55 (1991)

105. Burdman G, Donoghue JF. *Phys. Lett.* B280:287 (1992); Wise MB. *Phys. Rev. D* 45:2188 (1992); Burdman G, Ligeti Z, Neubert M, Nir Y. *Phys. Rev. D* 49:2331 (1994)

106. Anastassov A, et al. (CLEO Collab.) *Phys. Rev. D* 65:032003 (2002)

107. Fajfer S, Prelovsek S, Singer P. *Phys. Rev. D* 64:114009 (2001)

108. Kodama K, et al. (E653 Collab.) *Phys. Lett.* B274:246 (1992); Frabetti PL, et al. (E687 Collab.) *Phys. Lett.* B307:262 (1993)

109. Fajfer S, Prelovsek S, Singer P. *Phys. Rev. D* 58:094038 (1998)

110. Golowich E, Pakvasa S. *Phys. Rev. D* 51:1215 (1995)

111. Soares JM. *Phys. Rev. D* 53:241 (1996)

112. Beneke M, Buchalla G, Neubert M, Sachrajda CT. *Phys. Rev. Lett.* 83:1914 (1999); *Nucl. Phys. B* 591:313 (2000)

113. Burdman G. *Phys. Rev. D* 52:6400 (1995)

114. Bajc B, Fajfer S, Oakes RJ. *Phys. Rev. D* 54:5883 (1996)

115. Khodjamirian A, Stoll G, Wyler D. *Phys. Lett.* B358:129 (1995)

116. Fajfer S, Singer P. *Phys. Rev. D* 56:4302 (1997)

117. Fajfer S, Prelovsek S, Singer P. *Eur. Phys. J. C* 6:471 (1999)

118. Bajc B, Fajfer S, Oakes RJ. *Phys. Rev. D* 54:5883 (1996); Lebed RF. *Phys. Rev. D* 61:033004 (2000); Fajfer S, Prelovsek S, Singer P, Wyler D. *Phys. Lett.* B487:81 (2000)

119. Bauer M, Stech B, Wirbel M. *Z. Phys. C* 34:103 (1987)

120. Fajfer S, Singer P, Zupan J. *Phys. Rev. D* 64:074008 (2001)

121. Lunghi E, Masiero A, Scimemi I, Silvestrini L. *Nucl. Phys. B* 568:120 (2000)

122. Ibanez LE, Ross GG. *Nucl. Phys. B* 386:3 (1992)

123. Allanach BC, Dedes A, Dreiner HK. *Phys. Rev. D* 60:075014 (1999)

124. Agashe K, Graesser M. *Phys. Rev. D* 54:4445 (1996)

125. Adler S, et al. (E787 Collab.) *Phys. Rev. Lett.* 84:3768 (2000)

126. Bhattacharyya G, Choudhury D. *Mod. Phys. Lett.* A10:1699 (1995)

127. Burdman G. *Phys. Rev. D* 57:4254 (1998)

128. Akeroyd AG, Recksiegel S. *Phys. Lett.* B554:38 (2003)

129. Chivukula RS, Selipsky SB, Simmons EH. *Phys. Rev. Lett.* 69:575 (1992)

130. Randall L, Sundrum R. *Phys. Lett.* B312:148 (1993)

131. Grinstein B, Nir Y, Soares JM. *Phys. Rev. D* 48:3960 (1993)

132. Freyberger A, et al. (CLEO Collab.) *Phys. Rev. Lett.* 76:3065 (1996); erratum, *Phys. Rev. Lett.* 77:2147 (1996)

133. Aitala EM, et al. (E791 Collab.) *Phys. Lett.* B462:401 (1999)

134. Coan TE, et al. (CLEO Collab.) *Phys. Rev. Lett.* 90:101801 (2003)

135. Kodama K, et al. (E653 Collab.) *Phys. Lett.* B345:85 (1995)

136. Aitala EM, et al. (E791 Collab.) *Phys. Rev. Lett.* 86:3969 (2001)

137. Asner D, et al. (CLEO Collab.) *Phys. Rev. D* 58:092001 (1998)

138. Yabsley B. *Experimental limits on new physics from charm decay.* Presented at Lepton Photon 2003, XXI Int. Symp. Lepton Photon Interactions, Aug. 11–16, FNAL, Batavia, IL, and BELLE CONF-0346

139. Feldman GF, Cousins RD. *Phys. Rev. D* 57:3873 (1998)

140. Johns WE (FOCUS Collab.) *Rare decays, recent results from FOCUS (+theory).* Presented at First Symp. Flavor and CP Violation, Philadelphia, PA, May 16–18, 2002, hep-ex/0207015

141. Frabetti PL, et al. (E687 Collab.) *Phys. Lett.* B398:239 (1997)

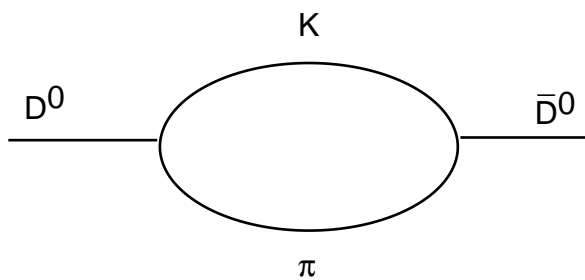142. Aitala EM, et al. (E791 Collab.) *Phys. Rev. Lett.* 86:3969 (2001)

Figure 1: Long-distance contribution from two charged pseudoscalar intermediate states.
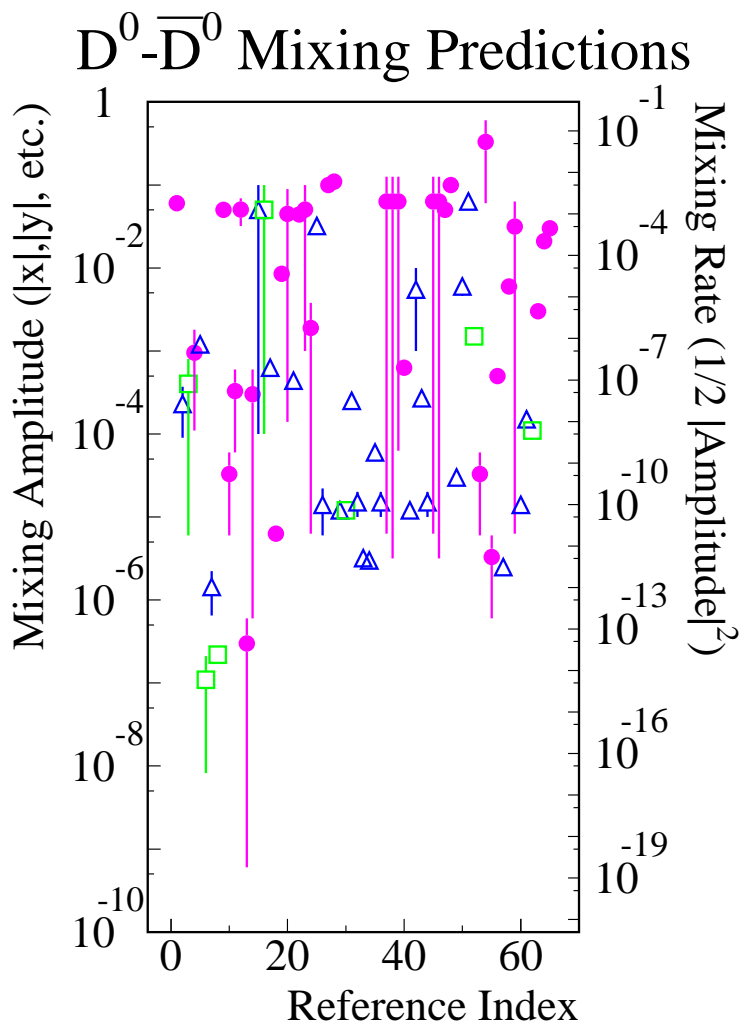

Figure 2: Predictions for $D^0 - \bar{D}^0$ mixing in the standard model and in some new-physics scenarios. From Reference (13). $\triangle$: Standard-model predictions for x. $\square$: standard-model predictions for y. $\bullet$: New-physics predictions for x. The horizontal axis corresponds to the references in Reference (13).

Table 1: Bounds on $(\delta^u_{12})_{LL}$, $(\delta^u_{12})_{LR}$ from D^0–$\bar{D}^0$ mixing (17) (neglecting the strong phase). All constraints should be multiplied by $(M_{\tilde{q}}/500 \text{ GeV})$.

$M^2_{\tilde{q}}/M^2_{\tilde{q}}$	$(\delta^u_{12})_{LL}$	$(\delta^u_{12})_{LR}$
0.3	0.03	0.04
1.0	0.06	0.02
4.0	0.14	0.02

Table 2: A comparison of the LEP experiments (35), CDF (36), E791 (37), FOCUS (38),CLEO (39), BaBar (40), and Belle (41). Each experiment has performed searches for charm mixing, rare decays, and CP violation. $K^-\pi^+$ is the number of reconstructed $D^0 \to K^-\pi^+$ used in published measurements. The proper time resolution for charm hadrons is denoted in σ_t.

	Fixed Target		e^+e^-			$p\bar{p}$
	E791	FOCUS	LEP	CLEO	BaBar/Belle	CDF
Beam	Hadron	Photon	$e^+e^- \to Z^0$	e^+e^-		$p\bar{p}$
$K^-\pi^+$	$\sim 2 \times 10^4$	$\sim 2 \times 10^5$	$\sim 10^4$ /expt.	$\sim 2 \times 10^5$	$\sim 10^6$	$\sim 5 \times 10^5$
σ_t	~ 40 fs	~ 40 fs	~ 100 fs	~ 140 fs	~ 160 fs	~ 50 fs

Table 3: Expected charm data sets for existing experiments and proposed facilities. "Current" is the size of the accumulated data set used in published physics analyses. "Full" is the size of the proposed complete data test, or the quantity of data collected per 10^7 s as indicated. Super Charm is not a proposed facility but is included for comparison. $K^+\pi^-$ is the number of reconstructed $D^0 \to K^-\pi^+$ in the full data set.

Experiment	Current	Full	$K^-\pi^+$
BaBar	91 fb^{-1}	500 fb^{-1}	6.6×10^6
Belle	46.2 fb^{-1}	500 fb^{-1}	6.6×10^6
CDF (Run II)	65 pb^{-1}	4.4 fb^{-1}	30×10^6
CLEO-c	-	3 fb^{-1}	5.5×10^5
BESIII	-	30 fb^{-1}	5.5×10^6
Super Charm	-	500 fb^{-1}	$9.2 \times 10^8/10^7$ s
SuperKEKB	-	2 ab^{-1}	$2.5 \times 10^7/10^7$ s
SuperBaBar	-	10 ab^{-1}	$1.3 \times 10^8/10^7$ s
BTeV	-		$\sim 6 \times 10^8/10^7$ s

Table 4: Comparison of the 95%-CL limits for the fit output parameters of BaBar, CLEO, and FOCUS when CP conservation is assumed in the fit, and when CP violation is allowed (denoted by CPV). The FOCUS entries are one dimensional limits. BaBar's limits include systematic uncertainties and were obtained in a fit that allowed $x'^2 < 0$.

	R_D	y'	x'	x'^2
CLEO [%]	(0.24, 0.69)	((−5.2, 0.2)	(−2.8, 2.8)	< 0.0076
BaBar [%]	(0.24, 0.49)	((−2.7, 2.2)	−	< 0.20
FOCUS [%]	(0.43, 1.78)	(−12.4, −0.6)	(−3.9, 3.9)	-
CLEO (CPV) [%]	(0.24, 0.71)	(−5.8, 1)	(−2.9, 2.9)	< 0.082
BaBar (CPV) [%]	(0.23, 0.52)	(−5.6, 3.9)	-	< 0.22

Table 5: Measurements of the time-integrated rate for the wrong-sign decay $D^0 \to K^+\pi^-$, normalized to the right sign decay $D^0 \to K^-\pi^+$

	$K^-\pi^+$	$K^+\pi^-$	$R_{\rm ws}[\%]$	$A_D[\%]$
E791 (66)	5.6K	not quoted	$0.68^{+0.34}_{-0.33} \pm 0.07$	-
ALEPH (67)	1038	19	$1.84 \pm 0.59 \pm 0.34$	-
FOCUS (68)	37K	150	$0.404 \pm 0.085 \pm 0.025$	-
CLEO (61)	13.5K	45	$0.332^{+0.063}_{-0.065} \pm 0.040$	$-2^{+19}_{-20} \pm 1$
Belle (63)	83K	317	$0.372 \pm 0.025^{+0.009}_{-0.014}$	-
BaBar (62)	120K	430	$0.357 \pm 0.022 \pm 0.027$	$9.5 \pm 6.1 \pm 8.3$
Average			0.368 ± 0.021	

Table 6: Current D^0 lifetime difference measurements. BaBar (New) is a measurement of $y\cos\phi$ and supersedes BaBar. Only the former is used to compute the world average value of y_{CP}.

	$K^-\pi^+$	K^-K^+	$\pi^-\pi^+$	y_{CP}	ref.
E791	35K	3.2K	−	$(0.8 \pm 2.9 \pm 1.0)\%$	(76)
FOCUS	120K	10K	−	$(3.4 \pm 1.4 \pm 0.7)\%$	(77)
CLEO	20K	1.9K	0.7K	$(−1.1 \pm 2.5 \pm 1.4)\%$	(78)
BaBar	158K	16.5K	8.4K	$(1.4 \pm 1.0^{+0.6}_{-0.7})\%$	(80)
Belle	214K	18.3K	−	$(−0.5 \pm 1.0 \pm 0.8)\%$	(79)
BaBar (New)	220K	26K	12.8K	$(0.8 \pm 0.4 \pm^{+0.5}_{-0.4})\%$	(81)

Table 7: Comparison of measurements in A_{CP} for D^0 modes, from E791 (89), FOCUS (90),CDF (88), and CLEO (78)

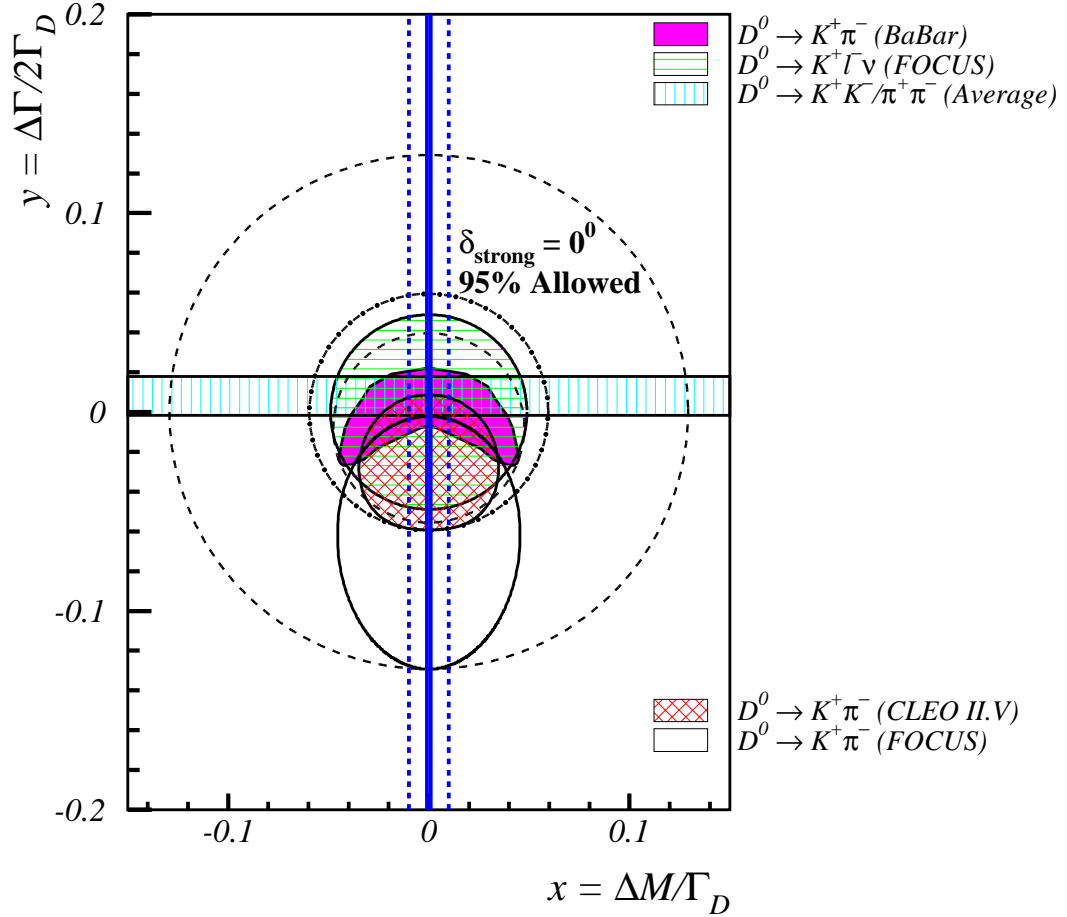|	Mode	A_{CP}	Mode	A_{CP}
CLEO	$D^0 \to K^+K^-$	$(0.0 \pm 2.2 \pm 0.8)\%$	$D^0 \to \pi^+\pi^-$	$(1.9 \pm 3.2 \pm 0.8)\%$
E791	$D^0 \to K^+K^-$	$(−1.0 \pm 4.9 \pm 1.2)\%$	$D^0 \to \pi^+\pi^-$	$(−4.9 \pm 7.8 \pm 2.5)\%$
FOCUS	$D^0 \to K^+K^-$	$(−0.1 \pm 2.2 \pm 1.5)\%$	$D^0 \to \pi^+\pi^-$	$(4.8 \pm 3.9 \pm 2.5)\%$
CDF	$D^0 \to K^+K^-$	$(2.0 \pm 1.7 \pm 0.6)\%$	$D^0 \to \pi^+\pi^-$	$(3.0 \pm 1.9 \pm 0.6)\%$
CLEO	$D^0 \to K^0_S\pi^0$	$(0.1 \pm 1.3)\%$	$D^0 \to \pi^0\pi^0$	$(0.1 \pm 4.8)\%$
CLEO	$D^0 \to K_SK^0_S$	$(−23 \pm 19)\%$		

Figure 3: Our present knowledge of D^0–$\bar{D}^0$ mixing. The solid vertical lines indicate a "typical" standard-model prediction for x. The dashed vertical lines indicate the upper range of non-standard-model predictions for x. The horizontal band is the world average 95% CL limit in y. The circle with horizontal shading is the 95% CL limit in (x, y). The strong-phase shift $\delta_{K\pi}$ between the Cabibbo-favored and doubly Cabibbo-suppressed decays is assumed to be zero in plotting the $D^0 \to K^+\pi^-$ results, where in each case CP conservation is assumed. For the CLEO and FOCUS measurements, the statistical error is included; for the BaBar measurement, both the statistical and systematic errors are included. The strong phase shift is expected to be close to zero, but until it is actually measured, the allowed region from the $D^0 \to K^+\pi^-$ measurements must be expanded to include the area swept out by rotating these regions about the origin. The three circles (small radius dashed, dot-dashed, and large radius dashed) are 2π rotations of the BABAR, CLEO, and FOCUS regions, respectively.
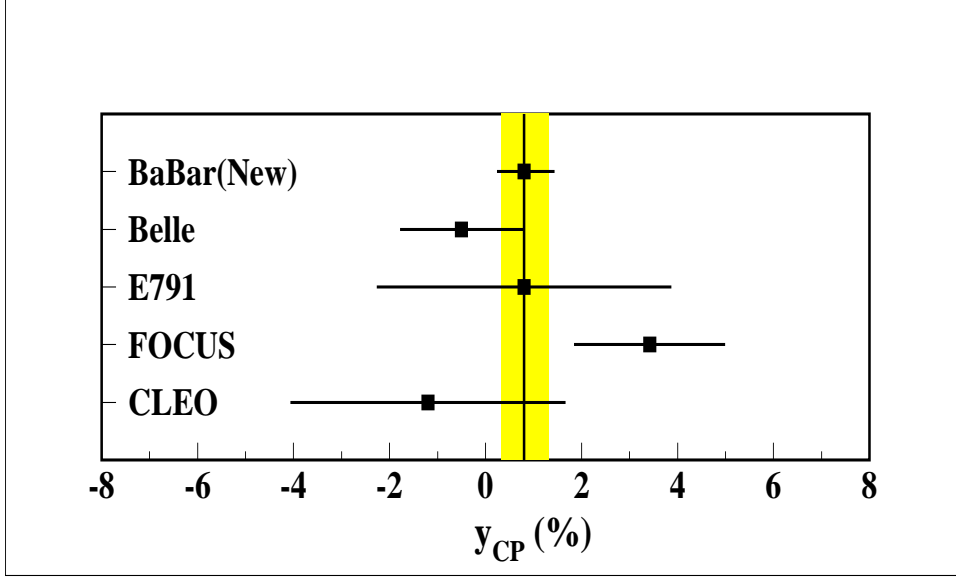
Figure 4: Comparison of experimental determinations of y_{CP}. The average value is indicated by the shaded band. We calculate the average of the measurements to be $\langle y_{CP}\rangle = (0.8\pm0.5)\%$.

Table 8: Comparison of measurements in A_{CP} for D^+ modes, from E791 (89) and FOCUS (90)

	Mode	A_{CP}
FOCUS	$D^+ \to K^- K^+ \pi^+$	$(0.6 \pm 1.1 \pm 0.5)\%$
	$D^+ \to K_S \pi^+$	$(-1.6 \pm 1.5 \pm 0.9)\%$
	$D^+ \to K_S K^+$ w.r.t. $(K^- \pi^+ \pi^+)$	$(6.9 \pm 6.0 \pm 1.5)\%$
	$D^+ \to K_S K^+$ w.r.t.$(K_S \pi^+)$	$(7.1 \pm 6.1 \pm 1.2)\%$
E791	$D^+ \to K^- K^+ \pi^+$	$(-1.4 \pm 2.9)\%$
	$D^+ \to \phi \pi^+$	$(-2.8 \pm 3.6)\%$
	$D^+ \to K^{*0}(892) K^+$	$(-1.0 \pm 5.0)\%$
	$D^+ \to \pi^+ \pi^- \pi^+$	$(-1.7 \pm 4.2)\%$

Table 9: Yields for direct CP violation in $\psi(3770) \to (CP$ Eigenstate 1$)(CP$ Eigenstate 2$)$ in one year at CLEO-c (52)

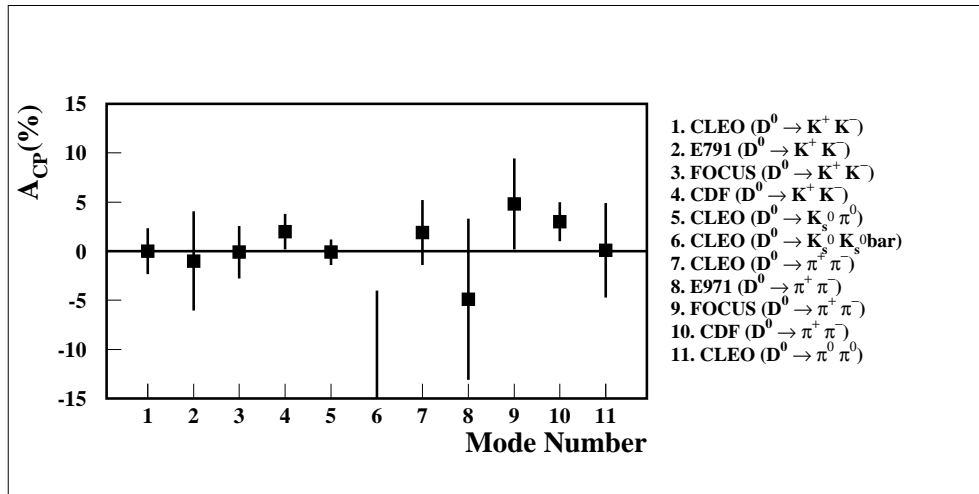| CP Eigenstate 1	CP Eigenstate 2	Events for 100% CP
$K^+ K^-$	$K^+ K^-$	174
$K^+ K^-$	$\rho^0 \pi^0$	171
$K_S \pi^0$	$K_S \pi^0$	183
$K_S K_S$	$K^+ K^-$	136

Figure 5: Measurements of A_{CP} for decay modes of the D^0.

Table 10: Direct CP-violation asymmetry δA reach from $\psi(3770) \to$ (flavor tag) (CP eigenstate), in one year at CLEO-c (52)

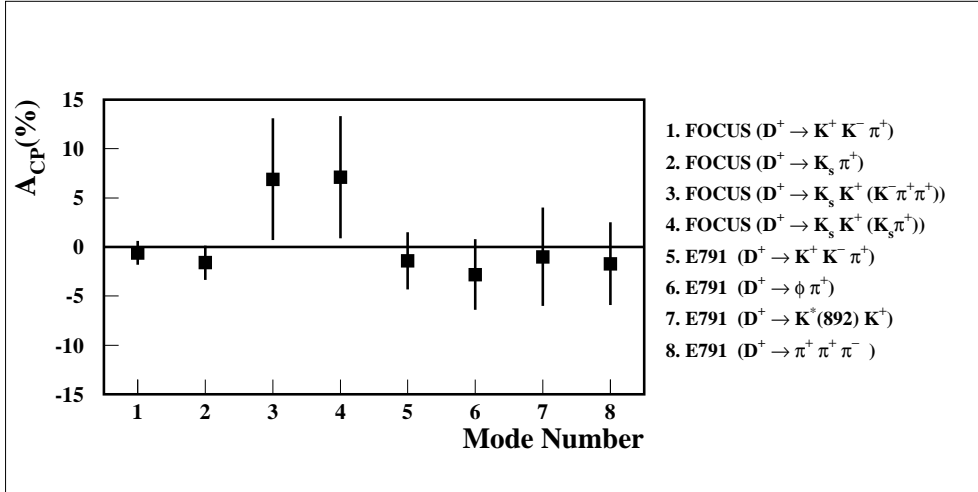| CP Eigenstate	Flavor-Tagged Sample	δA
$K^+ K^-$	10200	0.01
$K_S \pi^0$	10400	0.01
$K_S \omega$	3500	0.02

Figure 6: Measurements of A_{CP} for decay modes of the D^+.

Table 11: Projected CP asymmetry and sensitivity to rare decays for the full data set of existing experiments. For next-generation experiments, the sensitivities and rates are per year of 10^7 s. The yields at charm factories are computed without requiring a charm tag. Super Charm is not a proposed facility but is included for comparison. All entries are estimates by the authors.

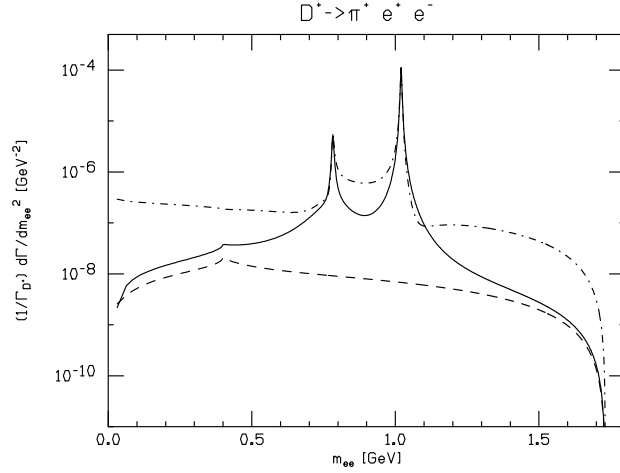| Experiment	δA_{CP}	$D \to \pi \ell^+ \ell^-$ limit	$D \to \pi \ell^+ \ell^-$ yield
BaBar	3×10^{-3}	1×10^{-6}	6
Belle	3×10^{-3}	1×10^{-6}	6
CDF (Run II)	1×10^{-3}	2×10^{-6}	4
CLEO-c	0.01	4×10^{-6}	4
BES III	3×10^{-3}	4×10^{-7}	40
Super Charm	2×10^{-4}	2×10^{-8}	700
Super-KEK-B	1×10^{-3}	5×10^{-7}	60
SuperBaBar	6×10^{-4}	3×10^{-7}	300
BTeV	3×10^{-4}	4×10^{-7}	200

Figure 7: The dilepton mass distribution for the $D^+ \to \pi^+ e^+ e^-$, normalized to Γ_{D^+}. The solid line shows the sum of the short- and long-distance standard-model contributions. The dashed line represents the short-distance contribution only. The dotted-dashed line includes the contribution of R-parity-violating terms in SUSY (see Section 3.2.2).

Figure 8: The dilepton mass distribution for the $D^0 \to \rho^0 e^+ e^-$, normalized to Γ_{D^0}. The solid line shows the sum of the short- and long-distance standard-model contributions. The dashed line represents the short-distance contribution only. The dotted-dashed line includes the contribution of R-parity-violating terms in SUSY (see Section 3.2.2).
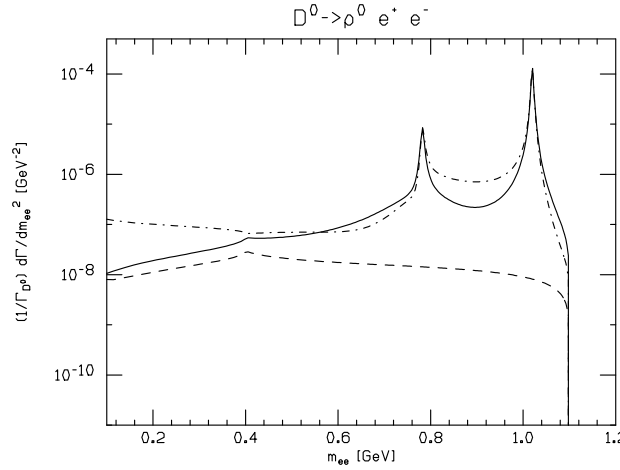
Table 12: Theoretical predictions for charm radiative decays ($Br \times 10^6$)

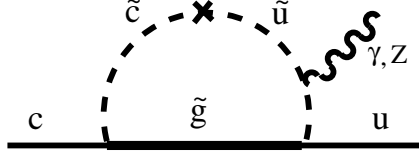| $D \to V\gamma$	Reference (97)	Reference (117)	Reference (115)
$D_s^+ \to \rho^+\gamma$	$6 - 38$	$20 - 80$	4.4
$D^0 \to \bar{K}^{*0}\gamma$	$7 - 12$	$6 - 36$	0.18
$D^0 \to \rho^0\gamma$	$0.1 - 0.5$	$0.1 - 1$	0.38
$D^0 \to \omega^0\gamma$	$\simeq 0.2$	$0.1 - 0.9$	$-$
$D^0 \to \phi^0\gamma$	$0.1 - 3.4$	$0.4 - 0.9$	$-$
$D^+ \to \rho^+\gamma$	$2 - 6$	$0.4 - 6.3$	0.43
$D_s^+ \to K^{*+}\gamma$	$0.8 - 3$	$1.2 - 5.1$	$-$

Figure 9: A typical contribution to $c \to u$ FCNC transitions in the MSSM. The cross denotes one mass insertion $(\delta^{12})_{\lambda\lambda'}$, with $\lambda, \lambda' = L, R$.
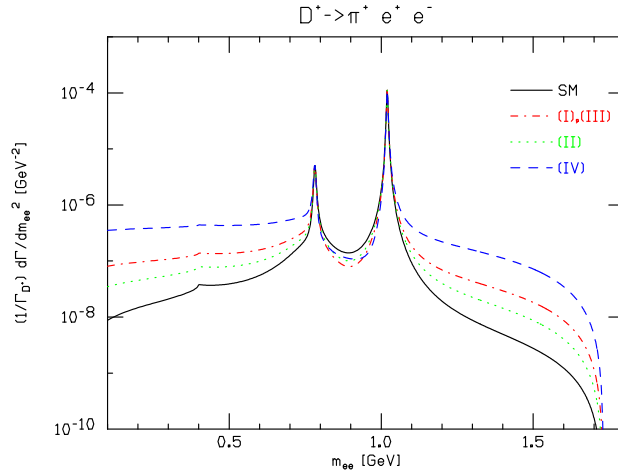

Figure 10: The dilepton mass distribution for $D^+ \to \pi^+ e^+ e^-$ (normalized to Γ_{D^+}) in the MSSM with nonuniversal soft breaking effects. The solid line is the standard model. (I) $M_{\tilde{g}} = M_{\tilde{q}} = 250$ GeV; (II) $M_{\tilde{g}} = 2\,M_{\tilde{q}} = 500$ GeV; (III) $M_{\tilde{g}} = M_{\tilde{q}} = 1000$ GeV; (IV) $M_{\tilde{g}} = (1/2)\,M_{\tilde{q}} = 250$ GeV.

Table 13: Most stringent (2σ) bounds for the R-parity violation couplings entering in rare D decays, from (a) charged-current universality, (b) R_π, and (c) $D \to K\ell\nu^*$. See Ref. (123) for details. All numbers should be multiplied by $(m_{\tilde{d}_R^k}/100$ GeV$)$.

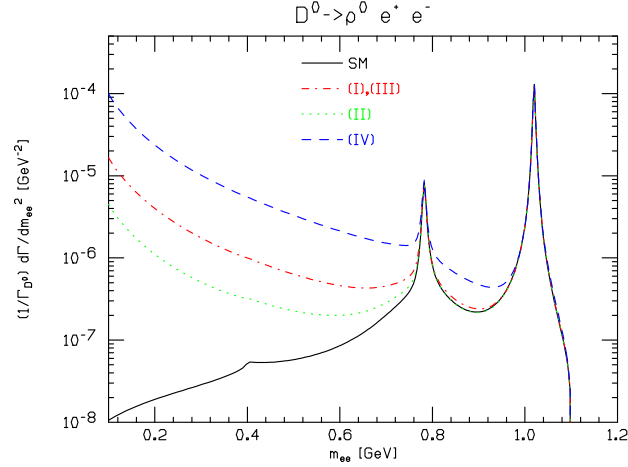| $\tilde{\lambda}'_{11k}$	$\tilde{\lambda}'_{12k}$	$\tilde{\lambda}'_{21k}$	$\tilde{\lambda}'_{22k}$
$0.02^{(a)}$	$0.04^{(a)}$	$0.06^{(b)}$	$0.21^{(c)}$

Figure 11: The dilepton mass distribution for $D^0 \to \rho^0 e^+ e^-$ (normalized to Γ_{D^0}) in the MSSM with nonuniversal soft breaking effects. The solid line is the standard model. (I) $M_{\tilde{g}} = M_{\tilde{q}} = 250$ GeV; (II) $M_{\tilde{g}} = 2\,M_{\tilde{q}} = 500$ GeV; (III) $M_{\tilde{g}} = M_{\tilde{q}} = 1000$ GeV; (IV) $M_{\tilde{g}} = (1/2)\,M_{\tilde{q}} = 250$ GeV.

Table 14: Comparison of various decay modes between the standard model and R-parity violation. The third column shows how large the R-parity–violating effect can be.

Decay Mode	Standard Model	$\not{R}_p$
$D^+ \to \pi^+ e^+ e^-$	2.0×10^{-6}	2.3×10^{-6}
$D^0 \to \rho^0 e^+ e^-$	1.8×10^{-6}	5.1×10^{-6}
$D^+ \to \pi^+ \mu^+ \mu^-$	1.9×10^{-6}	1.5×10^{-5}
$D^0 \to \rho^0 \mu^+ \mu^-$	1.8×10^{-6}	8.7×10^{-6}
$D^0 \to \mu^+ \mu^-$	3.0×10^{-13}	3.5×10^{-7}
$D^0 \to e^+ e^-$	10^{-23}	1.0×10^{-10}
$D^0 \to \mu^+ e^-$	0	1.0×10^{-6}
$D^+ \to \pi^+ \mu^+ e^-$	0	3.0×10^{-5}
$D^0 \to \rho^0 \mu^+ e^-$	0	1.4×10^{-5}

Table 15: FOCUS results with incorporated systematic errors for the modes shown (from Reference (140)) Each number represents a 90% upper limit for the branching ratio of the decay mode listed.
.

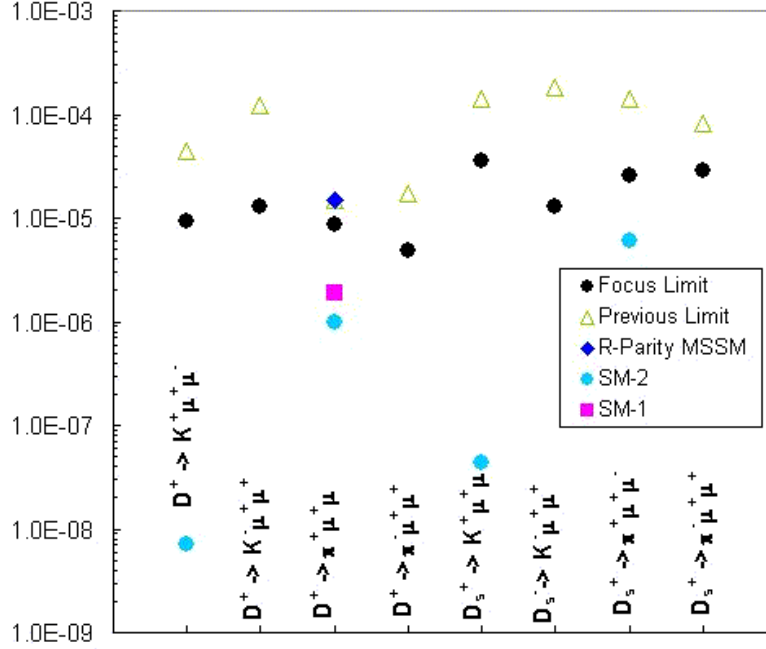| Decay Mode	Result
$D^+ \to K^+ \mu^+ \mu^-$	9.2×10^{-6}
$D^+ \to K^- \mu^+ \mu^+$	13.1×10^{-6}
$D^+ \to \pi^+ \mu^+ \mu^-$	8.8×10^{-6}
$D^+ \to \pi^- \mu^+ \mu^+$	4.8×10^{-6}
$D_S^+ \to K^+ \mu^+ \mu^-$	3.6×10^{-5}
$D_S^+ \to K^- \mu^+ \mu^+$	1.3×10^{-5}
$D_S^+ \to \pi^+ \mu^+ \mu^-$	2.6×10^{-5}
$D_S^+ \to \pi^- \mu^+ \mu^+$	2.9×10^{-5}

Figure 12: FOCUS limits and sensitivity from Reference (140), compared to other experiments and theory. (For a treatment of sensitivity, see (139).) The previous limits, except for the E687 $D^+ \to K^- \mu^+ \mu^+$ (141), are from the Fermilab experiment E791 (133). The theory estimates come from Reference (99) (R-parity MSSM and standard model–1) and Reference (107) (standard model–2). The results for four-body decays measured by E791 (142) are not shown.

Table 16: Current and projected 90%-CL upper limits in parts per million on rare D^0 decay modes.

Mode	$\Upsilon(4S)$CLEO Reference		Best Upper Limit Reference		B Factory	CLEO-c
e^+e^-	(132)	13	(133)	6.2	0.6	1.2
$\mu^+\mu^-$	(132)	34	(88)	2.4	3.4	1.2
$\mu^\pm e^\mp$	(132)	19	(133)	8.1	1.9	1.2
$\pi^0 e^+e^-$	(132)	45			1.0	4
$\pi^0 \mu^+\mu^-$	(132)	540	(135)	180	53	4
$\pi^0 \mu^\pm e^\mp$	(132)	86			8.5	4
$\bar{K}^0 e^+e^-$	(132)	110			2.6	7
$\bar{K}^0 \mu^+\mu^-$	(132)	670	(135)	260	46	7
$\bar{K}^0 \mu^\pm e^\mp$	(132)	100			2.3	7
ηe^+e^-	(132)	110			1.1	10
$\eta \mu^+\mu^-$	(132)	530			5.1	10
$\eta \mu^\pm e^\mp$	(132)	100			1	10

Table 17: Current and projected 90%-CL upper limits in parts per million on rare D^0 decay modes, (with the exception of $\phi\gamma$, where observation has been recently reported)

Mode	$\Upsilon(4S)$		Best Upper Limit		B Factory	CLEO-c
	Reference		Reference			
$\rho e^+ e^-$	(132)	100			9.9	2.5
$\rho\mu^+\mu^-$	(132)	490	(135)	230	48	2.5
$\rho\mu^\pm e^\mp$	(132)	49			4.8	2.5
$\omega e^+ e^-$	(132)	180			17	9
$\omega\mu^+\mu^-$	(132)	830			57	9
$\omega\mu^\pm e^\mp$	(132)	120			11	9
$K^*(892)^0 e^+ e^-$	(132)	140	(136)	24	14	4
$K^*(892)^0 \mu^+\mu^-$	(132)	1180	(136)	47	54	4
$K^*(892)^0 \mu^\pm e^\mp$	(132)	100	(136)	83	6.9	4
$\phi e^+ e^-$	(132)	52			5.1	5
$\phi\mu^+\mu^-$	(132)	410	(136)	31	28	5
$\phi\mu^\pm e^\mp$	(132)	34			3.4	5
$\pi^+\pi^-\pi^0\mu^+\mu^-$	none		(135)	810		6
$\rho\gamma$	(137)	240			26	1.5
$\omega\gamma$	(137)	240			26	8
$\phi\gamma$	(138)	$26^{+7+1.5}_{-6-1.7}$			21	4
$K^*(892)^0\gamma$	(137)	760			380	12
$\gamma\gamma$	(134)	29				1.2

Table 18: Current and projected 90%-CL upper limits on rare D^+ decay modes.

Mode	Best Upper Limit		CLEO-c
	Reference		
$\pi^+ e^+ e^-$	(133)	52	1.5
$\pi^+\mu^+\mu^-$	(140)	8.8	1.5
$\pi^+\mu^\pm e^\mp$	(133)	34	1.5
$\pi^- e^+ e^-$	(133)	96	1.5
$\pi^-\mu^+\mu^+$	(140)	4.8	1.5
$\pi^-\mu^+ e^+$	(133)	50	1.5
$K^+ e^+ e^-$	(133)	200	1.5
$K^+\mu^+\mu^-$	(140)	9.2	1.5
$K^+\mu^\pm e^\mp$	(133)	68	1.5
$K^- e^+ e^+$	(141)	120	1.5
$K^-\mu^+\mu^+$	(140)	13.1	1.5
$K^-\mu^+ e^+$	(141)	130	1.5

Table 19: Current and projected 90%-CL upper limits in parts per million on rare D^+ decay modes.

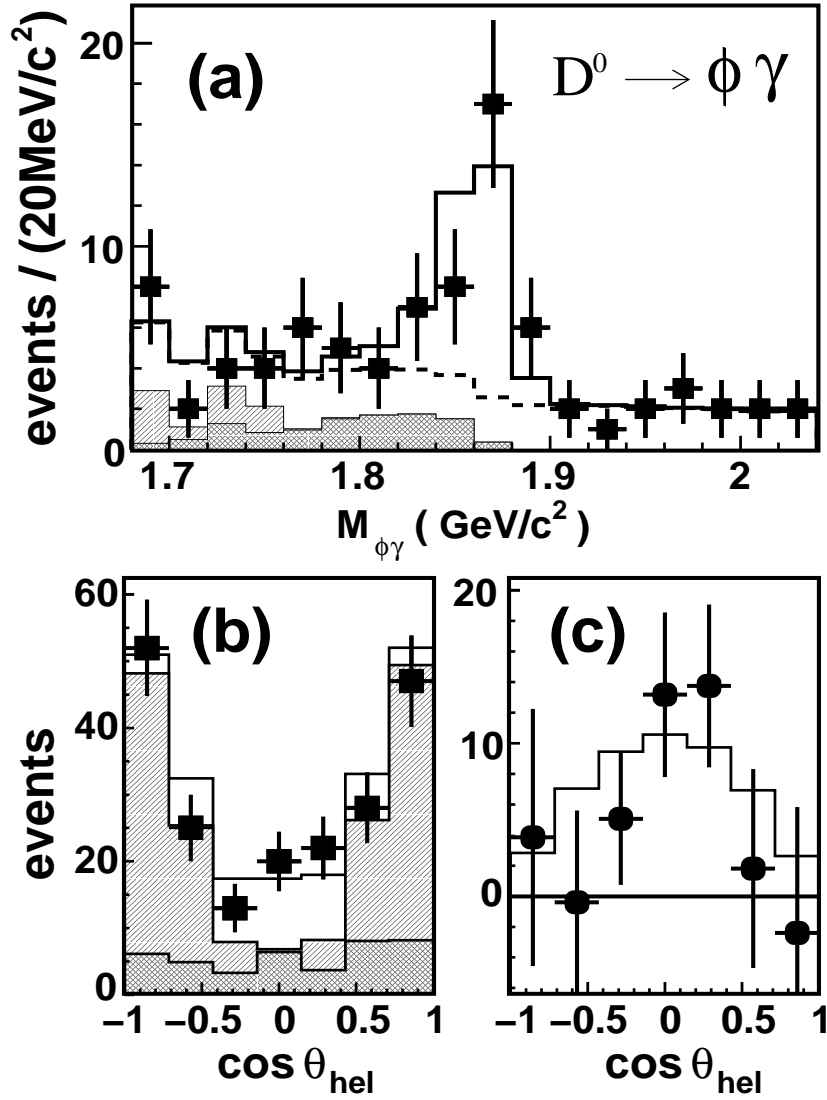| Mode	Best Upper Limit Reference		CLEO-c
$\rho^+ e^+ e^-$			7
$\rho^+ \mu^+ \mu^-$	(135)	560	7
$\rho^+ \mu^\pm e^\mp$			7
$\rho^- e^+ e^+$			7
$\rho^- \mu^+ \mu^+$	(135)	560	7
$\rho^- \mu^+ e^+$			7
$K^*(892)^+ e^+ e^-$			10
$K^*(892)^+ \mu^+ \mu^-$			10
$K^*(892)^+ \mu^\pm e^\mp$			10
$K^*(892)^- e^+ e^+$			10
$K^*(892)^- \mu^+ \mu^+$	(135)	850	10
$K^*(892)^- \mu^+ e^+$			10

Figure 13: The observation of $D^0 \rightarrow \phi\gamma$, $\phi \rightarrow K^+K^-$ by the BELLE collaboration ((138)). (a) The invariant mass distribution of $\phi\gamma$ pairs for data (points with error bars), the fit to the data (line), the background component of the fit (dashed line), $\phi\pi^0$ background (dark shaded histogram), and the sum of $\phi\eta$ and $D^+ \rightarrow \pi^+\pi^0$ backgrounds (light shaded histogram). (b) The helicity angle θ_{hel} distribution in the signal region, where θ_{hel} is defined as the angle between the direction of the K^+ momentum vector and the direction of the D^0 momentum vector in the rest frame of the ϕ meson. Data (points with error bars), MC prediction (line), total background (light shaded histogram), and non $\phi\pi^0$ background (dark shaded histogram. (c) Background subtracted θ_{hel} distribution in the signal region (points with error bars). The MC prediction is the line. The data are consistent with a $\sin^2\theta_{hel}$ distribution as expected for $D^0 \rightarrow \phi\gamma$.
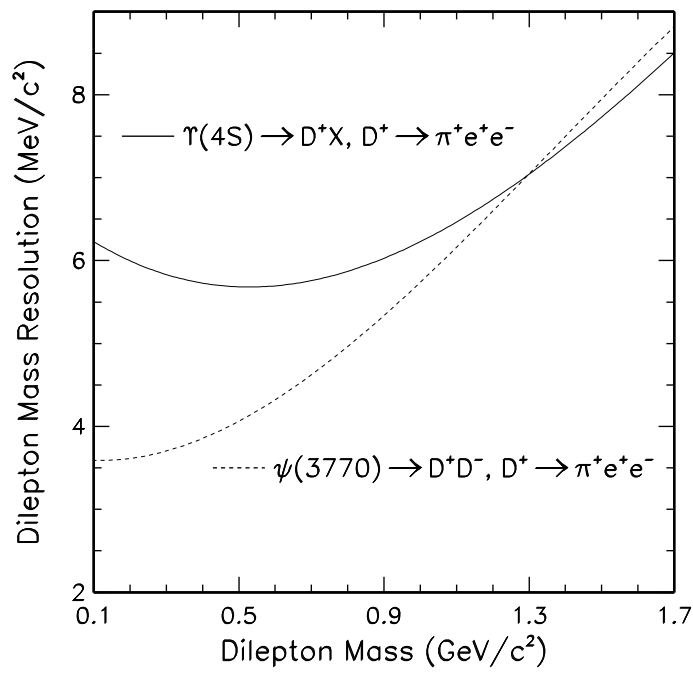
Figure 14: Dilepton mass resolution in $D^+ \to \pi^+ e^+ e^-$ for Ds produced at the $\Upsilon(4S)$ (solid) and at the $\psi(3770)$ (dashed).